



# NATIONAL AERONAUTICS AND SPACE ADMINISTRATION

DMS-DR-2443  
NASA CR-151769

PRESSURE AND HEAT TRANSFER TESTS OF THE 0.040-SCALE  
SPACE SHUTTLE ORBITER BASE HEATING MODEL (65-0) IN  
THE JOHNSON SPACE CENTER SPACE ENVIRONMENT SIMULATION  
LABORATORY THERMAL VACUUM CHAMBER A (CH79)

SPACE SHUTTLE

AEROTHERMODYNAMIC DATA REPORT

JOHNSON SPACE CENTER

HOUSTON, TEXAS

DATA MANAGEMENT services

SPACE DIVISION  CHRYSLER CORPORATION

March, 1979

DMS-DR-2443  
NASA CR-151769

PRESSURE AND HEAT TRANSFER TESTS OF THE 0.040-SCALE  
SPACE SHUTTLE ORBITER BASE HEATING MODEL (65-0) IN  
THE JOHNSON SPACE CENTER SPACE ENVIRONMENT SIMULATION  
LABORATORY THERMAL VACUUM CHAMBER A (CH79)

by

J. W. Foust  
Shuttle Aerosciences  
Rockwell International, Space Systems Group

Prepared under NASA Contract Number NAS9-13247

by

Data Management Services  
Chrysler Corporation Michoud Defense-Space Division  
New Orleans, La. 70189

for

Engineering Analysis Division

Johnson Space Center  
National Aeronautics and Space Administration  
Houston, Texas

WIND TUNNEL TEST SPECIFICS:

Test Number: JSC TVCA 61-A-78  
NASA Series Number OH79  
Model Number: 65-0  
Test Dates: June 26, 1978 through August 24, 1978  
Occupancy Hours: 372 Hours (252 test hours plus 120  
installation hours)

FACILITY COORDINATOR:

A. B. McIntyre  
Mail Code EL3  
NASA - Johnson Space Center  
Houston, Texas 77058

Phone: (713) 483-0123, Ext. 2254

PROJECT ENGINEERS:

J. W. Foust  
P. L. Lemoine  
Mail Code AD38  
Rockwell International  
Space Systems Group  
12214 Lakewood Boulevard  
Downey, CA 90241

A. L. Branscomb  
Mail Code EL3  
NASA - Johnson Space Center  
Houston, Texas 77058

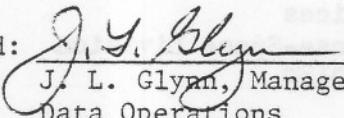
Phone: (713) 483-0123, Ext. 2254

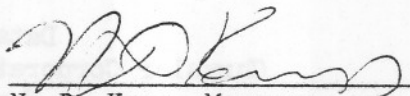
Phone: (213) 922-1463

DATA MANAGEMENT SERVICES:

Prepared by: Liaison--D. W. Hersey  
Operations--G. Richard Lutz

Reviewed by: G. G. McDonald

Approved:   
J. L. Glynn, Manager  
Data Operations

Concurrence:   
N. D. Kemp, Manager  
Data Management Services

Chrysler Corporation Michoud Defense-Space Division assumes responsibility  
only for publication and distribution of this document.

PRESSURE AND HEAT TRANSFER TESTS OF THE 0.040-SCALE  
SPACE SHUTTLE ORBITER BASE HEATING MODEL (65-0) IN  
THE JOHNSON SPACE CENTER SPACE ENVIRONMENT SIMULATION  
LABORATORY THERMAL VACUUM CHAMBER A (OH79)

by

J. W. Foust  
Rockwell International, Space Systems Group

ABSTRACT

Test OH79 was conducted in the NASA-Johnson Space Center Space Environment Simulation Laboratory (SESL) Thermal Vacuum Chamber A to determine space shuttle orbiter SSME plume-induced base pressure and heat transfer environments during simulated second-stage ascent trajectories. Specific objectives were (1) to provide verification of estimated environments used to design the SSME engine-mounted heat shield, (2) to provide environments for design of the SSME engine-mounted heat shield/orbiter-base heat shield interface seal, (3) to evaluate a central base heat shield flow protective device, (4) to provide SSME nozzle gimbaling limitation criteria for the ascent trajectories, (5) to provide detailed heating environments on the SSME nozzles, and (6) to evaluate heating penetration on the orbiter-base heat shield tile gap fillers.

Second-stage flight was simulated by firing the space shuttle main engines (SSME's) into the vacuum environment. The SSME's operated at one-half of full-scale chamber pressure. The O/F ratio and exhaust temperature were duplicated. To match the scaled SSME plume flow field,

ABSTRACT (Concluded)

simulated altitude pressures were reduced one half. The model was tested at simulated altitudes of 120, 150, 180 and 240 thousand feet.

All objectives of Test OH79 were fulfilled. Twenty-nine chamber entries consisting of 105 model firings were obtained to support all six objectives. Specifically, fifteen entries (58 firings) supported the first two objectives, three entries (9 firings) supported the third objective, two entries (7 firings) supported the fourth objective, six entries (21 firings) supported the fifth objective, and three entries (10 firings) supported the sixth objective.

Tabulated pressure and heat transfer data are not presented with this report; they may be obtained as shown in Appendix A.

The model configuration, instrumentation, test procedures, and data reduction are described in this report.

## TABLE OF CONTENTS

	Page
ABSTRACT	iii
INDEX OF MODEL FIGURES	2
INTRODUCTION	5
NOMENCLATURE	6
CONFIGURATIONS INVESTIGATED	10
INSTRUMENTATION	16
TEST FACILITY DESCRIPTION	20
TEST PROCEDURES	21
DATA REDUCTION	35
RESULTS AND DISCUSSION	46
REFERENCES	49
TABLES	
I. TEST CONDITIONS	50
II. DATA SET/RUN NUMBER COLLATION SUMMARY	51
III. MODEL DIMENSIONAL DATA	53
IV. MODEL 65-0 INSTRUMENTATION AND PATTERN SUMMARY	61
V. TEST SETUP SHEETS	79
VI. TEST DESCRIPTOR DEFINITION	81
VII. INSTRUMENTATION PATTERNS	84
FIGURES	
MODEL	85
APPENDIX A	
APPENDIX B	

## INDEX OF MODEL FIGURES

Figure	Title	Page
1.	Model 65-0 general arrangement.	85
2.	Instrumentation.	
	a. Base Heat Shield and Flow Diverter	86
	b. SSME Drain Line Nozzle	87
	c. SSME Firing Nozzle No. 1	88
	d. SSME Firing Nozzle No. 3	89
	e. SSME Smooth Wall Nozzle	90
	f. Body Flap	91
	g. Left OMS/RCS Pod	92
	h. Right OMS/RCS Pod	93
	i. Vertical Tail	94
	j. Tile Gap Base Heat Shield (Sheets 1 and 2)	95
	k. Tile Gap Body Flap	97
3.	Model 65-0 heat transfer gauges.	
	a. Left Side	98
	b. Right Side	99
	c. Center Base Heat Shield and Body Flap	100
4.	SSME hatband nozzle heat transfer gauges.	
	a. #1 SSME Position	101
	b. #2 SSME Position	102
	c. #3 SSME Position	103

## INDEX OF MODEL FIGURES (Continued)

Figure	Title	Page
5.	SSME smooth wall nozzle heat transfer gauges.	104
6.	Flow diverter heat transfer gauges.	
	a. Upper Flow Diverter	105
	b. Lower Flow Diverter	106
7.	Tile gap base heat shield and body flap heat transfer gauges.	
	a. Base Heat Shield	107
	b. Base Heat Shield	108
	c. Body Flap	109
8.	Model 65-0 installation and general arrangement.	
	a. Model, Thrust Stand, and Charge Tubes	110
	b. Model, Thrust Stand, and Pressurized Containers	111
9.	Model 65-0 strip connectors and wire bundles.	112
10.	Gas line arrangement inside Chamber A.	113
11.	Gas control panels.	114
12.	SSME operation pressure data.	115
13.	SSME operation timing data.	116
14.	Data acquisition equipment.	
	a. FACT	117
	b. Vidar	118
	c. Signal Conditioning and Amplifiers	119



## INDEX OF MODEL FIGURES (Concluded)

Figure	Title	Page
15.	SSME nozzle orientation.	
	a. Instrumentation Patterns 1, 4 and 6	120
	b. Instrumentation Pattern 2 (30° clocking)	121
	c. Instrumentation Pattern 2 (60° clocking)	122
	d. Instrumentation Pattern 7	123
	e. Instrumentation Pattern 8	124
16.	Instrumentation pattern 2 engine-mounted heat shield orientation.	
	a. 30° Clocking	125
	b. 60° Clocking	126
17.	Variation of thin-film gauge substrate (#7740 Pyrex) properties with temperature.	127

## INTRODUCTION

Between first-stage ascent and orbit, the space shuttle vehicle, in its second stage, passes through an almost vacuum region where the orbiter base environment is dominated by the plume flow field generated by the space shuttle main engines. Because the orbiter is not a conventional rocket launch vehicle, its base region can be complicated by SSME nozzle gimbaling and local altitude conditions beyond existing analytical prediction methods. To assist the design of thermal protection for the orbiter base, the plume-induced pressures and heat transfer rates must be determined experimentally.

This investigation, Test OH79, was undertaken to measure base pressure and heat transfer rates on a scaled model of the space shuttle orbiter base region with firing rocket engines, SSME, duplicating the plume flow field to simulate recirculation and impingement in a near-vacuum environment. One hundred five SSME firings were obtained at four simulated altitudes (120, 150, 180 and 240 thousand feet) with SSME nozzle gimbal angle varying to simulate numerous second-stage shuttle flight trajectory conditions. Results of the investigation are presented in this report.

## NOMENCLATURE

<u>PLOT SYMBOL</u>	<u>MNEMONIC</u>	<u>DEFINITION</u>
<u>Chamber Parameters</u>		
h	ALTITUDE	simulated altitude, ft.
<u>Model Parameters</u>		
	SSME 1	pitch and yaw gimbal angles, degrees
	SSME 2	pitch and yaw gimbal angles, degrees
	SSME 3	pitch and yaw gimbal angles, degrees
<u>Data Parameters</u>		
A <sub>t</sub>	NOZZLE THROAT AREA	total SSME nozzle throat area, in. <sup>2</sup>
c		specific heat of the thin-film gauge substrate, BTU/lbm-°F
C*	CHARACTERISTIC VELOCITY	actual SSME characteristic throat velocity, ft/sec
C* <sub>th</sub>	THEORETICAL CHARACTERISTIC VELOCITY	theoretical SSME characteristic throat velocity, ft/sec
CHI		high calibration signal on Vidar tape, counts
CLO		low calibration signal on Vidar tape, counts
FS		millivolt equivalent to the high calibration signal on Vidar tape, millivolts
g		gravitational constant (32.174 $\frac{\text{lbm ft}}{\text{lbf sec}^2}$ )
i		iteration variable
j		lower limit of averaging index interval
k		thermal conductivity of the thin-film gauge substrate, BTU/ft-sec-°F

NOMENCLATURE (Continued)

<u>PLOT SYMBOL</u>	<u>MNEMONIC</u>	<u>DEFINITION</u>
K		thin-film gauge substrate properties, BTU/ft <sup>2</sup> -sec <sup>1/2</sup> -°F
K <sub>c</sub>		thin-film gauge calibration sensitivity at 70°F, Ohms/°F
K <sub>T</sub>		thin-film gauge sensitivity at T <sub>a</sub> , Ohms/°F
K <sub>70</sub>		thin-film gauge sensitivity at 70°F, Ohms/°F
l		upper limit of averaging index interval
mV		signal value in millivolts
mV <sub>c</sub>		millivolt level corrected for RC circuit discharge
n		number of time intervals from 0 to t
N		upper limit of n
OFF		pressure transducer offset, psi
P	BPO0XX	low range absolute pressure, Mpsia
ΔP		differential pressure due to model firing, Mpsi
P <sub>A</sub>		chamber A internal pressure, TORR
PCOR		pressure correction, Mpsia
P <sub>c</sub>	PC0005	SSME chamber pressure, psia
P <sub>H2</sub>	HV0002	steady state hydrogen venturi pressure, psia
P <sub>O2</sub>	OV0001	steady state oxygen venturi pressure, psia
P <sub>0</sub>	OV0001 HV0002 OI0003 HI0004 PC0005	high range absolute pressure, psia

NOMENCLATURE (Continued)

<u>PLOT SYMBOL</u>	<u>MNEMONIC</u>	<u>DEFINITION</u>
$\Delta P_o$		differential pressure due to model firing, psi
$P_{ref}$		transducer reference pressure, psi
$\dot{q}$		instantaneous heat transfer rate, BTU/ft <sup>2</sup> -sec
$\dot{q}_c$		constant heat transfer rate, BTU/ft <sup>2</sup> -sec
$\bar{q}_{ss}$	HTXXXX	normalized heat transfer rate, BTU/ft <sup>2</sup> -sec
r	MIXTURE RATIO	oxidizer/fuel ratio
RAW		signal value in digital counts
$R_c$		thin-film gauge calibration resistance at 70°F, Ohms
$R_G$		thin-film gauge resistance at $T_a$ , Ohms
$R_L$		thin-film gauge circuit line resistance, Ohms
$R_p$		ratio of nominal to average SSME chamber pressure
S		pressure transducer bench calibration sensitivity, mV/psi
$S_g$		thin-film gauge conversion to °F, mV/°F
t		time, seconds
$\Delta t$		time increment, seconds
$\Delta T$		differential temperature due to model firing, °F
$T_a$		model steady state temperature prior to firing, °F
TCOR		reference temperature equivalent to $T_a$ , °F

NOMENCLATURE (Concluded)

<u>PLOT SYMBOL</u>	<u>MNEMONIC</u>	<u>DEFINITION</u>
$T_0$		reference time, seconds
$V_{ps}$		thin-film gauge circuit power supply voltage, Volts
$\dot{W}_{H_2}$	HYDROGEN WEIGHT FLOW	hydrogen weight flow rate, lb/sec
$\dot{W}_{O_2}$	OXYGEN WEIGHT FLOW	oxygen weight flow rate, lb/sec
$\dot{W}_T$	TOTAL NOZZLE WEIGHT FLOW	total nozzle weight flow rate, lb/sec
ZERO		millivolt equivalent to the low calibration signal on Vidar tape, millivolts
$\alpha$		reciprocal of the thin-film gauge signal conducting gain
$\eta_c$	COMBUSTION EFFICIENCY	SSME nozzle combustion efficiency
$\pi$		constant
$\rho$		density of the thin-film gauge substrate, lbm/ft <sup>3</sup>
$\tau$		RC circuit time constant, seconds

## CONFIGURATIONS INVESTIGATED

### General

Model 65-0 is an impulse type, hot firing 0.040-scale model of the aft portion of the orbiter vehicle 102 configuration. The propulsion simulation system is housed in a right circular cylinder of stainless steel and copper, to which the instrumented parts simulating the model external lines are rigidly mounted. For test OH79 the model was mounted on a thrust stand in the middle of the "lunar plane" of the test chamber firing vertically upward along the chamber axis. The propellants were gaseous hydrogen and oxygen.

The model lines simulate the OML of orbiter vehicle 102 aft of the base heat shield. Scaled components include the body flap, OMS/RCS pods and OMS engine nozzles, vertical tail, base heat shield, and SSME nozzles. The nozzles, both MPS and OMS, are correctly scaled internally (i.e., throat diameters, exit diameters, lengths, and internal contours). External nozzle contours are not precisely scaled because the nozzle wall thicknesses have been deliberately increased to allow for flush mounting of external instrumentation while preserving the ability to withstand the heat and pressure stresses of repeated model firings. The vertical tail is accurate as to planform and location, but simulates the undeflected rudder condition only. The body flap may be attached either in the nominal ( $\delta = 0^\circ$ ) position or deflected twenty degrees ( $\delta = +20^\circ$ ). All data taken during test OH79 were with the body flap in the undeflected position. A heat protective device, referred to as the flow

## CONFIGURATIONS INVESTIGATED (Continued)

diverter, was mounted to the central part of the base heat shield. The general arrangement of the model is shown in Figure 1.

### Propulsion Simulation System

Physically the propulsion simulation system consisted of a right circular cylinder of stainless steel and copper with internal passages for the flow of gaseous propellants and combustion products and external provisions for the attachment and support of model components and instrumentation harnesses and connectors. The upstream section of the propulsion simulation system attached to a flange or adapter which may be used to mount the model in any desired orientation.

Gaseous propellants (hydrogen and oxygen) were stored in external containers called charge tubes at the desired pressure (nominally 3000 psi) until model operation was required. The charge tubes are essentially stainless steel pipes of approximately one-inch internal diameter and lengths sufficient for an expansion wave reflection time exceeding 80 milliseconds. This wave time can be obtained with  $O_2$  and  $H_2$  charge tube lengths of 50 and 200 feet, respectively. The charge tubes were folded for installation alongside the model in the test chamber.

The propellant gases were supplied to the propulsion simulation system through a bipropellant autovalve attached to the upstream face of the mounting flange. The autovalve rapidly opens and closes the two propellant control valves, which are yoked together, to admit the propellant gases at pressures up to 3000 psi. The control valves remain



## CONFIGURATIONS INVESTIGATED (Continued)

open for a predetermined time interval, normally less than the wave time of the charge tubes. The duration of the "valves open" interval is preset, within close limits, by manual adjustment of time delay circuit parameters. The timing controls, together with other switches and controls, are located on the firing control panel. Energy for actuation of the autovalve is supplied by a regulated source of gaseous nitrogen at 3000 psi. The nitrogen is admitted to the open/close sides of the operating piston through solenoid-operated Valcor valves.

Because continuous burning of any large fraction of the propellant stored in the charge tubes would destroy the model, redundancy is provided in both the electrical signals and the nitrogen source (Valcor valve) to the "close" side of the operating piston. In the event that gas leakage past the bipropellant valves is sufficient to make long test chamber pumping times necessary, a pre-scored copper diaphragm may be installed between the autovalve and the flange. Operation of the bipropellant valves causes rupture and petalling of the weak diaphragm in the gas passages, and model firing operation is the same as without the diaphragm. It was not necessary to use the diaphragms during this test.

Within the propulsion simulation system, the propellant gases flowed through metering devices (venturis) before entering the injector passages. The venturi flowmeters are designed to remain choked under nominal model operating conditions. Upon autovalve opening, the charge tube gases are

## CONFIGURATIONS INVESTIGATED (Continued)

admitted, at essentially the loading pressure, to the venturi inlets. Venturi inlet pressures then remain constant until the reflected expansion shock waves generated by autovalve opening, return from the far end of the charge tubes. Under these conditions (choked venturis at constant inlet pressure), the propellant weight flow rates remained constant throughout the wave time of the charge tubes unless the autovalve closed prior to the wave return.

Propellant flows to the Main Propulsion System (MPS) were routed axially through the model. Downstream of the venturis the propellants entered the passages of a single injector, which mixed the fuel and oxidizer in a central combustion chamber, from which the burning gases were led off through separate passages to the three SSME nozzles. Ignition of the propellants in the central combustion chamber was accomplished with an automotive type spark plug. The timing of spark occurrence was controlled through adjustment of a potentiometer in the spark timing circuit. Closure of a microswitch during the autovalve opening stroke energized the spark timing circuit.

A set of metering venturis permitted metered (choked) flow to the MPS engines during three-engine firing simulation. The set of venturis was scaled to deliver weight flows at the nominal O/F ratio of 6 when the charge tubes were loaded to approximately the same pressure.

Two sets of SSME firing nozzles were provided. One set simulated such external nozzle features as the "hatband" stiffeners and coolant

## CONFIGURATIONS INVESTIGATED (Continued)

distribution pipes and manifolds. All four nozzles in this set bore heat transfer instrumentation; only three nozzles were used for test CH79. The other set of four nozzles had smooth external walls; three were non-instrumented, and one was instrumented and used for defining gimbaling limitation criteria. Both sets of nozzles faithfully reproduced the internal profiles of the full-scale engine nozzles, but wall thickness was not accurately scaled in either case. One instrumented, smooth-walled, non-firing nozzle was provided for simulated engine-out conditions; it was not used for test CH79.

Two sets of OMS nozzles were provided: one firing and one non-firing. Both non-firing nozzles had heat transfer gauges installed; only the left firing nozzle was instrumented. The firing nozzle internal profiles were correctly scaled, but the wall thicknesses were increased to permit flush-mounting of the external thin-film gauges and to provide strength and rigidity. Non-firing nozzles were installed; the OMS combustion system was not used for test CH79.

Interchangeable gimbal blocks were used to gimbal the MPS nozzles in discrete increments. The MPS nozzles could be gimballed in pitch, yaw, or a combination of pitch and yaw up to a total gimbal angle of 11 degrees. Gimbaling for the lower SSME nozzles was generally defined from the actuator null position ( $+10^{\circ}$  pitch,  $3.5^{\circ}$  yaw outboard). The only exceptions were entries 21 and 22 where gimbaling was defined from parallel yaw ( $+10^{\circ}$  pitch,  $0^{\circ}$  yaw).

## CONFIGURATIONS INVESTIGATED (Concluded)

Model 65-0 was distinguished from its predecessor, Model 25-0, by a redesign of the propulsion simulation system to reduce the firing steady-state response time. Model stabilization time (steady-state combustion chamber pressure achieved) appeared to be approximately 12-14 milliseconds for the MPS with three engines firing.

### Model Nomenclature

The following nomenclature is used to describe model components for the orbiter 102 (Vehicle 5) configurations:

B <sub>60</sub>	basic fuselage of vehicle 102 orbiter per Rockwell drawings
M <sub>18</sub>	orbital maneuvering system pods per Rockwell drawings
V <sub>5</sub>	vertical tail per Rockwell drawings
F <sub>14</sub>	body flap, per Rockwell drawings
N <sub>93,26</sub>	main propulsion system nozzles per Rockwell drawings
N <sub>8,90</sub>	orbiter maneuvering system nozzles per Rockwell drawings

Full-scale and model-scale dimensional data for the components of Model 65-0 are presented in Table III.

A more complete description of the model will be found in References 1 and 2.

## INSTRUMENTATION

### Pressure and Heat Transfer

Instrumentation on the external (lines) model part of model 65-0 consisted of static pressure taps and thin-film heat transfer gauges. Static pressures were measured with low-range piezo-electric pressure transducers mounted inside the model as close to the pressure orifice as possible. A small piece of flexible tubing was placed between the pressure transducer and orifice to attenuate acceleration when the model engines were fired. Thin-film heat transfer gauges were total gauges measuring a surface temperature-time history due to both convective and radiative heat transfer.

The instrumentation on model 65-0 used for test OH79 is presented in Table IV and Figure 2. Table IV lists the instrumentation on each model part and categorizes it according to instrumentation pattern; Figure 2 illustrates the instrumentation locations. The instrumentation used is summarized below and itemized on Figure 2.

#### Standard Base Heat Shield (Instrumentation Patterns 1, 2, 4, 7, 8):

Thin-film heat transfer gauges	128
--------------------------------	-----

Piezo-electric pressure transducers	20
-------------------------------------	----

#### Tile Gap Base Heat Shield (Instrumentation Pattern 6):

Thin-film heat transfer gauges	88
--------------------------------	----

Piezo-electric pressure transducers	2
-------------------------------------	---

### Reference

Reference instrumentation consisted of five internal static pressure

## INSTRUMENTATION (Continued)

measurements, five thermocouple measurements, and six discrete event signals.

Internal static pressures were measured with high-range piezo-electric pressure transducers. The pressures were hydrogen and oxygen venturi, hydrogen and oxygen injector, and SSME combustion chamber. All pressures were used to monitor the model firing. In addition, the venturi and combustion chamber pressures were used to calculate propellant weight flow rate and propulsion simulation system combustion efficiency.

Five thermocouples were mounted on the model to monitor temperature during repeated firings of a chamber entry. Two of the five were on opposite edges of the base heat shield, and their output before model firing was used as the initial thin-film gauge temperature for data reduction purposes. A third thermocouple was mounted on the aft wall of the combustion chamber. The remaining two thermocouples were mounted in the hydrogen and oxygen charge tubes.

The six discrete event signals were voltage signals used as cues for data processing operations and for monitoring the model firing sequence. The signals were:

1. Reference time ( $T_0$ )
2. Autovalve open signal ( $T_1$ )
3. Autovalve redundant close signal ( $T_2$ )
4. Autovalve primary close signal ( $T_3$ )

## INSTRUMENTATION (Continued)

5. Spark ignition signal ( $T_5$ )

6. Autovalve open/close trace ( $T_9$ )

### Sensor Description

Piezo-electric transducers responded only to pressure changes.

Piezo-electric materials inside the transducer sensed pressure changes on the transducer diaphragm. Each transducer was compensated for acceleration by a diaphragm wired opposite to the active diaphragm. Piezo-electric transducers were PCB type. High-range transducers were PCB Piezotronics model 111A22 dynamic pressure transducers rated for 5000 psid maximum. Low-range transducers were PCB Piezotronics model 103A sound pressure transducers, rated for 2 psid maximum.

The total heat transfer gauge was a thin-film gauge consisting of a thin resistance film of platinum fused to a Pyrex substrate (#7740 Pyrex). Silver tabs were fused to the platinum film terminals. Electrical connections were made to the silver with soft solder. The platinum film was insulated from the airstream by a thin dielectric coating of magnesium fluoride. All thin-film gauges measured the change in local surface temperature. The total gauge responded to both convective and radiative heating.

Thin-film gauges were contoured as required to match model curvature. Contouring was required on the hatband nozzles.

All thin-film gauges were bonded in place. Piezo-electric transducers were also bonded in place except for the high-pressure PCB's which

## INSTRUMENTATION (Concluded)

were threaded.

Further descriptions of the piezo-electric transducer and total heat transfer gauge can be found in Reference 3.

Figures 3 through 7 are various views of the base of the model showing excellent visualization of the heat transfer instrumentation. The small piezo-electric transducer pressure orifices are also visible on some views. Figure 3 shows overall views of the model illustrating heat transfer gauges on the base heat shield, body flap, OMS, and vertical tail. Figure 4 shows the heat transfer gauges on the SSME hatband nozzles. Heat transfer gauges on the SSME smooth-wall nozzle are shown on Figure 5. Figure 6 shows heat transfer gauges on the flow diverter mounted in place on the center base heat shield. Tile gap, base heat shield, and body flap heat transfer gauges are shown on Figure 7.



## TEST FACILITY DESCRIPTION

The Thermal Vacuum Chamber A of the NASA Johnson Space Center's Space Environment Simulation Laboratory is a large man-rated thermal vacuum chamber. The clear area inside the cold walls is 55 feet in diameter and extends 90 feet above the "Lunar Plane," the rotatable floor which supports the test articles and associated equipment. The internal free volume is approximately 350,000 cubic feet. The facility vacuum system is capable of bringing the test chamber to a simulated altitude of 300,000 feet ( $5 \times 10^{-4}$  torr) in approximately four and one-half hours.

## TEST PROCEDURES

### Installation

The model was mounted on a flange/adaptor bolted to a thrust stand in the center of the test chamber floor (lunar plane). The model was oriented so that the MPS engine plumes were directed vertically upward along the test chamber centerline. The propellant charge tubes, of schedule 80 stainless steel pipe, were folded within a rack to a package approximately 39 feet long. The accommodation of this package in the test chamber required positioning the charge tubes alongside the thrust stand and delivering propellants to the model from what had originally been the "fill" ends of the charge tubes. One of two pressurized containers near the model housed the "timer chassis," on which were mounted the model firing control electronic components and timer relays. The other container housed the model spark coils of other ignition system components. The physical arrangement of the model, thrust stand, charge tubes, and associated equipment in the test chamber is shown in Figure 8.

The instrumentation leads from each model component (nozzle, section of base heat shield, body flap, etc.) were grouped into bundles 36 inches in length with one half of a Cannon strip connector on the far end. The mating halves of the Cannon strip connectors were in turn attached to wire bundles 12 feet in length, which terminated at large Deutch connectors at the lunar plane beneath the model. From this point, facility wiring conducted measurement signals to amplifiers, signal conditioning equipment, and FM/FM tape recorders. The strip connectors and wire bundles are shown in Figure 9.

## TEST PROCEDURES (Continued)

### Installation (Continued)

Control panels for regulating gas supply to the charge tubes and autovalve were mounted near the exterior wall of Chamber A. The panels regulated pressure, vent, and purge of the hydrogen and oxygen charge tubes; pressure and vent of the autovalve; and pressure to the pressurized containers. An assortment of gases was supplied by bottles located near the panels. The autovalve and pressurized containers used only nitrogen. The oxygen charge tube used oxygen for model firings and nitrogen for purging and leak checking. The hydrogen charge tube used hydrogen for model firings, nitrogen for purging, and helium for leak checking. Figure 10 shows the gas line arrangement inside the chamber as the lines extend away from the thrust stand to the chamber wall. Figure 11 shows the gas control panels outside the chamber where the lines terminate.

Panels for controlling the model firing sequence were in the control room. One panel started the firing sequence while two other panels controlled the timer relays and spark ignition system housed in the two pressurized containers.

### Calibrations

All new thin-film heat transfer gauges were calibrated prior to installation in the model. Gauge resistance change with temperature was measured to determine a sensitivity factor,  $K_C$ . The temperature range was nominally 70°F to 150°F with three points being measured. Used thin-

## TEST PROCEDURES (Continued)

film gauges initially installed in the model for a previous test in Chamber A were not replaced or recalibrated if they were in good operating condition. The original calibrations were retained.

PCB piezo-electric pressure transducers were calibrated prior to installation in the model. Low-range PCB's, 0 to 2 psid, were calibrated at six points between 0 and 1.0 psi. High-range PCB's, 0 to 5000 psid, were calibrated at six points between 0 and 1900 psi. Because high-range PCB's were threaded in place, an unwanted stress imposed on the transducer during installation could alter the bench calibration. Therefore, "dead-end" calibrations with the nozzle exits blocked were performed on the high-range PCB's to guard against excessive change and to slightly alter the bench calibration if desired.

### Operating Procedure

Test preparation and test operation activities were conducted in accordance with the detailed test procedures for the OH79 base heating test (Reference 4). During a chamber entry, the procedures were followed step by step from the start of pumpdown until the chamber returned to atmospheric conditions.

Because multiple SSME firings were possible with the surface gap spark plug, refurbishment of the ignition system did not dictate the number of model firings during a chamber entry. In the past, SSME firings had to be limited to approximately ten due to heat deterioration of the SSME gimbal block O-rings; this was not a factor during test

## TEST PROCEDURES (Continued)

CH79 because of the relatively small test program. The number of SSME firings per chamber entry was simply determined by the proposed test altitude survey at each model configuration.

Four altitude conditions were required for test CH79 (see Table 1). For each model configuration, two, three, or four altitudes were scheduled to be surveyed. The number of SSME firings sometimes exceeded the number of scheduled altitude conditions. The primary reason to repeat SSME firings throughout the test was to improve data acquisition gain settings to obtain better quality data. The maximum SSME firings were 7 on Entry 15.

The order in which altitude data were obtained during a chamber entry remained flexible throughout the test program. Generally, the initial data were obtained at the lowest altitude or the lowest altitude where heating rates were significant. Subsequent data were obtained at altitudes in ascending order as long as the smooth flow of progress to reach the highest altitude was not significantly interrupted. Data not obtained on the ascending altitude curve could be obtained on the descending curve. Approximately four hours minimum was required to reach the highest altitude.

Pressures listed in Table 1 representing the test altitude conditions are one-half of the actual altitude pressure. Actual altitude pressures were determined by Reference 5. With the model SSME's operating at one-half full-scale chamber pressure, and Chamber A operating at one-half actual altitude pressure, the scaled SSME plume flow field was

## TEST PROCEDURES (Continued)

duplicated.

Two setup sheets were used to dictate the test activities for each day. The sheets contained pretest information, i.e., model configuration, model control pressures, planned test conditions, timer settings, etc., and post-test information, i.e., actual test conditions, actual model control pressures, IRIG time, model temperatures, etc. An example of the two setup sheets is shown in Table V.

The "descriptor" on Form I of the setup sheets is a nine-character code describing each model firing. Each test descriptor is listed in the run schedule in Table II. Each character of the "descriptor" is determined from the model and test configurations listed in Table VI.

SSME operation was initiated by a single switch on the firing control panel. When actuated, the switch set in motion a series of timing relays to operate the autovalve for proper charge tube gas flow to the combustion chamber (timing event signals  $T_1$ ,  $T_2$ ,  $T_3$ ) and to ignite the gas in the combustion chamber (timing event signal  $T_5$ ). Timing event signal  $T_5$ , which controlled the surface gap spark plug, was by far the most critical. Autovalve operation at this point, the fourth test of a base heating test series with this basic model, has become reliable and predictable making the  $T_1$ ,  $T_2$ , and  $T_3$  timer settings a matter of routine.  $T_5$ , on the other hand, must be set to actuate the spark within two to three milliseconds after charge tube gas flow reaches the combustion chamber, and then the time tolerance for spark occurrence

## TEST PROCEDURES (Continued)

is less than one millisecond for safe and reliable SSME operation. If the spark occurs too soon, the combustion chamber may contain insufficient gas mixture or insufficient pressure for ignition. If the spark occurs too late, the combustion chamber may contain too much pressure before ignition causing overpressure during ignition which could result in structural damage to the model. Standard practice was to ignite the cold gas mixture before the pressure exceeded 100 psi. Because of the critical timing of the charge tube gas flow and spark, the reliable autovalve operation was a significant plus factor. Spark occurrence was also reliable once a timer setting had been established. Timer setting changes were not necessary unless the spark plug was replaced or unless the microswitch which actuated the  $T_5$  timing event was replaced. The spark plug was changed twice during the test program, prior to chamber entries 11 and 26, respectively. These two occasions were not required changes but were precautions to prevent erosion and subsequent welding of the spark plug threads to the steel helicoil insert in the combustor housing. The microswitch did, however, require replacement on several occasions. There were two microswitches actuated when the autovalve opened: one initiated the primary closing timer relay, and one initiated the spark timer relay. If either one partially broke during repeated use, a new set was installed. When either the spark plug or microswitch was replaced, a new  $T_5$  timer setting had to be established by comparing the spark event with the combustion chamber pressure trace. Typical examples of the pressure and

## TEST PROCEDURES (Continued)

timing event data obtained to monitor SSME operation are shown in Figures 12 and 13.

Model refurbishment between chamber entries generally consisted of updating the model configuration and instrumentation checkout. Model configuration changes centered around the SSME gimbal pattern which was changed for almost every entry. At the same time, other required configuration changes and maintenance were completed, i.e., SSME nozzle rotation, SSME engine adapter O-rings,  $P_c$  transducer diaphragm insulation tape, flow diverter, etc. Each time the SSME gimbal pattern was changed, a low-pressure leak check was performed by plugging the SSME nozzle throats and pressurizing the model with approximately 150 psi helium to detect leaks around the gimbal block Marmon clamps. Each time the SSME chamber pressure transducer was removed to replace or install new insulation tape, or each time the spark plug was replaced, a high-pressure leak check was performed by blocking the aft end of the SSME gimbal blocks and pressurizing the model with helium at approximately 400 psi. Instrumentation checkout between chamber entries consisted of a "quick fix" effort to correct noisy channels or thin-film gauges and piezo-electric pressure transducers that showed no response. A faulty amplifier was replaced or wiring was repaired when feasible, but faulty thin-film gauges or intricate wiring problems were ignored. When a thin-film gauge or its wiring were determined to be beyond repair, a substitute gauge was patched into the data acquisition system. Low-range piezo-electric pressure transducers



## TEST PROCEDURES (Continued)

were reliable enough not to warrant replacement throughout the test. Of the high-range piezo-electric pressure transducers, only the SSME combustion chamber transducer required replacement on one occasion. Model refurbishment did not delay any chamber entry throughout the test program except after the first entry when numerous instrumentation and data acquisition problems required checkout.

### Data Acquisition

Three types of data acquisition systems were used for test OH79: FLEX, FACT, and Vidar.

FLEX allowed visual display in the control room of selected model and Chamber A parameters for easy analysis. The parameters were:

Autovalve operation pressures

Charge tube pressures

Charge tube temperatures

Model base thermocouple temperatures

Model system power supply voltages

Chamber A pressure

FACT is the facility's "Fast Automatic Circuit Tester" equipment used to record steady-state thin-film gauge data. FACT is capable of recording up to 144 individual channels of data; however, a maximum of only ninety-four were used for test OH79. The steady-state data measurement consisted of thin-film gauge resistance plus the line resistance from the gauge to the FACT equipment. FACT data were recorded before each model

## TEST PROCEDURES (Continued)

firing. A final FACT recording was also obtained after the last model firing of a chamber entry. A minimum of twenty minutes elapsed between model firing and FACT recording to allow the model thin-film gauges to stabilize. FACT data were used for data reduction and to assess thin-film gauge integrity. A good thin-film gauge maintained relatively constant resistance.

Vidar is an analog system for recording data during model firing. Two Vidar systems were used for test OH79. Vidar 1 was a 60-channel, 100-millivolt, full-scale system with 12 tracks of 5 channels each. Its data consisted of:

- 31 to 35 thin-film gauge measurements
- 2 or 20 low-range pressure measurements
  - 1 timing event ( $T_0$ )
  - 2 IRIG time channels

Vidar 2 was a 78-channel, 500-millivolt, full-scale system with 13 tracks of 6 channels each. Its data consisted of:

- 53 to 59 thin-film gauge measurements
- 5 high-range pressure measurements
- 6 timing events
- 2 IRIG time channels

Pressure transducer signal conditioning was provided by a 110V multi-channel power unit built specifically for the PCB transducer. The

## TEST PROCEDURES (Continued)

power supply unit provided 22V and 12mA current excitation for the transducers. Being highly sensitive, approximately 1500 mV/psi, the low-range PCB transducers did not require additional amplification. High-range PCB transducers with a sensitivity of approximately 1 mV/psi also did not require amplification, but they did require a voltage divider in the circuits because their output ranged from 1500 mV to 3000 mV. Venturi and injector transducer outputs were divided by a factor of six (3000 mV output = 500 mV full scale); SSME chamber pressure transducer output was divided by a factor of four (2000 mV output = 500 mV full scale). PCB transducer circuit time constants were approximately 3 seconds for the low-range transducers and approximately 5 seconds for the high-range transducers.

Thin-film gauge signal conditioning consisted of signal conditioning circuitry requiring 12V excitation and amplifiers to boost the signal ( $\approx 1\text{mV}/^{\circ}\text{F}$ ) for Vidar recording. The circuit time constant was 2.4 seconds. Amplifiers for the two Vidar systems were as follows:

### Vidar 1 (Dual Amplifiers):

Pre-Amp Gain Settings = 0.01, 0.03, 0.1, 0.3, 1, 3, 10

Post-Amp Gain Settings = 0.1, 1, 10, 100

### Vidar 2 (Single Amplifier):

Gain Settings = 1, 2, 5, 10, 20, 50, 100, 200, 500, 1000

Amplifier bandwidth was set at 10K Hz.

Data acquisition equipment is shown in Figures 14a through 14c.

## TEST PROCEDURES (Continued)

Figure 14a shows the FACT equipment in the center background. Figure 14b shows the two Vidar systems with the visicorder playback. Figure 14c shows the amplifiers and signal conditioning equipment; amplifiers for Vidar 1 are on the left, signal conditioning equipment is in the middle, and amplifiers for Vidar 2 are on the right.

Amplifier gains were established for the initial entry of each instrumentation pattern and then were updated as required between model firings or chamber entries to improve the signal-to-noise ratio for better quality data. Gains were changed to raise the signal out of the noise level or to eliminate or prevent saturation. It was common practice to have two or three gain patterns for each chamber entry and a new gain pattern at the start of each entry.

Six instrumentation patterns were developed for test CH79. They were determined by model configuration or model geometry. The six patterns are outlined in Table VII.

Instrumentation configurations were designated by two digits. The first digit was a number signifying one of the instrumentation patterns listed in Table VII. The second digit was a letter signifying a particular amplifier gain pattern for that particular instrumentation pattern.

SSME nozzles and the orientation of their instrumentation varied with instrumentation pattern. Four SSME nozzles were used throughout the test program: drain line, #1, #3 and smooth wall. The SSME nozzles and

## TEST PROCEDURES (Continued)

instrumentation orientation for each instrumentation pattern are shown in Figures 15A through 15e. The figures are viewed looking forward along each nozzle axis.

Each engine-mounted heat shield (eyeball, see Figure 2a) was rigidly attached to the SSME nozzle. The basic instrumentation orientation of each engine-mounted heat shield at the #1, #2, and #3 SSME nozzle positions is as shown in Figure 2a. This basic orientation was maintained throughout instrumentation patterns 1, 4, 6, 7, and 8. Because repeat data were not essential, the engine-mounted heat shields were allowed to rotate with the nozzles for instrumentation pattern 2, i.e., whatever angle the SSME nozzles were rotated away from the instrumentation pattern 1 orientation, the engine-mounted heat shields were rotated by an equal amount. Engine-mounted heat shield instrumentation orientation for instrumentation pattern 2 is shown in Figures 16a and 16b.

Instrumentation pattern changes usually required switching of thin-film gauges only. An exception was pattern 6 where low-range PCB transducers were also eliminated. Unless new model parts were installed, thin-film gauge switching was accomplished at the input to the signal conditioning units. The output of the signal conditioning units was then patched to the correct FACT and Vidar system channels if changes were required. This switching procedure applied to patterns 1 and 2 where model configuration hardware did not change. Patterns 4, 6, 7, and 8, where new model hardware was added or installed, also required patching

## TEST PROCEDURES (Continued)

at the Cannon strip connectors inside Chamber A. Spare cables were used whenever possible to eliminate unnecessary work. Whenever any thin-film gauge or PCB transducer patching changes were made, a continuity check from the gauge or transducer to the Vidar systems insured proper hookup.

Thin-film gauge line resistances were determined by inserting a shorted connector in place of the gauge at the Cannon strip connectors and recording the resultant line resistance on the FACT system.

Data were reviewed immediately after each model firing to:

1. Verify satisfactory model operation
2. Verify sufficient data and their integrity

Either selected or all Vidar tracks could be immediately played back on Visicorder upon request. Tracks from Vidar 2 containing model high-range internal pressure and event data were received first to verify model operation. Then, all or selected tracks from both Vidars were received to verify thin-film gauge and low-range pressure data. Vidar playback data, as a rule, spanned one inch full scale, i.e., 100 mV or 500 mV was equal to a one-inch deflection. Because of the need for increased sensitivity, hydrogen venturi, oxygen venturi, and SSME chamber pressure playback data were spanned to 3.9 inches full scale. Standard practice was to review all Vidar channels of the first firing of each entry, and thereafter select three or four thin-film gauge and low-range pressure data tracks for review. If data review was not complete by the time the next ascending altitude was reached, the model firing was skipped,

## TEST PROCEDURES (Concluded)

and the chamber proceeded to the next altitude. At the highest altitude of an entry, all playback data were reviewed before descending. Any data missed during ascent or any data requiring repeat were obtained on descent to atmospheric conditions.

## DATA REDUCTION

### Chamber A Pressure

Measured Chamber A internal pressure was converted to units of Torr (mm of H<sub>g</sub>) by the FLEX data system for display in the control room.

### Thermocouples

Model charge tube and base thermocouple measurements were converted to degrees Fahrenheit by the FLEX data system for display in the control room.

### Data Reduction Procedures

Routine procedures, equipment, and software programs by which the Vidar analog data were converted to digital data and subsequently processed into the desired format are detailed in Reference 6. The computer program (SOBHR) for calculating final reduced data from the digital data is documented in Reference 7.

### A-D Conversion

Vidar analog data were converted to digital data for storage on tape. Each Vidar analog channel was processed at 2000 samples per second. The full-scale range of each channel was equivalent to 2000 counts.

### Millivolt Data

Digital count data were converted to units of millivolts by Equation (1).

$$(1) \quad \text{mV} = \frac{(\text{FS-ZERO})(\text{RAW-CLO})}{\text{CHI} - \text{CLO}} + \text{ZERO} \quad (\text{millivolts})$$



## DATA REDUCTION (Continued)

where:

mV = millivolt value  
FS = millivolt equivalent to high calibration level  
ZERO = millivolt equivalent to low calibration level  
RAW = digital count value  
CLO = low calibration count value  
CHI = high calibration count value

High and low calibration signals were generated on each Vidar tape for each model firing within one hour before the firing.

### Tare Correction

Immediately following reference time,  $T_0$ , forty data points were averaged and used as a tare correction for each data point in the data processing interval. The forty data points spanned 20 milliseconds of time (0.5 milliseconds per data point). The tare correction was applied to all pressure and thin-film gauge data; event signals did not require data processing.

### Code Sheets

Various parameters and preliminary data were input by cards to the SOEHR data processing program. These parameters and data were supplied on "code sheets" for card key punching. Code sheets were required for each model firing. The basic code sheet information consisted of:

1. Time information - data processing time interval, data tabulation time interval, data averaging time interval, etc. (Time information was extracted from Vidar playback model operation pressure and event data.)

## DATA REDUCTION (Continued)

2. Model performance coefficients.
3. Header information.
4. Pressure conversion from millivolts to psi.
5. Thin-film gauge temperature conversion from millivolts to °F.
6. Thin-film gauge gain setting information.
7. Pressure transducer and thin-film gauge circuit time constants.

### Voltage Signal Correction

Pressure transducer and thin-film gauge electronic circuits were subjected to a typical RC circuit discharge rate depending on the time constant of the circuit. As an example, a 2-second circuit time constant will reduce an analog voltage response by approximately 5 percent in 100 milliseconds. To correct for any voltage signal loss, Equation (2) was applied to all pressure transducer and thin-film gauge measurements before final data processing.

$$(2) \text{ mVc}(t_n) = \text{mVc}(t_{n-1}) + \text{mV}(t_n) - \text{mV}(t_{n-1}) e^{-\Delta t/\tau} \text{ (millivolts)}$$

where:

mVc = corrected voltage

mV = actual voltage measurement

t = time at which voltage is being corrected

n = number of time intervals from 0 to t

$\Delta t$  =  $t/n$  = data sampling period ( $\Delta t = 0.5$  milliseconds)

$\tau$  = RC circuit time constant

## DATA REDUCTION (Continued)

### Average Data

Pressure and heat transfer data were averaged over a time interval corresponding to stable model operation and peak level of sensor output to obtain a steady-state value. The averaging interval always spanned 13 milliseconds or 26 data points during the last half of SSME operation.

### Low-Range Pressures

Low-range PCB transducer measurements of base pressures during model firing were reduced according to Equation (3).

$$(3) \quad P = \Delta P + P_{\text{ref}} + \text{PCOR} \quad (\text{Mpsia})$$

where:

$$(4) \quad \Delta P = \text{mVc} / \left( \frac{S}{1000} \right) + \text{OFF} \quad (\text{Mpsi})$$

$$(5) \quad \text{PCOR} = \frac{P_A \text{ psi}}{51.7 \text{ Torr}} \times 1000 \quad (\text{Mpsia})$$

$\Delta P$  = differential pressure due to model firing

$P_{\text{ref}}$  = reference pressure

PCOR = pressure correction

OFF = transducer offset

$P_A$  = Chamber A internal pressure, Torr

mVc = millivolt output of transducer (corrected)

S = transducer bench calibration, mV/psi

For all low-range pressure data processing,  $P_{\text{ref}}$  and OFF were zero; PCOR calculated by Equation (5) was used as the actual transducer reference pressure. Therefore, Equations (3) and (4) are simplified to:

DATA REDUCTION (Continued)

$$(6) \quad P = \Delta P + PCOR \quad (\text{Mpsia})$$

$$(7) \quad \Delta P = mVc / \left( \frac{S}{1000} \right) \quad (\text{Mpsi})$$

High-Range Pressures

High-range PCB transducer measurements of model internal operating pressures were reduced according to Equation (8).

$$(8) \quad P_o = \Delta P_o + P_{ref} + PCOR \quad (\text{psia})$$

where:

$$(9) \quad \Delta P_o = mVc/S + OFF \quad (\text{psi})$$

Terms of Equations (8) and (9) are as defined in the preceding section. Bench calibration sensitivity, S, is corrected to account for installation effects. For all high-range pressure data processing,  $P_{ref}$  was zero; OFF was zero for all model firings except for the SSME chamber pressure transducer during entries 28 and 29, where a large transducer zero shift (see Results and Discussion) was accounted for by OFF.

PCOR, Equation (5), was used as the actual reference pressure for the high range transducers. Noting that PCOR is 1000 times the actual Chamber A pressure in units of psia, a slight error is introduced into Equation (8). Maximum error is approximately 2.4% at 120K feet; minimum error is approximately 0.01% at 240K feet.

Equations (8) and (9) can now be simplified to:

$$(10) \quad P_o = \Delta P_o + PCOR \quad (\text{psia})$$

$$(11) \quad \Delta P_o = mVc/S + OFF \quad (\text{psi})$$

DATA REDUCTION (Continued)

Heat Transfer Rates

Thin-film gauge output was a surface temperature time history which is analogous to homogeneous one-dimensional, semi-infinite slab theory for unsteady heat conduction. The numerical technique used to extract instantaneous heating rates from the surface temperature-time history, i.e., the solution to the unsteady, one-dimensional heat conduction equation for a semi-infinite body, is described in Reference 8.

Three heat transfer rates were calculated from a thin-film gauge temperature time history:

1. Constant heating rate (Equation (12))
2. Instantaneous heating rate (Equations (13), (14), and (15))
3. Normalized heating rate (Equation (16))

Normalized heating rates were used for the tabulated summary data.

$$(12) \quad \dot{q}_{cn} = \frac{\pi K \Delta T_n}{2 \sqrt{t_n}} \quad (\text{BTU/ft}^2\text{-sec})$$

$$(13) \quad \dot{q}_n = K \left[ \frac{\Delta T(t_n)}{\sqrt{t_n}} + \sum_{i=2}^{n-1} \left\{ \frac{\Delta T(t_n) - \Delta T(t_i)}{\sqrt{t_n - t_i}} - \frac{\Delta T(t_n) - \Delta T(t_{i-1})}{\sqrt{t_n - t_{i-1}}} \right. \right. \\ \left. \left. + 2 \frac{\Delta T(t_i) - \Delta T(t_{i-1})}{\sqrt{t_n - t_i} + \sqrt{t_n - t_{i-1}}} \right\} + \frac{\Delta T(t_n) - \Delta T(t_{n-1})}{\sqrt{\Delta t}} \right]$$

for  $n = 3, 4, 5, \dots, N$  (BTU/ft<sup>2</sup>-sec)

for  $n = 1,$

$$(14) \quad \dot{q}_1 = 0$$

DATA REDUCTION (Continued)

For  $n = 2$ ,

$$(15) \quad \dot{q}_2 = \frac{\pi K \Delta T_2}{4\sqrt{t_2}} \quad (\text{BTU}/\text{ft}^2\text{-sec})$$

$$(16) \quad \bar{q}_{ss} = \frac{R_p^{0.8}}{(\ell - j) + 1} \sum_{n=j}^{\ell} \dot{q}_n \quad (\text{BTU}/\text{ft}^2\text{-sec})$$

Parameters in Equations (12) through (16) are defined as follows:

$K$  = thin-film gauge substrate properties (Equation (17))

$\Delta T$  = surface temperature change from the temperature-time history (Equation (18))

$t$  = time at which heating rate is being determined

$\Delta t$  =  $t/n$  = data sampling period ( $\Delta t = 0.5$  milliseconds)

$n$  = number of time intervals from 0 to  $t$

$N$  = upper limit of  $n$

$i$  = iteration variable

$\ell, j$  = averaging index interval

$R_p$  = ratio of nominal to average SSME chamber pressure

Thin-film gauge substrate properties were determined from a third-order curve fit of Figure 17. The resulting equation is:

$$(17) \quad K = \frac{1}{\sqrt{\pi}} \left( \frac{\sqrt{\rho c k}}{\sqrt{\rho c k_{70}}} \right) \sqrt{\rho c k_{70}} = \frac{1}{\sqrt{\pi}} \left( 6.94848 \times 10^{-2} + 6.4165929 \times 10^{-5} T_a \right. \\ \left. - 6.8729213 \times 10^{-8} T_a^2 + 2.671248 \times 10^{-11} T_a^3 \right) \\ (\text{BTU}/\text{ft}^2\text{-sec}^{1/2}\text{-}^\circ\text{F})$$

DATA REDUCTION (Continued)

where

$\rho$  = density

$c$  = specific heat

$k$  = thermal conductivity

$T_a$  = TCOR = model steady-state temperature prior to firing  
(average of base heat shield thermocouples)

Surface temperature change,  $\Delta T$ , was determined by a sliding average of the differential temperature computed by Equation (18).

$$(18) \quad \Delta T(t) = mVc \frac{\alpha}{S_g} \quad (^\circ F)$$

where

$\alpha$  = reciprocal of the signal conducting gain

$S_g$  = gauge conversion to  $^\circ F$

One characteristic of Equation (13) is that the surface temperature-time history must be a smooth curve in order to produce a smooth heating rate-time history. A smooth temperature-time history was attained by calculating a sliding average of the actual surface temperature-time history. Equations (19) and (20) were applied three successive times to the data generated by Equation (18) before using the data in heating rate Equations (12) and (13).

$$(19) \quad \Delta T(t_1) = \frac{\Delta T(t_1) + \Delta T(t_2)}{2} \quad (^\circ F)$$

$$(20) \quad \Delta T(t_2 \dots t_n) = \frac{\Delta T(t_{n-1}) + \Delta T(t_n) + \Delta T(t_{n+1})}{3} \quad (^\circ F)$$

## DATA REDUCTION (Continued)

Gauge conversion,  $S_g$ , used in Equation (18) was calculated by Equation (21).

$$(21) \quad S_g = K_T V_{ps} \frac{1000^2}{(1000 + R_L + R_G)(1220 + R_L + R_G)} \quad (\text{mV}/^\circ\text{F})$$

$$(22) \quad K_T = K_{70} (1.018 - 2.59 \times 10^{-4} T_a) \quad (\text{Ohms}/^\circ\text{F})$$

$$(23) \quad K_{70} = \frac{R_G}{\frac{R_c}{K_c} + (T_a - 70)} \quad (\text{Ohms}/^\circ\text{F})$$

where

$K_T$  = sensitivity at  $T_a$

$K_{70}$  = sensitivity at  $70^\circ\text{F}$

$K_c$  = calibration sensitivity at  $70^\circ\text{F}$

$R_c$  = calibration resistance at  $70^\circ\text{F}$

$R_G$  = resistance at  $T_a$

$R_L$  = line resistance

$T_a$  = model steady state temperature prior to firing

$V_{ps}$  = circuit power supply voltage (12V)

Model steady-state temperature,  $T_a$ , was determined from the average of the two thermocouples mounted on the edges of the base heat shield. Gauge resistance was recorded by FACT. Actual FACT data consisted of  $R_L + R_G$ . Line resistances were recorded by FACT as described in the data acquisition section.

### Model Performance

Model performance was determined by the SSME nozzle combustion



DATA REDUCTION (Continued)

efficiency which is a ratio of actual to ideal characteristic throat velocity.

$$(24) \quad \eta_c = \frac{C^*}{C^*_{th}}$$

where

$C^*$  = actual characteristic throat velocity

$C^*_{th}$  = theoretical characteristic throat velocity

Actual characteristic throat velocity was computed by:

$$(25) \quad C^* = \frac{P_c A_t g}{\dot{W}_T} \quad (\text{ft/sec})$$

where

$P_c$  = SSME chamber pressure

$A_t$  = SSME nozzle throat area

$g$  = gravitational constant

$\dot{W}_T$  = total weight flow rate

Theoretical characteristic throat velocity was computed by:

$$(26) \quad C^*_{th} = 9397.5 - 305.0r - (39.832r^2 - 505.8664r + 1410.0552) \log \left( \frac{P_c}{100} \right) \quad (\text{ft/sec})$$

where

$r$  = oxidizer/fuel ratio

Total weight flow rate and oxidizer/fuel ratio were calculated from the individual hydrogen and oxygen weight flow rates as follows:

DATA REDUCTION (Concluded)

$$(27) \quad \dot{W}_T = \dot{W}_{O_2} + \dot{W}_{H_2} \quad (\text{lb/sec})$$

$$(28) \quad r = \frac{\dot{W}_{O_2}}{\dot{W}_{H_2}}$$

where

$\dot{W}_{O_2}$  = oxygen weight flow rate

$\dot{W}_{H_2}$  = hydrogen weight flow rate

Oxygen and hydrogen weight flow equations were determined from venturi calibrations. They are:

$$(29) \quad \dot{W}_{O_2} = 8.1526029 \times 10^{-4} P_{O_2} + 2.0558974 \times 10^{-8} P_{O_2}^2 \quad (\text{lb/sec})$$

$$(30) \quad \dot{W}_{H_2} = 1.4813399 \times 10^{-4} P_{H_2} - 1.404687 \times 10^{-9} P_{H_2}^2 \quad (\text{lb/sec})$$

where

$P_{O_2}$  = steady-state oxygen venturi pressure

$P_{H_2}$  = steady-state hydrogen venturi pressure

## RESULTS AND DISCUSSION

Test OH79 data consisted of heating rates and pressures varying as a function of time during model firing. By selecting a time interval to average data, as described in the preceding section, each sensor output during the firing was summarized by a single steady-state value.

Two types of data were received: tabulated and plotted. Tabulated summary data consisted of (1) chamber and model header information, (2) a listing of card inputs to the data reduction program, (3) model performance data, and (4) summary heat transfer and pressure data. Plotted data consisted of the same plus heat transfer and pressure data in engineering units displayed as a function of model firing time. Plotted pressure data were each low-range PCB transducer measurement or each high-range PCB transducer measurement displayed versus model firing time in milliseconds. Plotted heat transfer data were differential temperature, instantaneous heating rate, and constant heating rate from each thin-film gauge measurement displayed versus model firing time in milliseconds.

Analog data were generally of good quality with a high signal-to-noise ratio. Some channels did experience a relatively higher noise level than others or experienced 60-cycle noise, but it usually did not result in data loss or inhibit the steady-state data level. Filtering of some channels by reducing the bandwidth to 1K Hz did not appear to improve signal quality. Pressure data at low altitudes (120K and 150K) were mostly noise, possibly caused by acceleration due to the model

## RESULTS AND DISCUSSION (Continued)

firing into a higher surrounding pressure. At higher altitudes, pressure data were relatively clean with good response.

Model combustion efficiency was usually around 0.90 which is a measure of how well the SSME engines simulated the theoretical characteristic throat velocity. This high combustion efficiency does lend credibility to the SSME plume flow field and to the heating rates and pressures generated by it.

SSME combustion chamber pressure usually fluctuated around the desired value of 1500 psia. Late in the test program beginning with Entry 27, the pressure level decreased to approximately 1200 to 1300 psia with a large zero shift. A new transducer was installed without performing an in-place check calibration. The problem persisted which led to the conclusion that the PCB power supply channel circuit was the problem. Switching to a new channel solved the problem, but transducer output was higher than anticipated probably due to a slight calibration shift during installation. In view of the above, the actual SSME chamber pressure was most likely normal for Entry 27 through Entry 31.

Return waves caused by reflection from the chamber walls were not evidenced in the test OH79 data. Results of the previous test in Chamber A indicated that return waves might be a problem. This was not the case. A negative shift in some of the SSME nozzle heating rate data was experienced, but it could not be linked to return waves. It was attributed to electrical noise.

## RESULTS AND DISCUSSION (Concluded)

Tabulated source data are not supplied with this document but are available through the Rockwell International, STS Aerosciences Department as shown in Appendix A.

Plotted source data are also available through the Rockwell International, STS Aerosciences Department as shown in Appendix A.

Appendix B contains factors to correct the tabulated summary heat transfer data. Parameter  $R_p$  in Equation (16) which is a card input to the data reduction via the code sheets, was in error for all model firings.  $R_p$  should be the ratio of nominal to average SSME chamber pressure; actually, the inverse was entered on the code sheets. A correction factor for each model firing to account for this error is presented in Appendix B (corrected data = correction factor x tabulated summary data).

#### REFERENCES

1. W. P. Garton and B. J. Herrera, "Pretest Information for Test (OH78) of the 0.040-Scale Space Shuttle Orbiter Base Heating Model 65-0 in the Johnson Space Center Space Environment Simulation Laboratory Thermal Vacuum Chamber A," Rockwell International Space Division Report SD75-SH-0240, dated March 5, 1976.
2. E. Chee, "Pretest Information for Test (OH79) of the 0.040-Scale Space Shuttle Orbiter Base Heating Model 65-0 in the Johnson Space Center Space Environment Simulation Laboratory Thermal Vacuum Chamber A," Rockwell International Space Division Report SD78-SH-0058, dated February 15, 1978.
3. L. Bogdan, "Instrumentation Techniques for Short Duration Test Facilities," CAL No. WTH-030, dated March 31, 1967.
4. "Shuttle OH79 Base Heating Test Series Test No. 61-A-78 Detailed Test Procedure," Space Environment Simulation Laboratory, Johnson Space Center, Houston, Texas, dated May 15, 1978.
5. O. E. Smith and D. K. Weidner, "A Reference Atmosphere for Patrick AFB, Florida, Annual (1963 Revision)," NASA TM X-53139, NASA-Marshall Space Flight Center, dated September 23, 1964.
6. H. D. Hefner, "Data Processing Plan for Thermal Vacuum Testing of the Shuttle Orbiter Base Heating Model 65-0," Lockheed Electronics Company, Inc., Aerospace Systems Division Report LEC-7791 (JSC-11195), dated May, 1976.
7. J. D. McBryde, "Program Documentation, Shuttle Orbiter Base Heating Rate Program (SOEHR)," Lockheed Electronics Company, Inc., Aerospace Systems Division Report LEC-8326 (JSC-11386), dated August, 1976.
8. W. T. Cook and E. J. Felderman, "Reduction of Data from Thin-Film Heat Transfer Gauges: A Concise Numerical Technique," AIAA Journal, Vol. 4, No. 3, dated March, 1966.

TABLE I. TEST CONDITIONS

SIMULATED ALTITUDE	CHAMBER A PRESSURE	
	(K ft.)	PSIA X 1000
120	35.400	1.83
150	10.522	$5.44 \times 10^{-1}$
180	3.346	$1.73 \times 10^{-1}$
240	0.2456	$1.27 \times 10^{-2}$

NOTE: Test conditions are nominal.

TABLE II. DATA SET/RUN NUMBER COLLATION SUMMARY

Test 0479		SPACE DIVISION NORTH AMERICAN ROCKWELL CORPORATION										Prepared By:	Page No. 1 of 2
												Checked By:	Report No.
												Date:	Model No.
1	2	3	4	5	6	7	8	9	10	11	12	13	15
Dataset	Chamber	Test	Test	FIRINGS		Configuration		*Descriptor		Instr.	SSME	Gimb	Ang
Identifire	Entry	Simulated	Simulated	Altitude	Altitude					Pattern	Chamber	H/SSME	H/SSME
		120K	150K	150K	240K						Pressure	P	P
001	2	7	6	5	4	Parallel Pitch	Yaw, Gimbal	INFA401XB		1	1500	-5 0	-5 -3.5
002	3	1	4	3	2			INFA101XB				-2 0	-2 -3.5
003	4	1	1	3	2			INFA001XB				0 0	0 -3.5
004	5			1	2			INFA201XB				+2 0	+2 -3.5
005	6			1	2			INFA301XB				+5 0	+5 -3.5
006	7	1	5	2,4	3			INFA501XB				-5 +0.7	-5 -2.8
007	8	1	4	2	3			INFA601XB				-5 -0.7	-5 -4.2
008	9	1	2	3	4			INFA701XB				-2 +0.7	-2 -2.8
009	10	2	3	4	5			INFA801XB		Y	Y	-2 -0.7	-2 -4.2
010	11		1,4	3	2		Benign Gimbal (Actuator Null)	INFA901XB		1	1500	0 0	0 0
011	12	1	2,5	3	4			INFAA01XB				+5 0	+5 0
012	13			1,3	2			INFAB01XB				-5 0	-5 0
013	14			1,3	2			INFAE01XB				-5 0	-5 -5
014	15	1,7	2,6	3	4,5			INFAD01XB				+5 0	+5 -5
015	16		5	2,4	3			INFAC01XB		Y	Y	0 0	0 +5
016	17		4	2	3		Flow Blocking Device	4NFAA001XA		4	1500	0 0	0 -3.5
017	19			1	2			4NFA301XA				+5 0	+5 -3.5
018	20	4	1	2	3			4NFA401XA		Y	Y	-5 0	-5 -3.5
019*	21	3	1	2			Roll Gimbal (Smooth)	8NFAD#01XB		8	1500	0 +1	10.77 -2.23
020*	22	4	1	2,3			Roll Gimbal (Smooth) with Nozzle	7NFEG01XB		7		0 -1	-10.77 +2.23



TABLE II. DATA SET/RUN NUMBER COLLATION SUMMARY (Concluded)

Test 0H79			SPACE DIVISION				NORTH AMERICAN ROCKWELL CORPORATION				Prepared By:		Page No. 2 of 2				
			NORTH AMERICAN ROCKWELL CORPORATION								Report No.						
											Checked By:		Model No.				
											Date:						
1	2	3	4	5	6	7	8	9	10	11	12	13		15			
Dataset Identifier	Chamber Entry	Simulated 120K	Test 150K	FIRings ALTitudes 180K 240K		Configuration		**Descriptor		Insire. Pattern	SSME Chamber Pressure	P	Y	Ang	rs		
021	23		2,5	3	4	Clock SSME's 30°		2NFB00XB		2	1500	0	0	-3.5	0	+3.5	
022	24			1,3	2			2NFB30XB				+5	0	-3.5	+5	+3.5	
023	25	1	4	2	3			2NFB40XB				-5	0	-3.5	-5	+3.5	
024	26	2	5	3	4	Clock SSME's 60°		2NFC40XB		2	1500	-5	0	-5	-3.5	-5	+3.5
025	27		4	1,3	2			2NFC00XB				0	0	-3.5	0	+3.5	
026	28			1	2			2NFC30XB				+5	0	-3.5	+5	+3.5	
027	29		1,4	2	3	Heat Shield w/Gaps		6NFA00XB		6	1500	0	0	-3.5	0	+3.5	
028	30	4	1	2	3			6NFA30XB				+5	0	-3.5	+5	+3.5	
029	31			1	2			6NFA40XB				-5	0	-3.5	-5	+3.5	
* Gimbal angles are defined from parallel yaw. All other gimbal angles are defined from actuator null (lower SSME's 3.5° outboard).																	
** X=1 @ 120K																	
X=4 @ 150K																	
X=6 @ 180K																	
X=8 @ 240K																	

TABLE III. MODEL DIMENSIONAL DATA

MODEL COMPONENT: BODY - B60

GENERAL DESCRIPTION: The body is to the Baseline Definition Space Shuttle Vehicle Configuration 5, MCR 200, Rev. 7 dated 10/17/74.

MODEL SCALE: 0.040

DRAWING NUMBER: VC70-000002, MDV-70 Baseline IML

DIMENSIONS:	<u>FULL SCALE</u>	<u>MODEL SCALE</u>
Ref. Length	1290.3	51.612
Length IML	1288.4	51.536
Length OML	1293.3	51.732
OML Max. Width, in.	262.7184	10.508
IML Max. Width, in.	260.7184	10.428
OML Max. Depth, in.	248.575	9.943
IML MAX. Depth, in.	246.575	9.863
OML Fineness Ratio	5.1365	5.1365
IML Fineness Ratio	5.1525	5.1525
Area		
Max. Cross-Sectional, Ft. <sup>2</sup> @ X <sub>0</sub> 1463.316	340.82	0.545

TABLE III. MODEL DIMENSIONAL DATA (Continued)

MODEL COMPONENT: CMS PODS (CML) - M18 Revised 11/11/75

GENERAL DESCRIPTION: Orbiter maneuvering system pod, short pod for orbiter 102/vehicle 5, MCR 1750 R1 baseline.

MODEL SCALE: 0.040

DRAWING NUMBER: VC70-000002A, VL70-008410, MD-V70

DIMENSIONS:	<u>FULL SCALE</u>	<u>MODEL SCALE</u>
Length, in., including RCS package (X <sub>O</sub> 1311 to X <sub>O</sub> 1569.64)	258.64	10.386
Length, in. (X <sub>O</sub> 1311 to X <sub>O</sub> 1511)	200.00	8.000
Max. Width, in. (X <sub>P</sub> 304, X <sub>O</sub> 1511)	135.546	5.421
Max. Depth, in. (X <sub>P</sub> 304, X <sub>O</sub> 1511)	74.36	2.974
Area, ft. <sup>2</sup>		
Max. Cross-Sectional @ X <sub>P</sub> = 304	59.091	2.363

Supersedes M18 values of 11/25/74 Revision

TABLE III. MODEL DIMENSIONAL DATA (Continued)

MODEL COMPONENT: VERTICAL - V<sub>5</sub>  
 GENERAL DESCRIPTION: Centerline vertical tail, doublewedge airfoil with rounded leading edge.

MODEL SCALE: 0.040

DRAWING NUMBER: VL70-000095

DIMENSIONS:	<u>FULL SCALE</u>	<u>MODEL SCALE</u>
TOTAL DATA		
Area (Theo.), ft <sup>2</sup> Planform	413.25	0.66120
Span (Theo.), in.	315.72	12.629
Aspect Ratio	1.675	1.675
Rate of Taper	0.507	0.507
Taper Ratio	0.404	0.404
Sweep Back Angles, degrees		
Leading Edge	45.000	45.000
Trailing Edge	26.249	26.249
0.25 Element Line	41.130	41.130
Chords:		
Root (Theo.) WP	268.50	10.740
Tip (Theo.) WP	108.47	4.339
MAC	199.81	7.992
Fus. Sta. of .25 MAC	1463.50	58.54
W.P. of .25 MAC	635.522	25.421
B.L. of .25 MAC	0.0	0.0
Airfoil Section		
Leading Wedge Angle, deg.	10.00	10.00
Trailing Wedge Angle, deg.	14.920	14.920
Leading Edge Radius	2.00	0.080
Void Area	13.17	0.0211
Blanketed Area	12.67	0.0203

TABLE III. MODEL DIMENSIONAL DATA (Continued)

MODEL COMPONENT: BODY FLAP (OUTER MOLD LINES) F<sub>14</sub>

GENERAL DESCRIPTION: Orbiter body flap vehicle 5 configuration MCR 200  
Rev. 7 "OML" to be used with B<sub>63</sub> HL X<sub>0</sub> 1532.0 Y<sub>0</sub> = 128.0

MODEL SCALE: 0.040

DRAWING NUMBER: VC70-000002, MDV-70

DIMENSIONS:	<u>FULL SCALE</u>	<u>MODEL SCALE</u>
Total Area, Ft <sup>2</sup>	134.125	5.365
Span (equivalent), In.	238.444	9.538
Inb'd equivalent chord, In.	81.00	3.240
Outb'd equivalent chord, In.	81.00	3.240
Ratio movable surface chord/ total surface chord		
At Inb'd equiv. chord		
At Outb'd equiv. chord		
Sweep Back Angles, degrees		
Leading Edge	0.0	0.0
Trailing Edge	0.0	0.0
Hingeline	0.0	0.0
Area Moment (MAC X Total area, Ft. <sup>3</sup> )	905.343	0.0579
Mean Aerodynamic Chord, In.	81.0	3.240

TABLE III. MODEL DIMENSIONAL DATA (Continued)

MODEL COMPONENT: MPS NOZZLES - N<sub>93</sub>

GENERAL DESCRIPTION: The main propulsion nozzles are laval-bell shaped and are located on the aft planes of the orbiter.

MODEL SCALE: 0.040

DRAWING NUMBER: VC70-000002; VC70-08144; RS009107; 13M15000

DIMENSIONS:	<u>FULL SCALE</u>	<u>MODEL SCALE</u>
MACH NO.		
Length, in.		
Gimbal Point to Exit Plane	157.00	6.280
Throat to Exit Plane	121.00	4.840
Diameter, in.		
Exit (ID)	90.414	3.616
Throat	10.3054	0.412
Area, in. <sup>2</sup>		
Exit (ID)	6420.384	10.272
Throat	83.405	0.133
Gimbal Point (Station), in.		
Upper Nozzle		
X	1445.000	57.800
Y	0.00	0.00
Z	443.000	17.720
Lower Nozzle		
X	1468.170	58.727
Y	± 53.00	± 2.120
Z	342.640	13.706
Null Position, Degrees		
Upper Nozzle		
Pitch	16.0	16.0
Yaw	0.0	0.0
Lower Nozzle		
Pitch	10.0	10.0
Yaw	3.5	3.5

TABLE III. MODEL DIMENSIONAL DATA (Continued)

MODEL COMPONENT: MPS NOZZLES - N<sub>26</sub>

GENERAL DESCRIPTION: MPS nozzle, configuration 2A.

MODEL SCALE: 0.040

DRAWING NUMBER: VL70-000089B

DIMENSIONS:	<u>FULL SCALE</u>	<u>MODEL SCALE</u>
MACH NO.		
Diameter, in.		
Exit	92.0	3.68
Area, ft. <sup>2</sup>		
Max Cross-sectional	46.16396	0.7386
Gimbal Point (Station), in.		
Upper Nozzle, in. F.S.		
X	1445.00	57.80
Y	0	0
Z	443.	17.72
Lower Nozzle		
X	1468.17	58.727
Y	± 53.	± 2.12
Z	543.36	21.734
Null Position, Degrees		
Upper Nozzle		
Pitch (Pitch ± 11°, Yaw ± 9°)	16.	0
Lower Nozzle		
Pitch (Pitch ± 11°, Yaw ± 9°)	10.	3.5 outb'd

TABLE III. MODEL DIMENSIONAL DATA (Continued)

MODEL COMPONENT: NOZZLES - N8

GENERAL DESCRIPTION: Basic OMS nozzle of configuration 2A per Rockwell Lines VL70-008306 and VL70-000089B. Intersection of nozzle exit plane and nozzle centerline at  $X_0 = 1570.75$ ,  $Y_0 = + 99.25$ ,  $Z_0 = 507.25$ .

MODEL SCALE: 0.040

DRAWING NUMBER: VL70-008306, 000089B, SS-A00092

DIMENSIONS:	<u>FULL SCALE</u>	<u>MODEL SCALE</u>
MACH NO.		
Diameter, in.		
Exit	50.0	2.0
Throat	N/A	N/A
Inlet	28.00	0.720
Area, ft. <sup>2</sup>		
Exit	13.635	0.545
Gimbal Point (Station), in.		
Nozzle		
X	1518.0	60.720
Y	± 88.0	± 3.52
Z	492.0	19.68
Null Position, Degrees		
Nozzle		
Pitch	15°49'	15°49'
Yaw	± 12°17'	± 12°17'



TABLE III. MODEL DIMENSIONAL DATA (Concluded)

MODEL COMPONENT: NOZZLES - N<sub>90</sub>

GENERAL DESCRIPTION: OMS nozzle for MCR 500 configuration.

MODEL SCALE: 0.040

DRAWING NUMBER: Fig. 4. APS Interface to OMS Engine and Interconnect

DIMENSIONS:	<u>FULL SCALE</u>	<u>MODEL SCALE</u>
MACH NO.		
Length, in.		
Gimbal Point to Exit Plane	56.0	2.240
Throat to Exit Plane	56.0	2.240
Diameter, in.		
Exit (ID)	43.088	1.7235
Throat (ID)	5.812	0.23248
Gimbal Point (Station), in.		
Nozzle		
X	1518.	60.72
Y	88.	3.520
Z	492.	19.680
Null Position, Degrees		
Nozzle		
Pitch	15°49'	15°49'
Yaw	6°30'	6°30'

TABLE IV. MODEL 65-0 INSTRUMENTATION AND PATTERN SUMMARY

a. Base Heat Shield

PARAMETER	TYPE	INSTRUMENTATION PATTERNS					
		1	2	4	6	7	8
HT0100	Thin-Film Gauge	X		X		X	X
HT0101		X	X	X		X	X
HT0102		X		X		X	X
HT0103		X	X	X		X	X
HT0104		X		X		X	X
HT0105		X	X	X		X	X
HT0106		X					
HT0108		X		X		X	X
HT0109		X		X		X	X
HT0110		X	X	X		X	X
HT0111		X	X	X		X	X
HT0112		X	X	X		X	X
HT0113		X		X		X	X
HT0115		X					
HT0116		X		X		X	X
HT0121		X					
HT0124		X		X		X	X
HT0125		X	X	X		X	X
HT0131		X	X	X		X	X

TABLE IV. MODEL 65-0 INSTRUMENTATION AND PATTERN SUMMARY (Continued)

a. Base Heat Shield (Continued)

PARAMETER	TYPE	INSTRUMENTATION PATTERNS					
		1	2	4	6	7	8
HTO132	Thin-Film Gauge	X	X	X		X	X
HTO133		X	X	X		X	X
HTO134		X		X		X	X
HTO135		X	X	X		X	X
HTO137		X		X		X	X
HTO138		X					
HTO139		X		X		X	X
HTO193		X		X		X	X
HTO405		X	X	X		X	X
HTO406		X	X	X		X	X
HTO431		X	X	X		X	X
HTO432		X	X	X		X	X
HTO434		X	X	X		X	X
HTO435		X	X	X		X	X
BPO002	Low Pressure	X	X	X		X	X
BPO003		X	X	X		X	X
BPO004		X	X	X		X	X
BPO005		X	X	X		X	X
BPO006		X	X	X		X	X



TABLE IV. MODEL 65-0 INSTRUMENTATION AND PATTERN SUMMARY (Continued)

b. SSME Engine Mounted Heat Shields

PARAMETER	TYPE	INSTRUMENTATION PATTERNS					
		1	2	4	6	7	8
<u>Engine #1</u>							
HTO107	Thin-Film Gauge	X	X	X		X	X
HTO130	↓	X	X	X		X	X
HTO407	↓	X	X	X		X	X
HTO430	↓	X	X	X		X	X
BPO012	Low Pressure	X	X	X	X	X	X
<u>Engine #2</u>							
BPO016	Low Pressure	X	X	X	X	X	X
<u>Engine #3</u>							
HTO117	Thin Film Gauge	X	X	X		X	X
HTO126	↓	X	X	X		X	X
HTO136	↓	X	X	X		X	X
HTO140	↓	X	X	X		X	X
HTO436	↓	X	X	X		X	X

TABLE IV. MODEL 65-0 INSTRUMENTATION AND PATTERN SUMMARY (Continued)

c. Center Base Heat Shield Flow Diverter

PARAMETER	TYPE		INSTRUMENTATION PATTERNS					
			1	2	4	6	7	8
HTO400	Thin-Film Gauge				X			
HTO403	X	X			X			
HTO404	X	X			X			
HTO410	X	X			X			
		X						
X	X	X						
X	X	X						
X	X	X						
X	X	X						
X	X	X						
X	X	X						
X	X	X						
X	X	X						
X	X	X						
X	X	X						

TABLE IV. MODEL 65-0 INSTRUMENTATION AND PATTERN SUMMARY (Continued)

d. SSME Drain Line Nozzle (Hatband)

PARAMETER	TYPE	INSTRUMENTATION PATTERNS					
		1	2	4	6	7	8
HT4200	Thin-Film Gauge	X	X	X		X	
HT4201		X	X	X		X	
HT4202		X	X	X		X	
HT4203		X	X	X		X	
HT4205		X					
HT4206		X	X	X		X	
HT4207		X	X	X		X	
HT4208		X	X	X		X	
HT4209		X	X	X		X	
HT4210		X	X	X		X	
HT4211		X	X	X		X	
HT4220		X	X	X		X	
HT4221		X	X	X		X	
HT4231		X	X	X		X	
HT4282		X	X	X		X	

TABLE IV. MODEL 65-0 INSTRUMENTATION AND PATTERN SUMMARY (Continued)

e. SSME Firing Nozzle No. 1 (Hatband)

PARAMETER	TYPE	INSTRUMENTATION PATTERNS					
		1	2	4	6	7	8
HT1201	Thin-Film Gauge		X				
HT1202		X	X	X		X	X
HT1203		X	X	X		X	X
HT1204		X	X	X		X	X
HT1206		X	X	X		X	X
HT1208			X				
HT1210		X	X	X		X	X
HT1211		X					
HT1212		X	X	X		X	X
HT1213			X				
HT1221		X	X	X		X	X
HT1222		X	X	X		X	X
HT1223			X				
HT1251			X				
HT1252		X	X	X		X	X
HT1253		X	X	X		X	X
HT1271			X				
HT1272		X	X	X		X	X
HT1273		X	X	X		X	X
HT1281			X				
HT1282		X	X	X		X	X
HT1283		X	X	X		X	X



TABLE IV. MODEL 65-0 INSTRUMENTATION AND PATTERN SUMMARY (Continued)

f. SSME Firing Nozzle No. 3 (Hatband)

PARAMETER	TYPE	INSTRUMENTATION PATTERNS					
		1	2	4	6	7	8
HT3201	Thin-Film Gauge	X	X	X			X
HT3202		X					
HT3203		X	X	X			X
HT3204		X	X	X			X
HT3205		X					
HT3206		X	X	X			X
HT3208		X	X	X			X
HT3210		X	X	X			X
HT3211		X	X	X			X
HT3212		X	X	X			X
HT3213			X				
HT3221		X	X	X			X
HT3222		X	X	X			X
HT3223			X				
HT3251			X				
HT3252		X	X	X			X
HT3253		X	X	X			X
HT3271			X				
HT3272		X	X	X			X
HT3273		X	X	X			X
HT3281			X				
HT3282		X	X	X			X
HT3283		X	X	X			X

TABLE IV. MODEL 65-0 INSTRUMENTATION AND PATTERN SUMMARY (Continued)

g. SSME Smooth Wall Nozzle

PARAMETER	TYPE	INSTRUMENTATION PATTERNS					
		1	2	4	6	7	8
HTO200	Thin-Film Gauge					X	X
HTO201	↓					X	X
HTO202	↓					X	X
HTO204	↓					X	X
HTO205	↓					X	X
HTO206	↓					X	X
HTO207	↓					X	X
HTO208	↓					X	X
HTO209	↓					X	X
HTO210	↓					X	X
HTO211	↓					X	X

TABLE IV. MODEL 65-0 INSTRUMENTATION AND PATTERN SUMMARY (Continued)

h. Body Flap

PARAMETER	TYPE	INSTRUMENTATION PATTERNS					
		1	2	4	6	7	8
HTO164	Thin-Film Gauge	X	X	X		X	X
HTO168	↓	X	X	X		X	X
HTO170	↓	X	X	X		X	X
HTO174	↓	X					
BPO047	Low Pressure	X	X	X		X	X
BPO055	↓	X	X	X		X	X

TABLE IV. MODEL 65-0 INSTRUMENTATION AND PATTERN SUMMARY (Continued)

i. Left OMS/RCS Pod

PARAMETER	TYPE	INSTRUMENTATION PATTERNS					
		1	2	4	6	7	8
HTO146	Thin-Film Gauge	X					
HTO150	↓	X					
HTO151	↓	X	X	X		X	X
HTO152	↓	X	X	X		X	X
HTO160	↓	X	X	X		X	X

TABLE IV. MODEL 65-0 INSTRUMENTATION AND PATTERN SUMMARY (Continued)

j. Right CMS/RCS Pod

PARAMETER	TYPE	INSTRUMENTATION PATTERNS					
		1	2	4	6	7	8
BPO038	Low Pressure	X	X	X		X	X
BPO043	↓	X	X	X		X	X
BPO046	↓	X	X	X		X	X



TABLE IV. MODEL 65-0 INSTRUMENTATION AND PATTERN SUMMARY (Continued)

1. Tile Gap Base Heat Shield

PARAMETER	TYPE	INSTRUMENTATION PATTERNS					
		1	2	4	6	7	8
HT5011	Thin-Gilm Gauge				X		
HT5012					X		
HT5013					X		
HT5021					X		
HT5022					X		
HT5023					X		
HT5031					X		
HT5032					X		
HT5033					X		
HT5041					X		
HT5042					X		
HT5043					X		
HT5051					X		
HT5052					X		
HT5053					X		
HT5061					X		
HT5062					X		
HT5063					X		
HT5071					X		
HT5072					X		

TABLE IV. MODEL 65-0 INSTRUMENTATION AND PATTERN SUMMARY (Continued)

1. Tile Gap Base Heat Shield (Continued)

PARAMETER	TYPE	INSTRUMENTATION PATTERNS					
		1	2	4	6	7	8
HT5073	Thin-Film Gauge				X		
HT5081					X		
HT5082					X		
HT5091					X		
HT5101					X		
HT5111					X		
HT5112					X		
HT5121					X		
HT5122					X		
HT5131					X		
HT5132					X		
HT5141					X		
HT5142					X		
HT5151					X		
HT5152					X		
HT5161					X		
HT5162					X		
HT5171					X		
HT5172					X		
HT5181					X		



TABLE IV. MODEL 65-0 INSTRUMENTATION AND PATTERN SUMMARY (Continued)

1. Tile Gap Base Heat Shield (Continued)

PARAMETER	TYPE	INSTRUMENTATION PATTERNS					
		1	2	4	6	7	8
HT5182	Thin-Film Gauge				X		
HT5211					X		
HT5212					X		
HT5213					X		
HT5221					X		
HT5222					X		
HT5223					X		
HT5231					X		
HT5232					X		
HT5233					X		
HT5241					X		
HT5242					X		
HT5243					X		
HT5251					X		
HT5252					X		
HT5253					X		
HT5261					X		
HT5262					X		
HT5263					X		

TABLE IV. MODEL 65-0 INSTRUMENTATION AND PATTERN SUMMARY (Continued)

1. Tile Gap Base Heat Shield (Concluded)

PARAMETER	TYPE	INSTRUMENTATION PATTERNS					
		1	2	4	6	7	8
HT5271	Thin-Film Gauge				X		
HT5272					X		
HT5273					X		
HT5281					X		
HT5282					X		
HT5291					X		
HT5292					X		
HT5301					X		
HT5302					X		
HT5311					X		
HT5312					X		
HT5321					X		
HT5322					X		
HT5323					X		
HT5331					X		
HT5332					X		
HT5333					X		
HT5341					X		
HT5342					X		
HT5351					X		
HT5352					X		



TABLE V. TEST SETUP SHEETS

OH-79 ENTRY CONFIGURATION

DESCRIPTOR									ENTRY:
1	N	F	A	6	0	1	1,4,6,8	B	08
NOTES:									
	120K	1	VIDAR gain pattern						
	150K	4	LF						
	180K	6							
	240K	8							

PART NUMBERS						
	ENG	NOZZLE P/N	FIRING	GIMPAL BLOCK P/N	ALPHA	BETA
S S M E	1	SS-H-01529	YES	SS-H-00507-7	-5	-0.7
	2	"	"	"	-5	-4.2
	3	"	"	"	-5	+2.8
O T H E R	Nozzle orientation: No change.					

ADDITIONAL INSTRUCTIONS:

INITIATOR: W. F. Braddock      DATE: 7/26/78

TABLE V. TEST SETUP SHEETS (Concluded)

OH-79 TEST RUN CONDITIONS

OBJECTIVE: PARALLEL YAW, PITCH GIMBAL	ENTRY: 08
--	--------------

RUN NUMBER		08-1	08-3	08-2	08-4	
DESCRIPTOR		1NFA6011B	1NFA6018B	1NFA6016B	1NFA6014B	
P R E S S U R E S	GO <sub>2</sub> (PSI)	BEFORE	2770	2780	2770	2780
		AFTER	2655	2680	2665	2680
	GH <sub>2</sub> (PSI)	BEFORE	2625	2625	2625	2625
		AFTER	2565	2565	2565	2565
	GN <sub>2</sub> (PSI)	OPEN	2510	2510	2510	2510
		CLOSE	2980	2980	2980	2980
		HOLD	1310	1310	1310	1310
	COMBUSTOR (PSI)		1500	1500	1500	1500
A L T (TORR)	SIMULATED (KFT)		120	240	180	150
	PCH (TORR)	REQ'D	1.83	1.27 x 10 <sup>-2</sup>	1.73 x 10 <sup>-1</sup>	5.44 x 10 <sup>-1</sup>
		ACTUAL	1.84	1.38 x 10 <sup>-2</sup>	1.725 x 10 <sup>-1</sup>	5.47 x 10 <sup>-1</sup>
T I M E	CLOCK		09:49:24	11:59:48	10:59	12:39:50
	IRIG-B		207 days 9:49:25:355	207 days 11:59:21:824	207 days 10:59:28:596	207 days 12:39:56:244
BASE TEMPS (°F)		76.0 76.1	77.2 81.2 81.3	85.6 79.4 79.5	81.1 84.6 84.7	88.0

REMARKS:	T <sub>1</sub> = 1.0
	T <sub>2</sub> = 3.5
	T <sub>3</sub> = 1.8
	T <sub>S</sub> = 2.1

INITIATOR: P. L. Lemoine	DATE: 7/26/78
--------------------------	---------------

TABLE VI. TEST DESCRIPTOR DEFINITION

FIRST CHARACTER: Instrumentation Configuration

- 1 = Basic cold base
- 2 = Basic cold base with nozzle clocking
- 4 = Basic cold base with flow block device
- 6 = Tile gap heat shield and body flap
- 7 = Smooth wall nozzle #2, #3 hatband in #1 position
- 8 = Smooth wall nozzle #2, drainline in #1 position

SECOND CHARACTER: Body Flap Configuration

- N = Body flap undeflected ( $\delta_{BF} = 0^\circ$ )

THIRD CHARACTER: SSME Chamber Pressure

- F = 1500 psi

FOURTH CHARACTER: SSME Operating Pattern

- A = All operating, SSME hatband nozzles @  $\phi = 0^\circ$
- B = All operating, SSME hatband nozzles @  $\phi = 30^\circ$
- C = All operating, SSME hatband nozzles @  $\phi = 60^\circ$
- D = All operating, #1 ( $\phi = 240^\circ$ ), #2 ( $\phi = 120^\circ$ ), #3 ( $\phi = 60^\circ$ )
- E = All operating, #1 ( $\phi = 270^\circ$ ), #2 ( $\phi = 150^\circ$ ), #3 ( $\phi = 90^\circ$ )

FIFTH CHARACTER: SSME Gimbal Pattern

- 0 = Pitch null, parallel burn
- 1 =  $-2^\circ$  pitch, parallel burn
- 2 =  $+2^\circ$  pitch, parallel burn
- 3 =  $+5^\circ$  pitch, parallel burn
- 4 =  $-5^\circ$  pitch, parallel burn

TABLE VI. TEST DESCRIPTOR DEFINITION (Continued)

FIFTH CHARACTER: SSME Gimbal Pattern (Continued)

- 5 = (-5, +0.7), (-5, -2.8), (-5, +4.2)
- 6 = (-5, -0.7), (-5, -4.2), (-5, +2.8)
- 7 = (-2, +0.7), (-2, -2.8), (-2, +4.2)
- 8 = (-2, -0.7), (-2, -4.2), (-2, +2.8)
- 9 = (0, 0), (0, 0), (0, 0) benign gimbal (actuator null)
- A = (+5, 0), (+5, 0), (+5, 0) benign gimbal
- B = (-5, 0), (-5, 0), (-5, 0) benign gimbal
- C = (0, 0), (0, +5), (0, -5) benign gimbal (increased yaw)
- D = (+5, 0), (+5, +5), (+5, -5) benign gimbal (precant)
- E = (-5, 0), (-5, +5), (-5, -5) benign gimbal (precant)
- F = (0, +1), (+10.77, -2.23), (-10.77, -2.23) + roll gimbal
- G = (0, -1), (-10.77, +2.23), (+10.77, +2.23) - roll gimbal

It is again noted that F and G gimbal angles are measured from the parallel yaw position; all others are from actuator null (lower SSME's at 3.5° outboard yaw).

SIXTH CHARACTER: OMS Engine Chamber Pressure

- 0 = Zero psi (off)

SEVENTH CHARACTER: OMS Gimbal Angles

- 1 = Stowed (non-firing) position (+6°, ±7°)

TABLE VI. TEST DESCRIPTOR DEFINITION (Concluded)

EIGHTH CHARACTER: Simulated Pressure Altitude

- 1 = 120K feet
- 4 = 150K feet
- 6 = 180K feet
- 8 = 240K feet

NINTH CHARACTER: Flow Diverter

- A = Instrumented
- B = Off



TABLE VII. INSTRUMENTATION PATTERNS

PATTERN NO.	CHAMBER ENTRIES USED	DESCRIPTION	VIDAR DATA ACQUISITION CHANNELS				IRIG TIME
			TFG	LOW-RANGE PCB	HIGH-RANGE PCB	EVENT SIGNALS	
1	2 - 16	Parallel Yaw and Benign Gimbal Configurations	90 Or 91	20	5	7	4
2	23 - 28	SSME Nozzle Clocking Configurations	90	20	5	7	4
4	17, 19, 20	Flow Diverter Configurations	94	20	5	7	4
6	29 - 31	Tile Gap Base Heat Shield and Body Flap Configuration	88	2	5	7	4
7	22	Roll Gimbal Configuration	86	20	5	7	4
8	21	Roll Gimbal Configuration	88	20	5	7	4

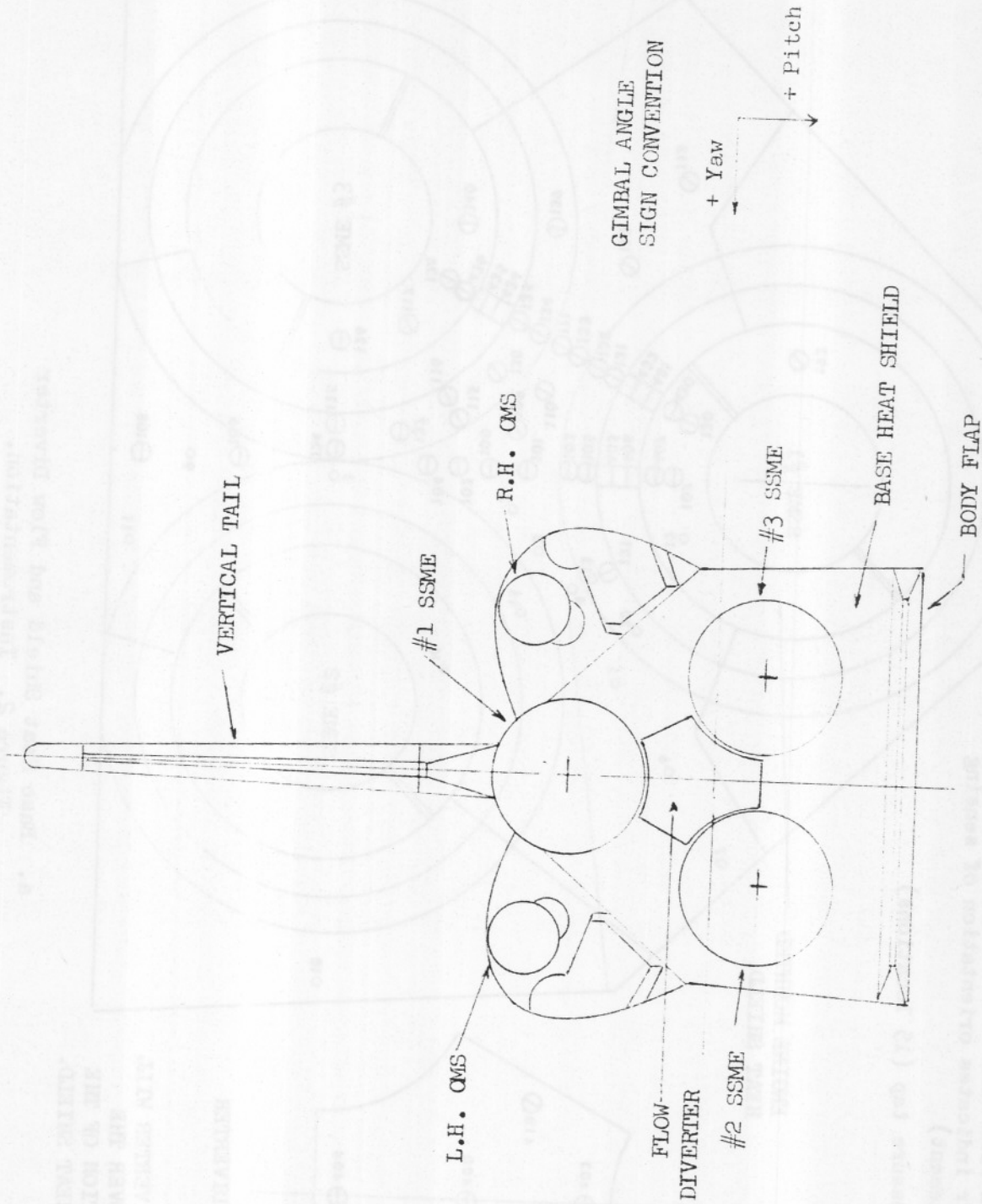
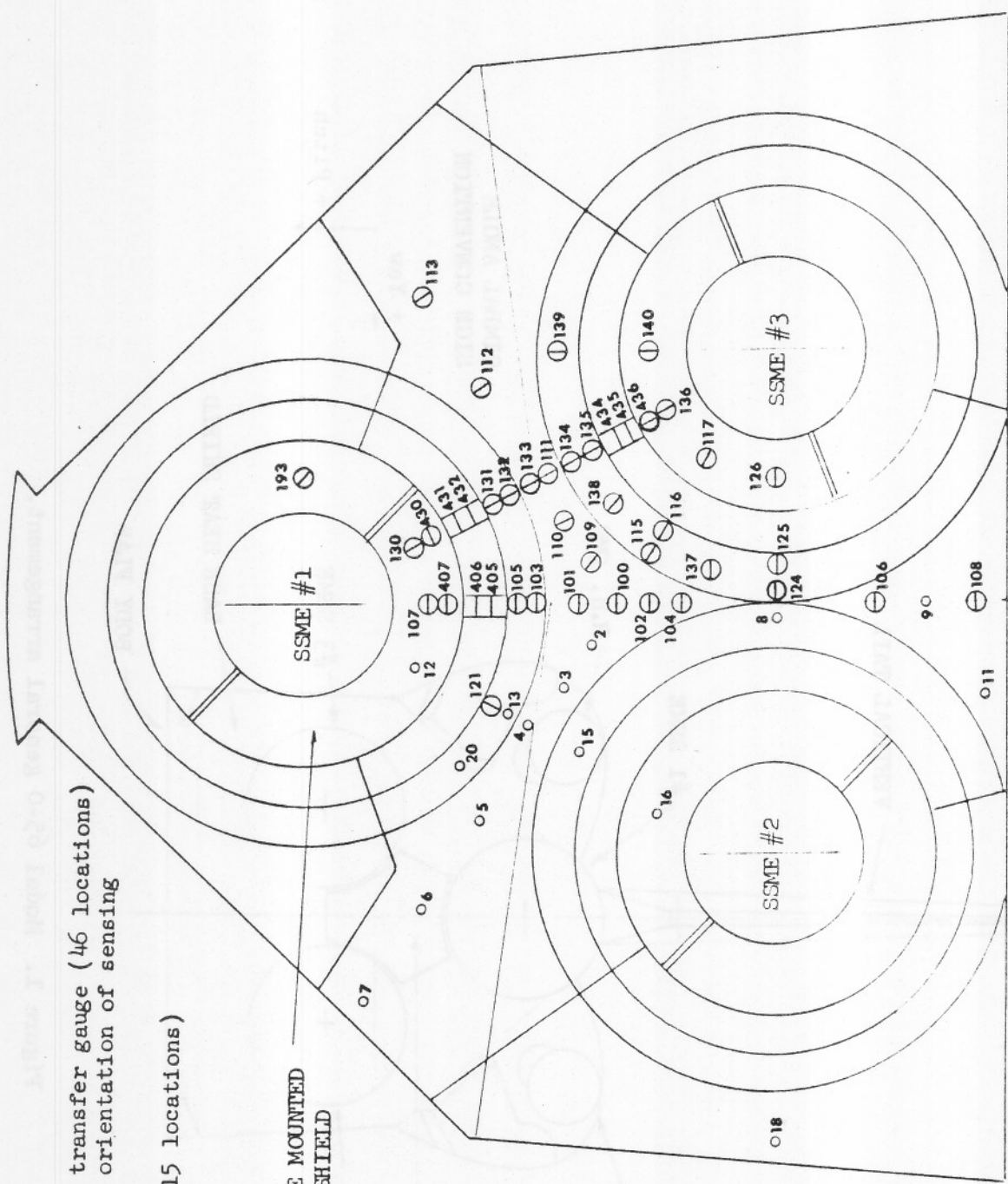


Figure 1. Model 65-0 general arrangement.



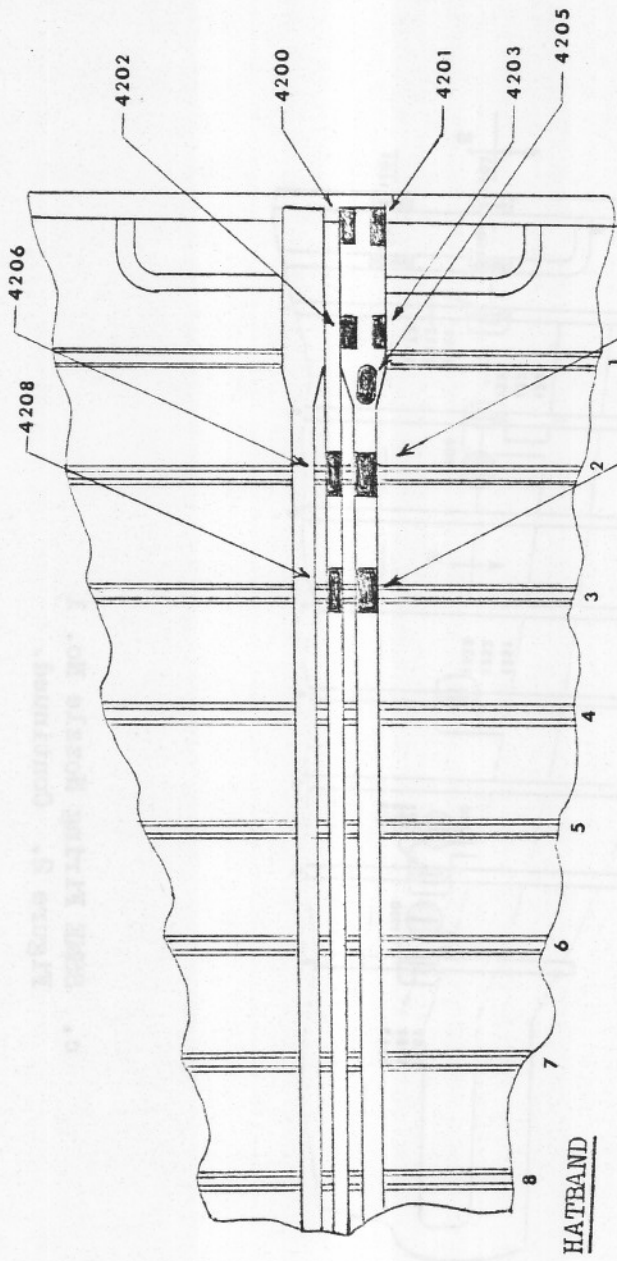
Thin-film heat transfer gauge (46 locations)  
 ○ IXX - (bar indicates orientation of sensing element)  
 ○ - Pressure tap (15 locations)

ENGINE MOUNTED  
 HEAT SHIELD

FLOW DIVERTER

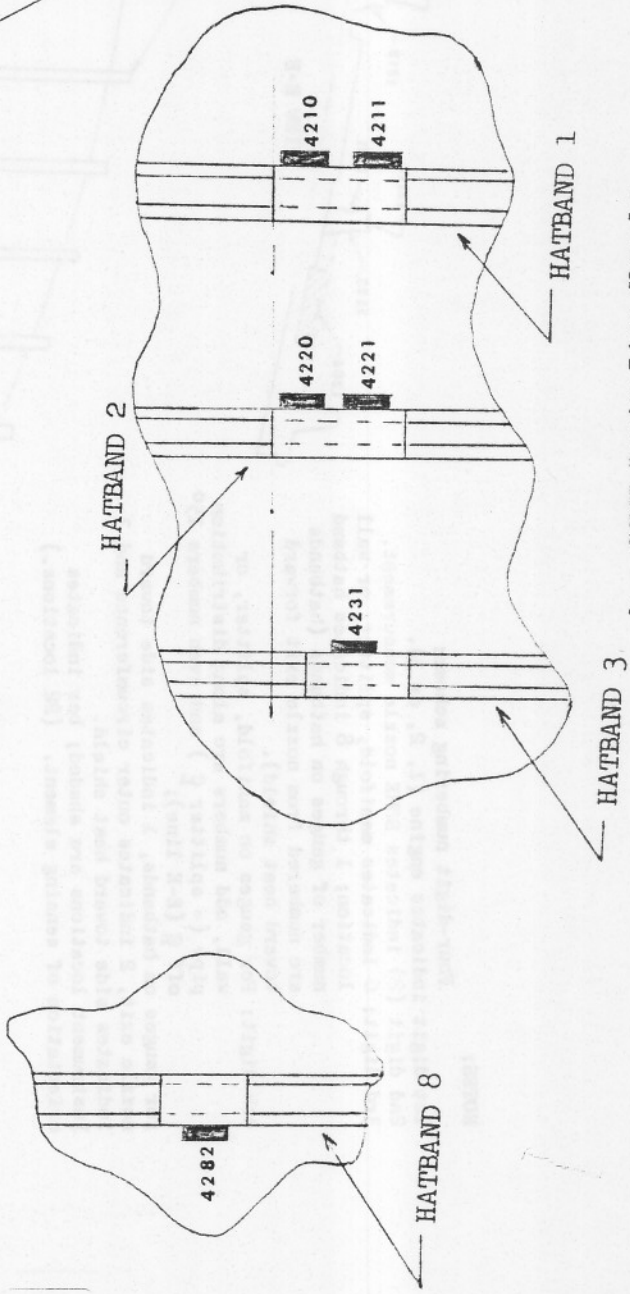
NOTE:  
 THE FLOW DIVERTER WILL  
 BE PLACED OVER THE  
 CENTER SECTION OF THE  
 COLD BASE HEAT SHIELD.

a. Base Heat Shield and Flow Diverter  
 Figure 2. Instrumentation.



HATBAND

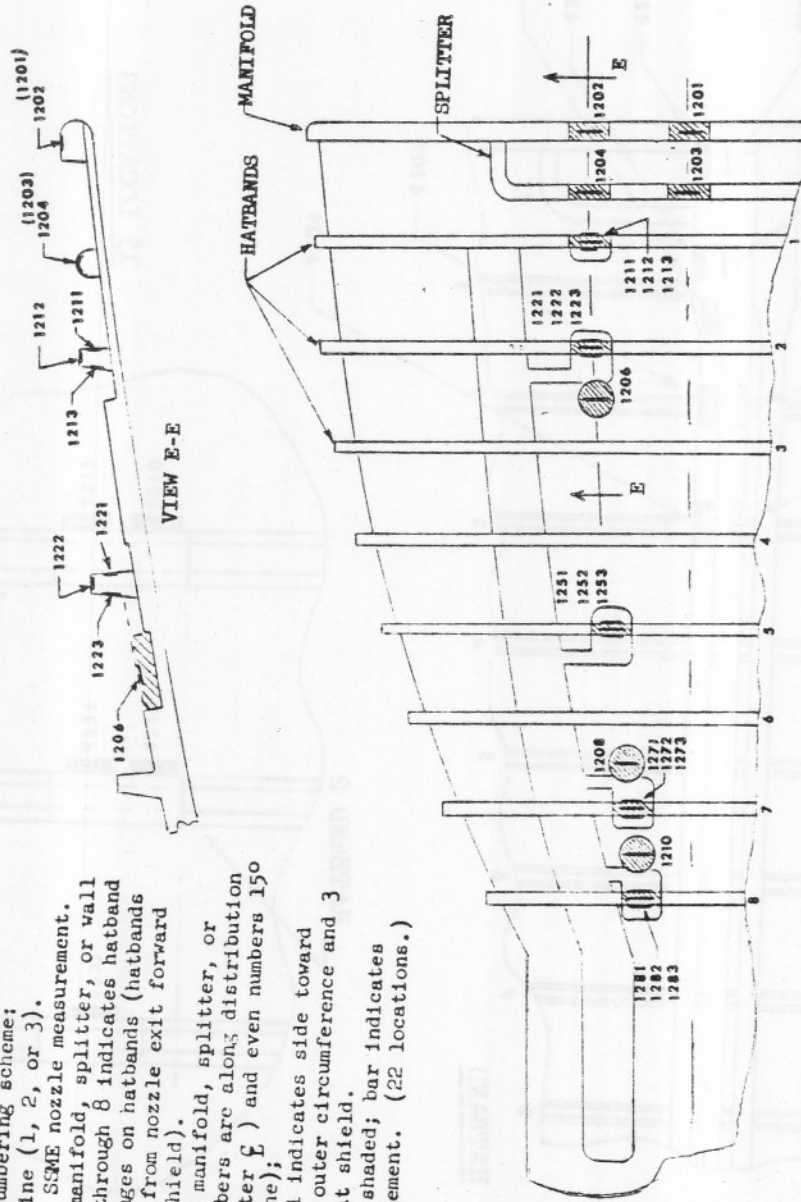
15 LOCATIONS



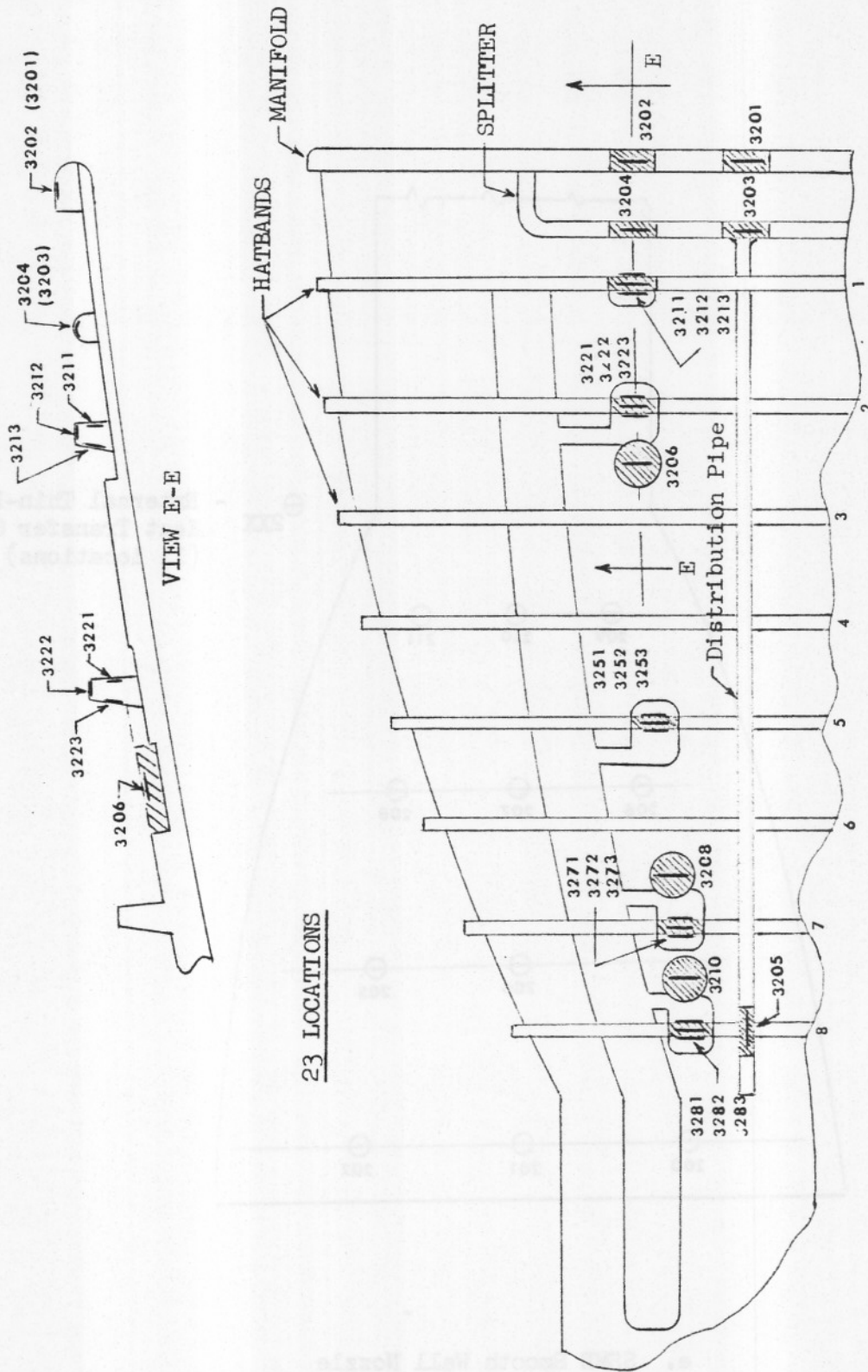
b. SSME Drain Line Nozzle  
Figure 2. Continued.

NOTES:

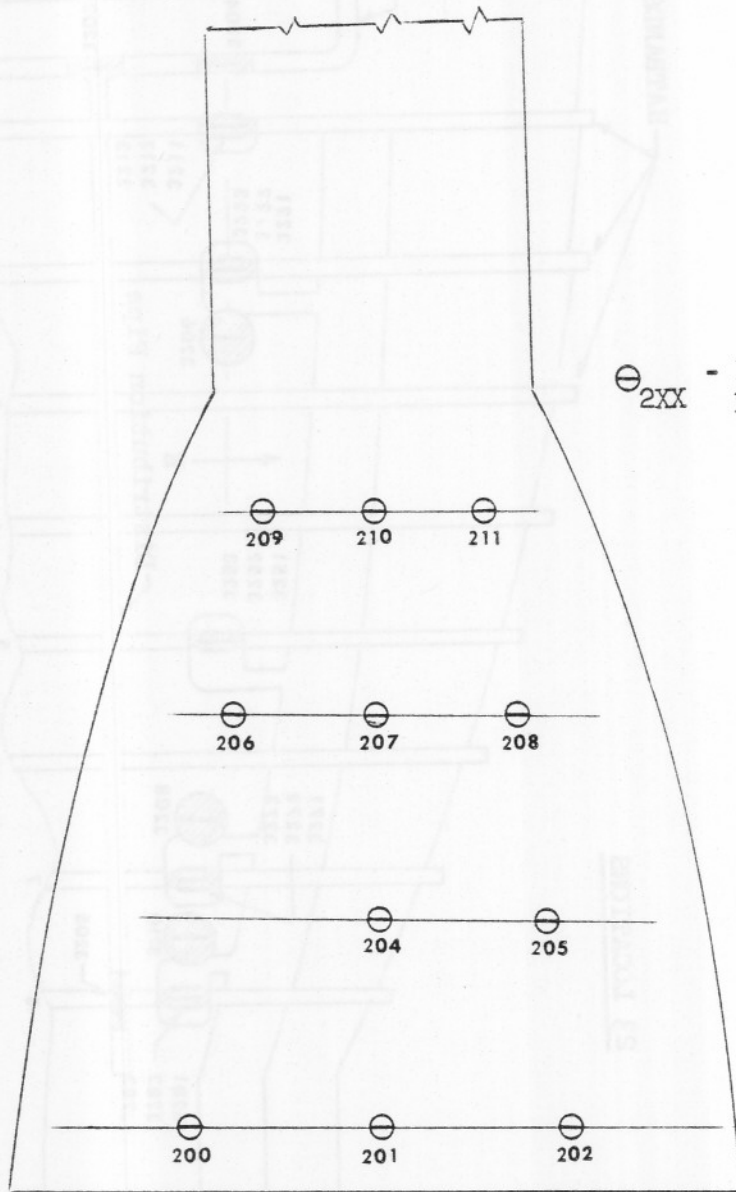
Four-digit numbering scheme:  
 1st digit indicates engine (1, 2, or 3).  
 2nd digit (2) indicates SSME nozzle measurement.  
 3rd digit: 0 indicates manifold, splitter, or wall location; 1 through 8 indicates hatband number of gauges on hatbands (hatbands are numbered from nozzle exit forward toward heat shield).  
 4th digit: For gauges on manifold, splitter, or wall, odd numbers are along distribution pipe (= splitter E) and even numbers 150 off E (E-E line);  
 for gauges on hatbands, 1 indicates side toward nozzle exit, 2 indicates outer circumference and 3 indicates side toward heat shield.  
 Instrument locations are shaded; bar indicates orientation of sensing element. (22 locations.)



c. SSME Firing Nozzle No. 1  
 Figure 2. Continued.



d. SSME Firing Nozzle No. 3  
Figure 2. Continued.

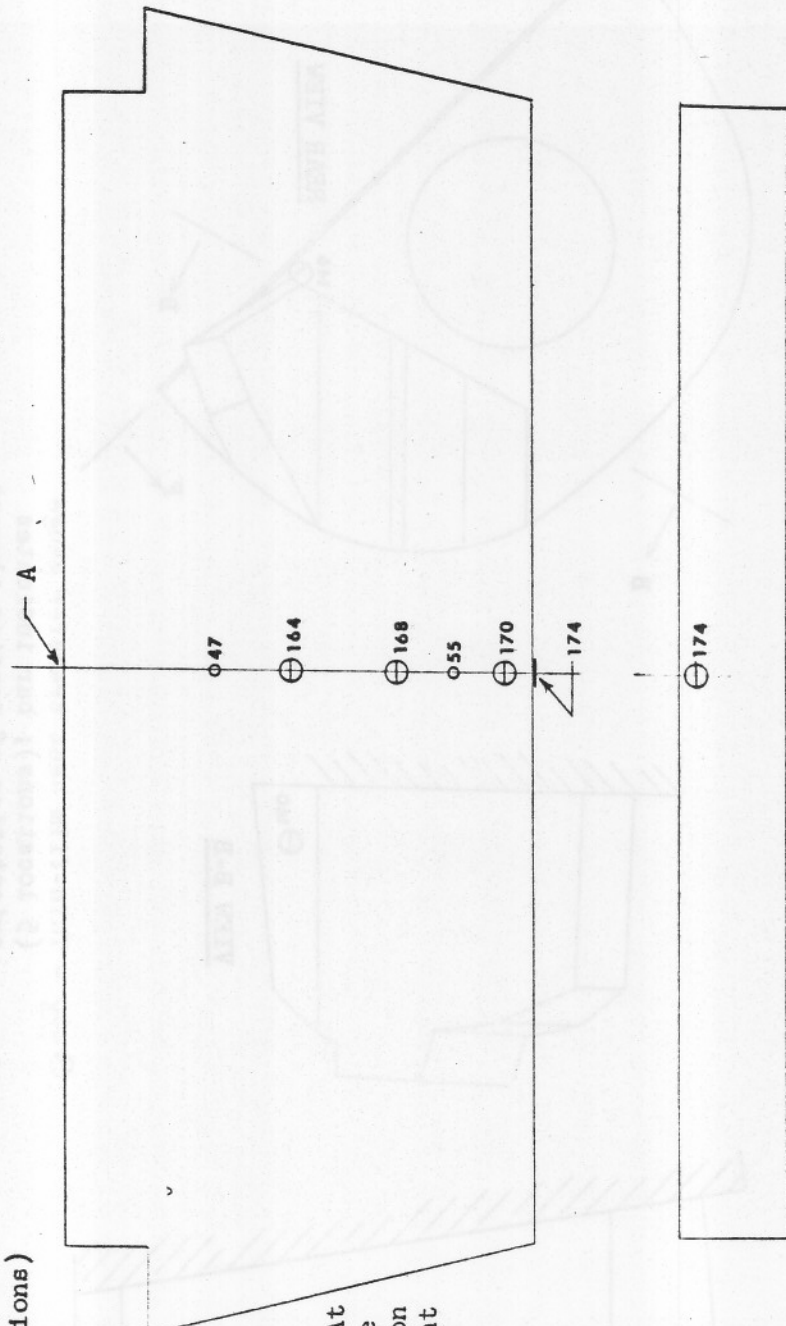


⊖<sub>2XX</sub> - External Thin-Film Heat Transfer Gauge (11 locations)

e. SSME Smooth Wall Nozzle  
Figure 2. Continued.

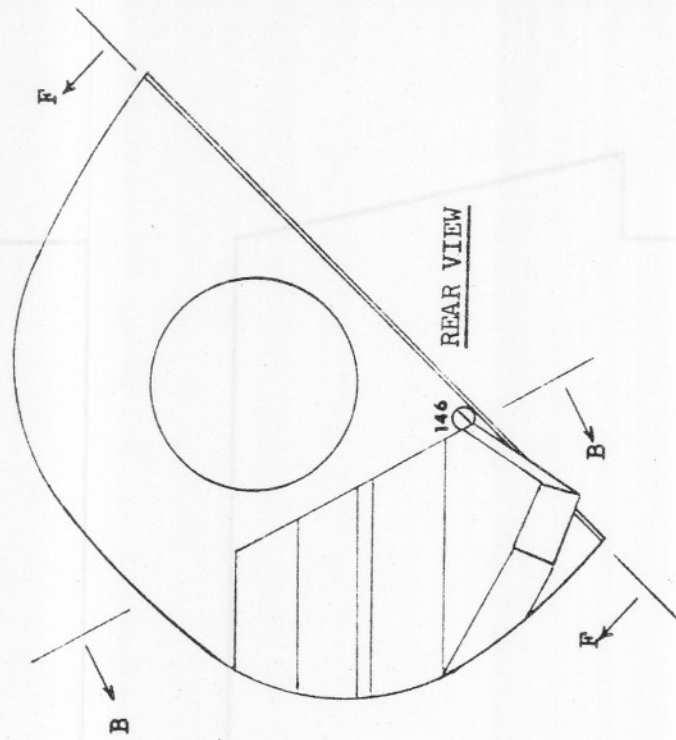
o XX - Pressure tap (2 locations)

⊖ IXX - Thin-film heat transfer gauge (4 locations); bar indicates orientation of sensing element: At right angles to a line from the gauge location to point "A" (mid-point of body flap leading edge).



f. Body Flap  
Figure 2. Continued.





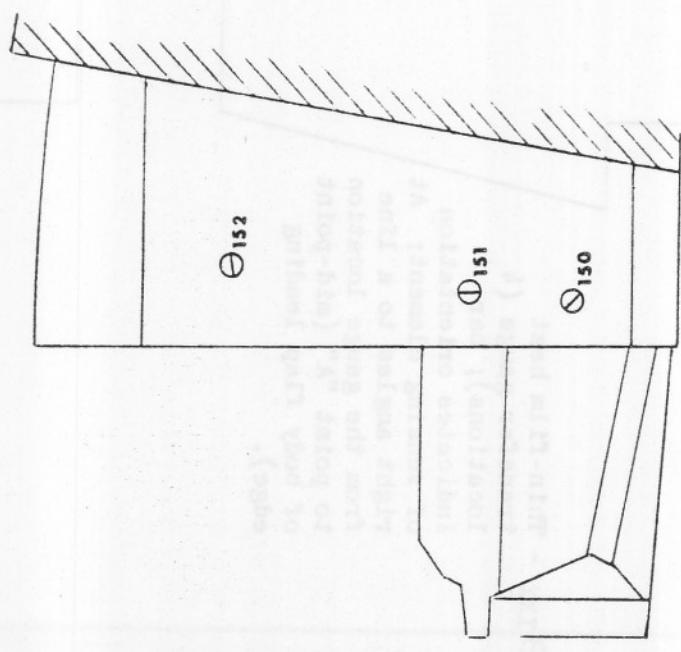
REAR VIEW

146

B

B

F



VIEW F-F

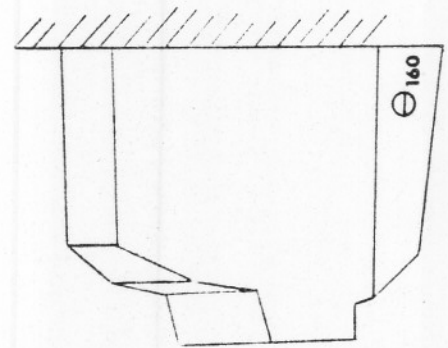
152

151

150

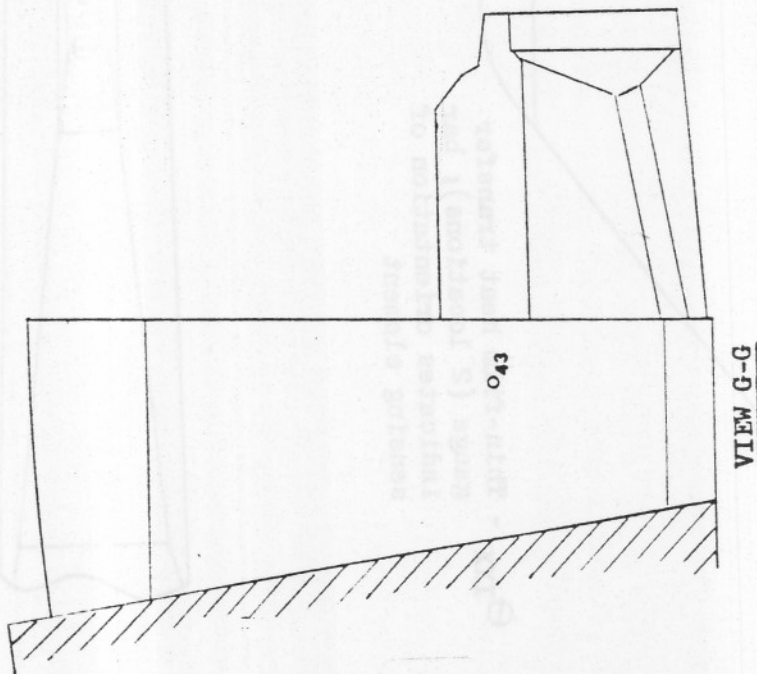
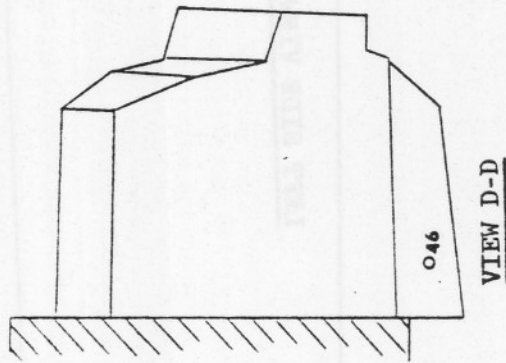
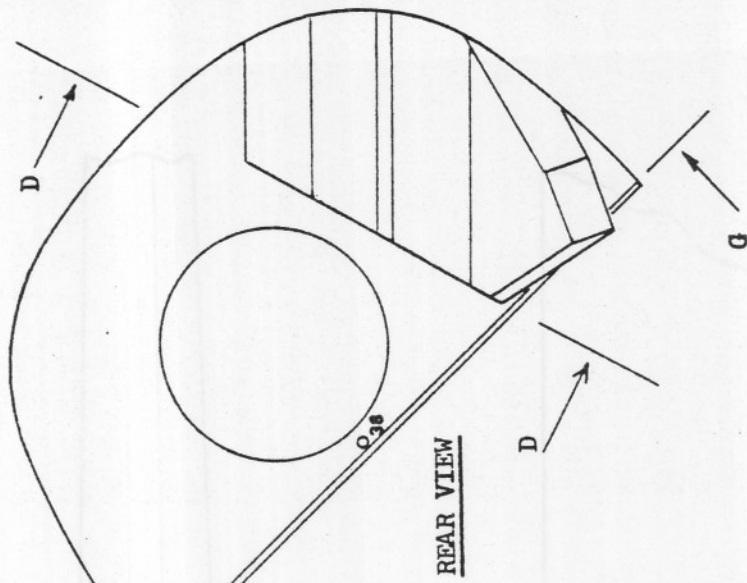
160

VIEW B-B



⊙ IX - Thin-film heat transfer gauge  
(5 locations); bar indicates  
orientation of sensing element

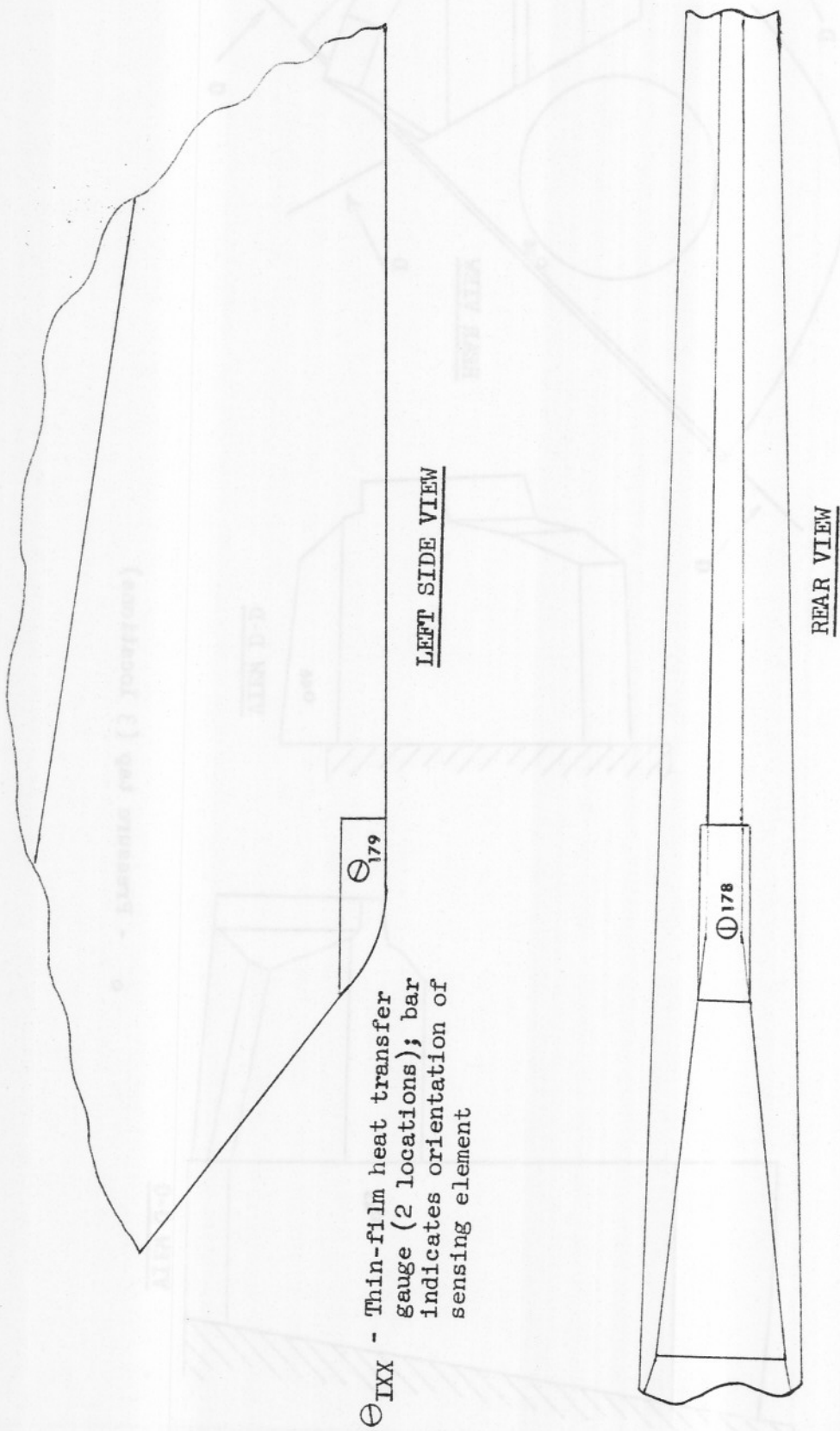
g. Left QMS/RCS Pod  
Figure 2. Continued.



o - Pressure tap (3 locations)

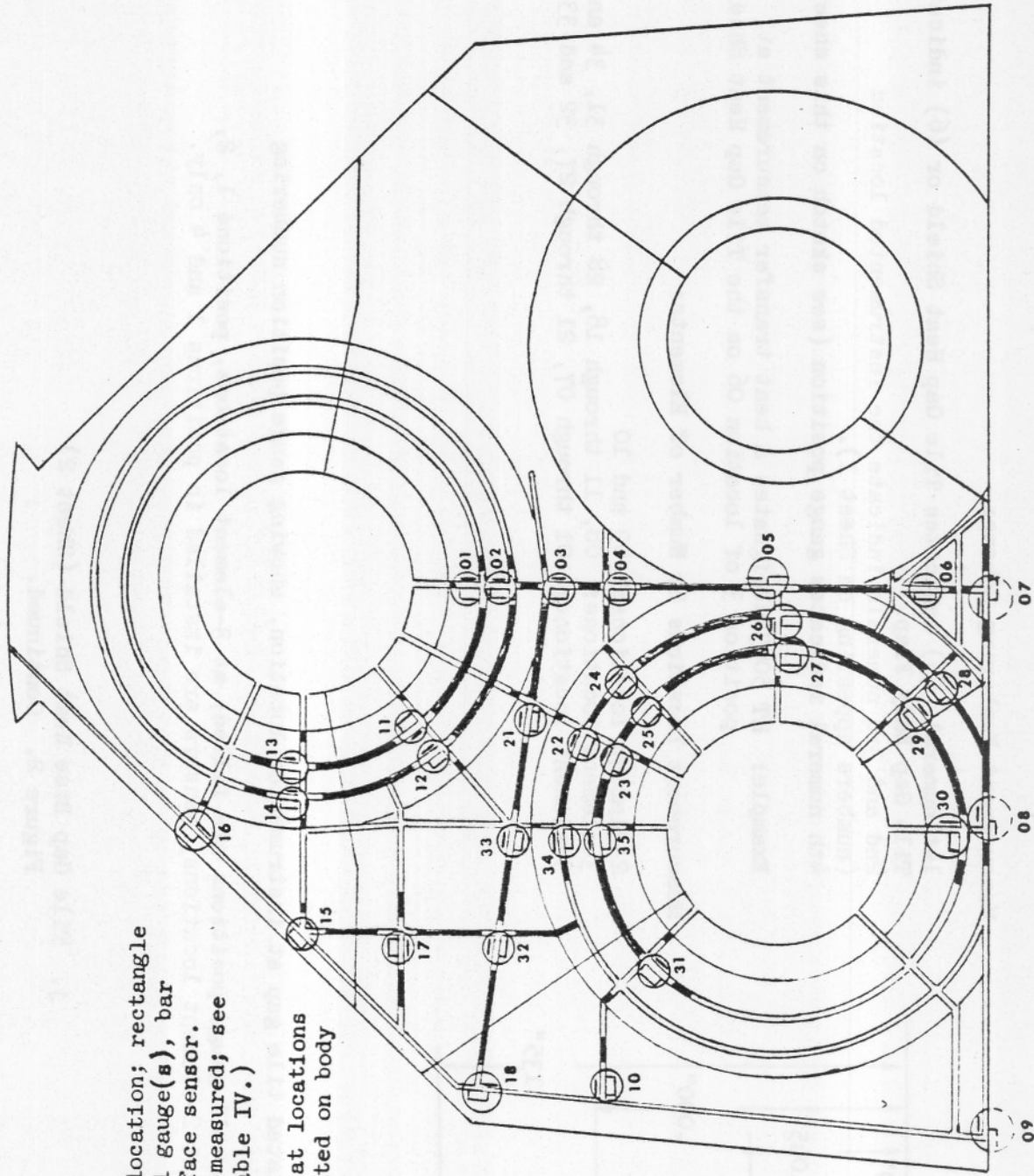
h. Right OMS/RCS Pod  
Figure 2. Continued.

Figure 5. CONTINUED  
P. 1104 (10/10/50 504)



① IXX - Thin-film heat transfer gauge (2 locations); bar indicates orientation of sensing element

i. Vertical Tail  
Figure 2. Continued.



XX - Instrumented location; rectangle indicates wall gauge(s), bar indicates surface sensor. (80 locations measured; see Sheet 2 and Table IV.)

Note that wall gauges at locations 07, 08 and 09 are mounted on body flap.

J. Tile Gap Base Heat Shield (Sheet 1)  
 Figure 2. Continued.

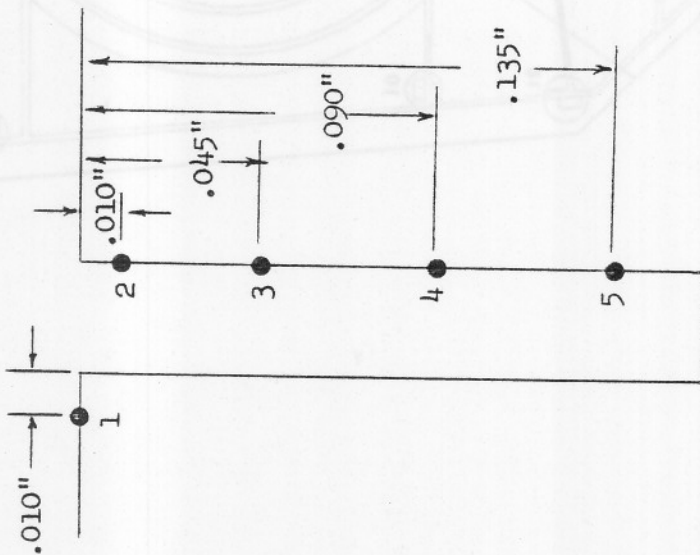
Measurement Numbering Scheme:

- 1st numeral (5) indicates Tile Gap Heat Shield or (6) indicates Tile Gap Body Flap.
- 2nd and 3rd numerals indicate the instrumented location (numbers appearing on Sheet 1).
- 4th numeral indicates gauge position (see sketch on this sheet)

Example: HT 5063 designates a heat transfer measurement at position 3 of location 06 on the Tile Gap Heat Shield

Measurement Locations by Number of Elements:

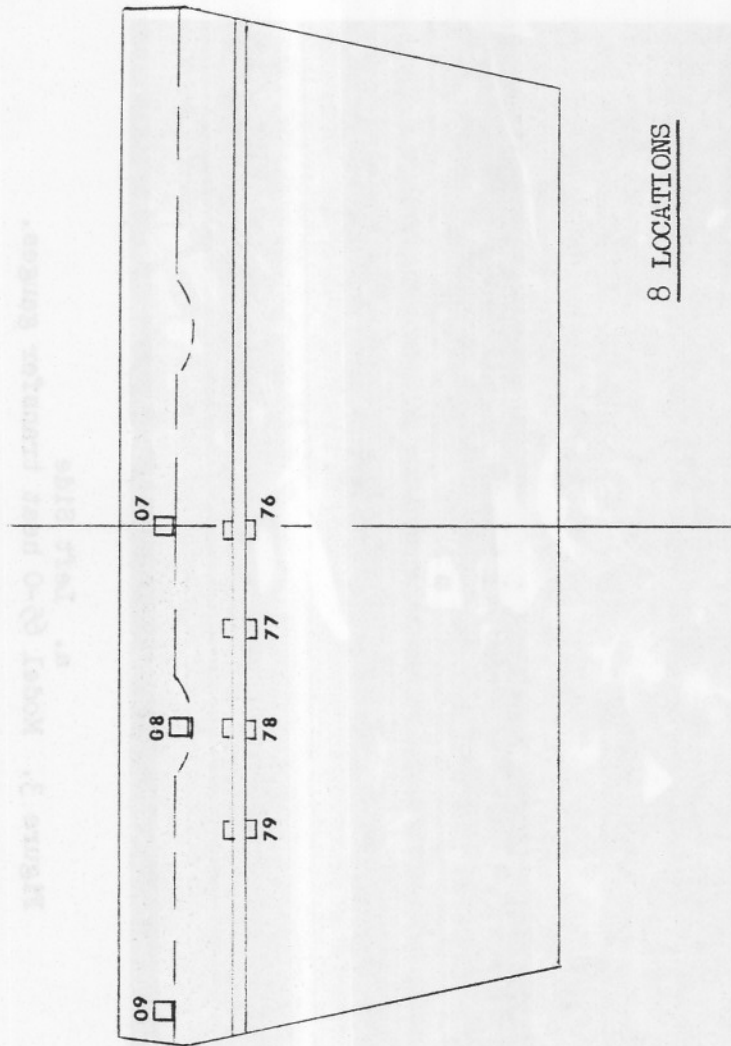
- 2-element locations: 09 and 10
- 3-element locations: 08, 11 through 18, 28 through 31, 34 and 35
- 5-element locations: 01 through 07, 21 through 27, 32 and 33



Cross-section of simulated tile gap at instrumented location, showing gauge position numbering

At 5-element locations, all gauge positions are filled; at 3-element locations, positions 1, 2, and 4 are filled; and at 2-element locations, sensors are installed in positions 1 and 4 only.

J. Tile Gap Base Heat Shield (Sheet 2)  
Figure 2. Continued.



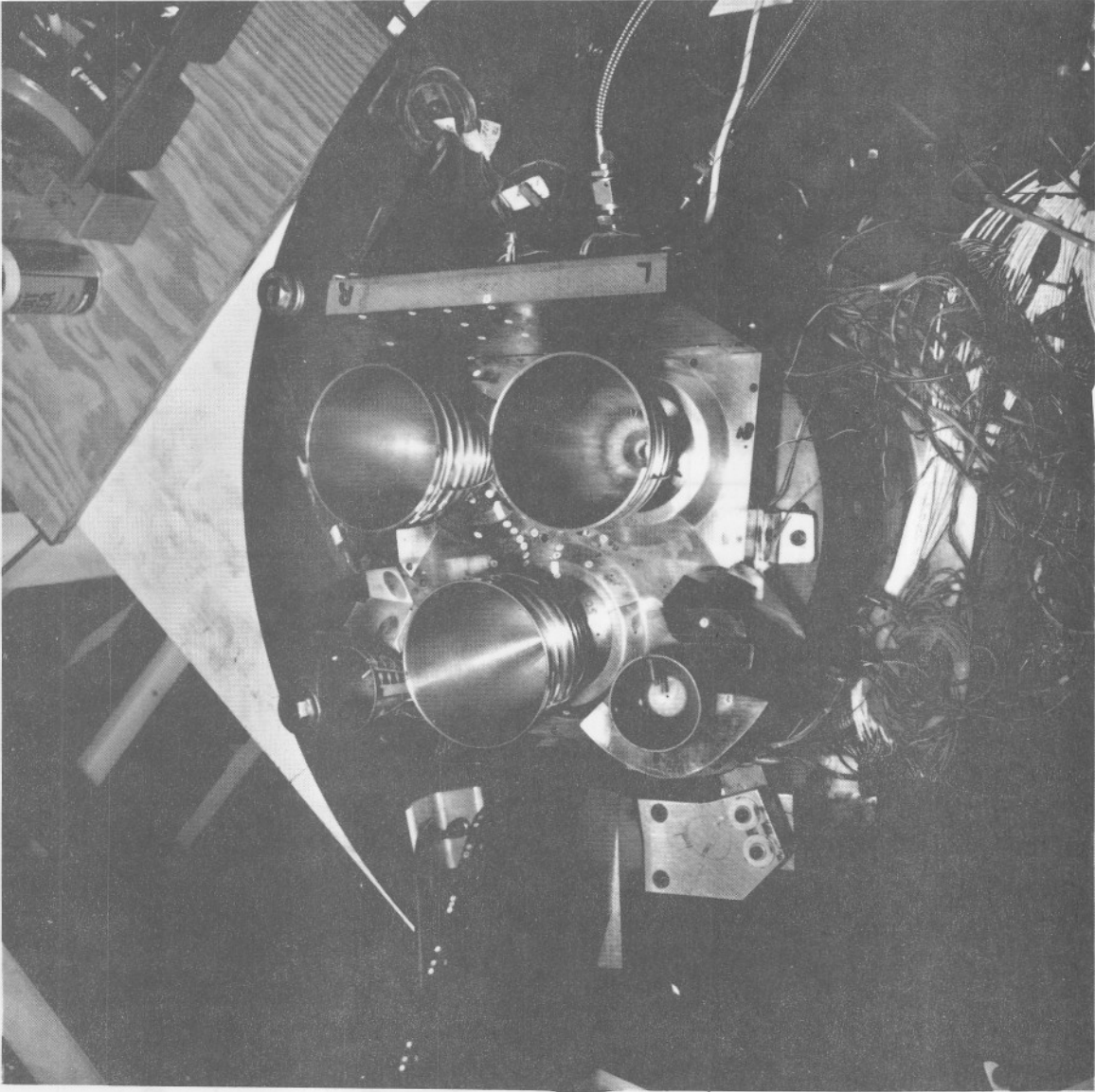
8 LOCATIONS

Notes: (1) Wall gauges for base heat shield locations 07, 08 and 09 are shown on Sheet 1 of Figure 2j.

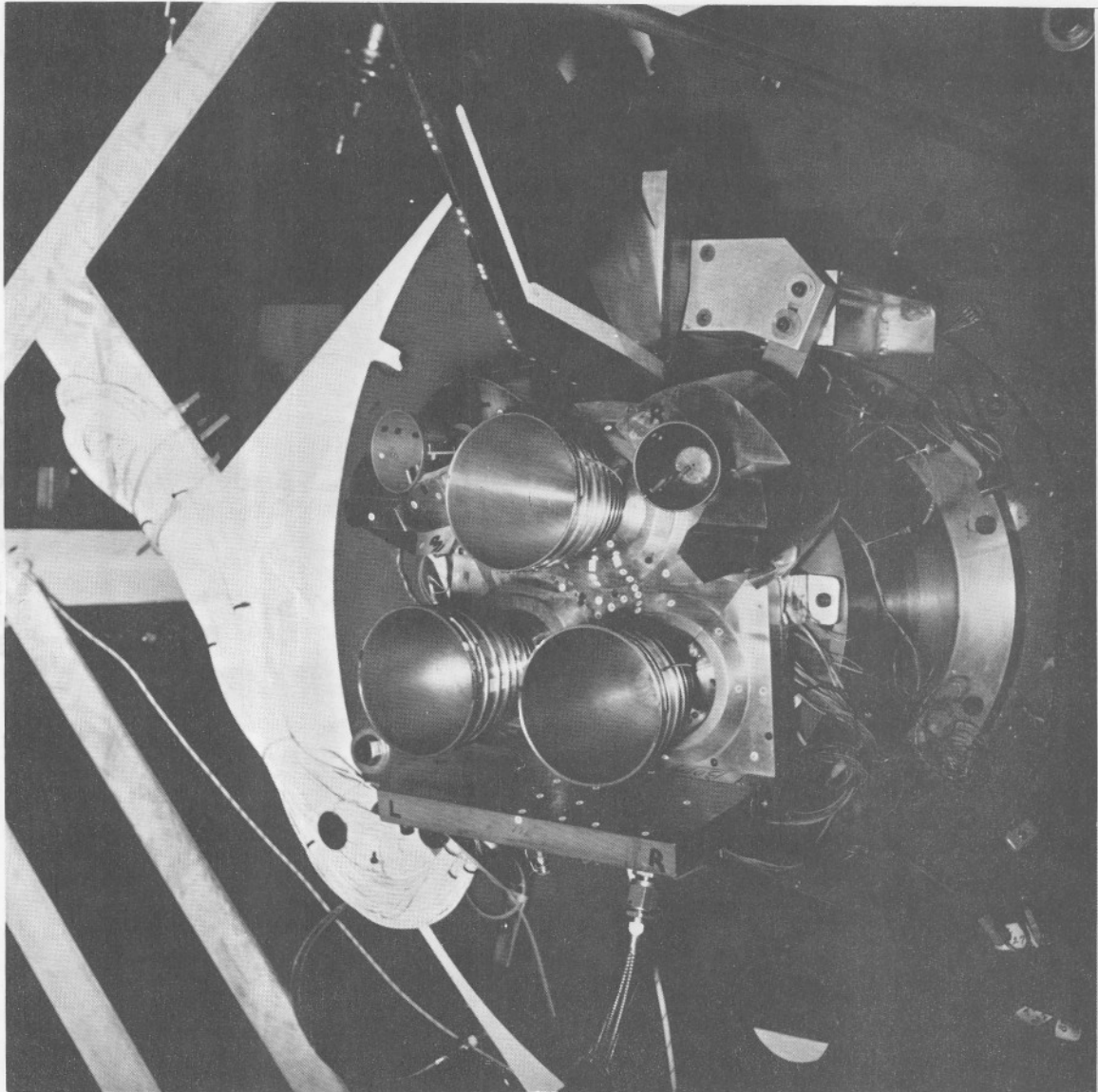
<u>Gauge Locations</u>	<u>No. of Sensors</u>
76	5
77	3
78	3
79	2

(3) For sensor placement at each gauge location see Sheet 2 of Figure 2j.

k. Tile Gap Body Flap  
Figure 2. Concluded.

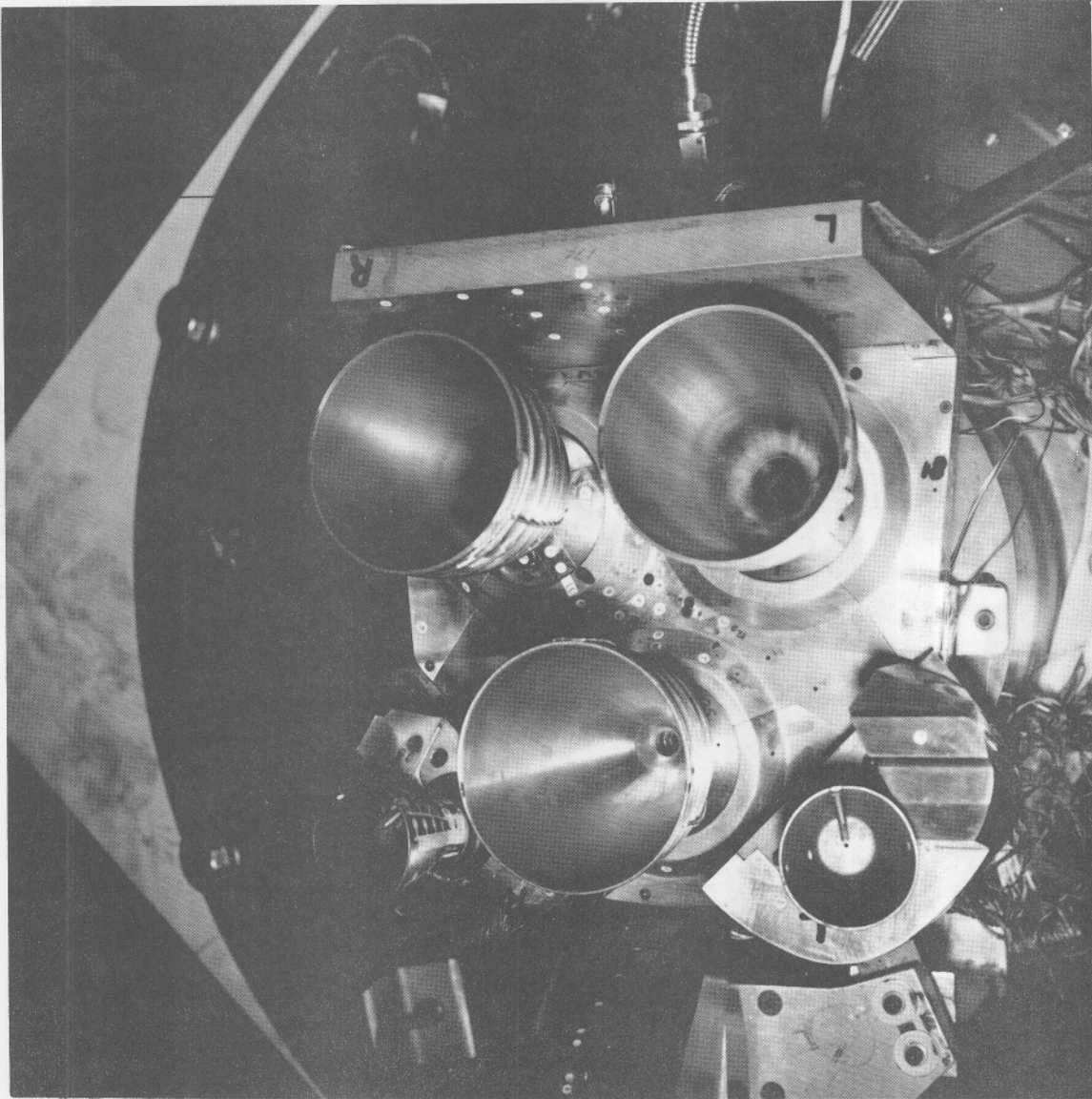


a. Left Side  
Figure 3. Model 65-0 heat transfer gauges.

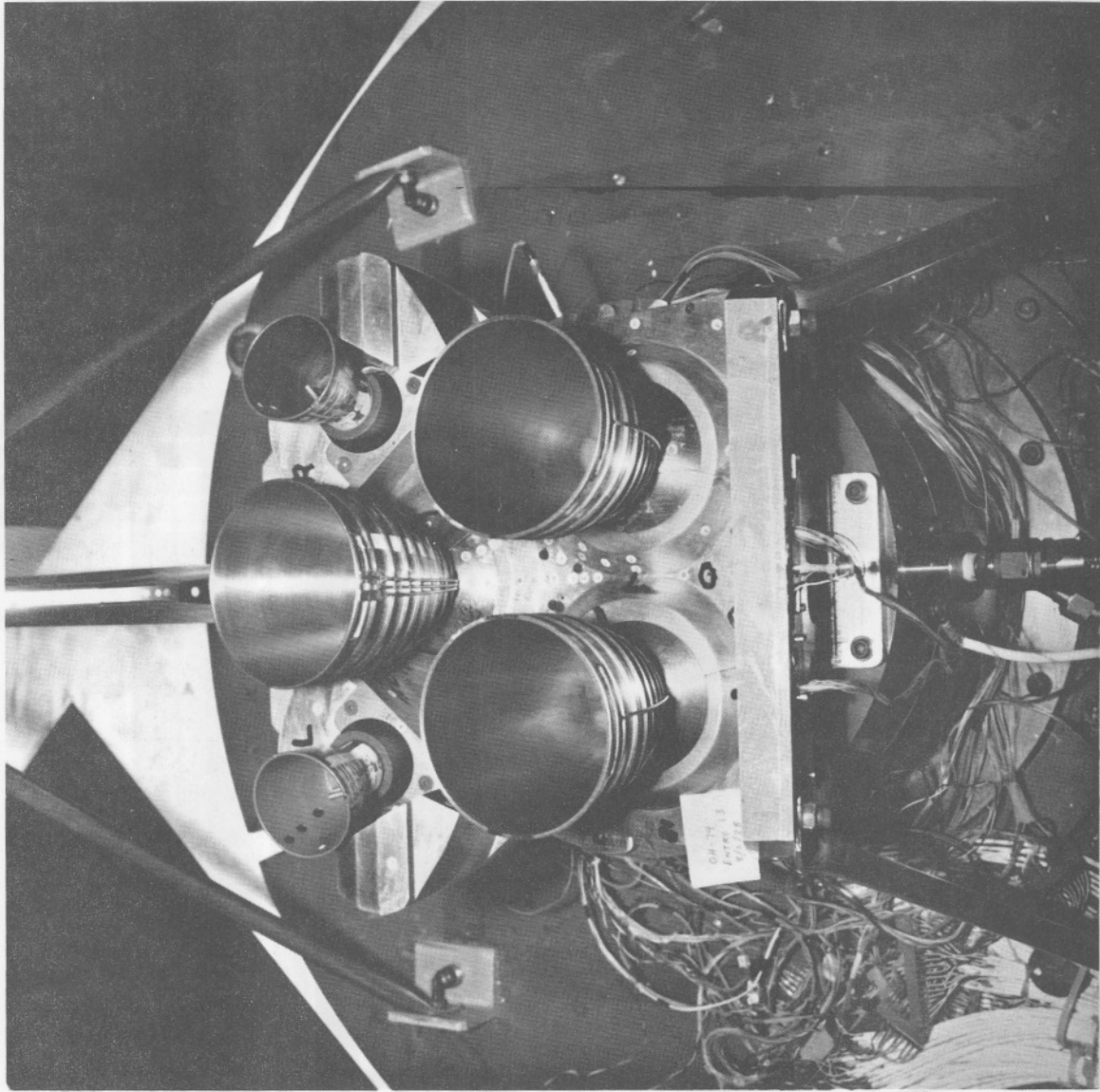


b. Right Side  
Figure 3. Continued.

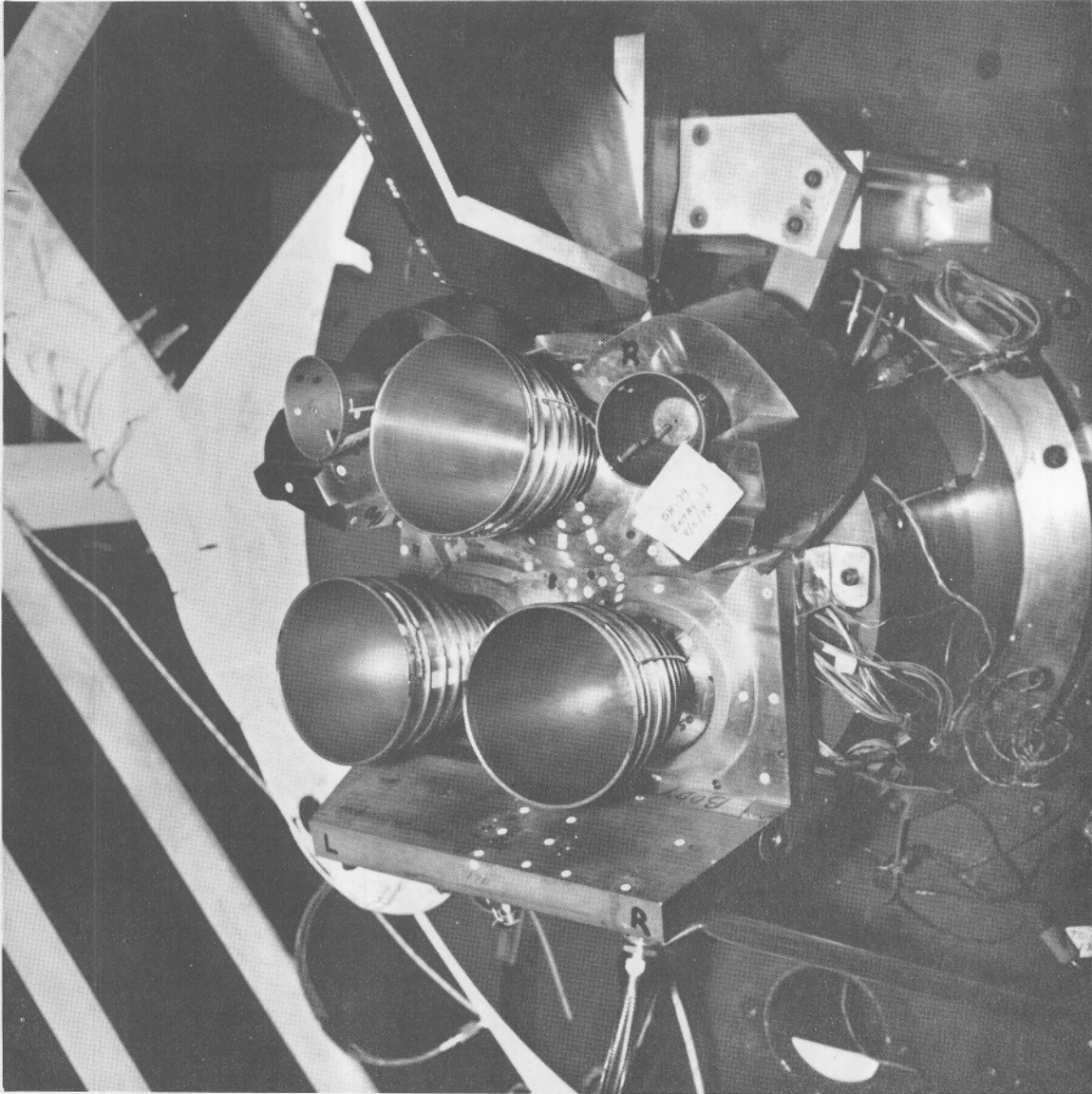




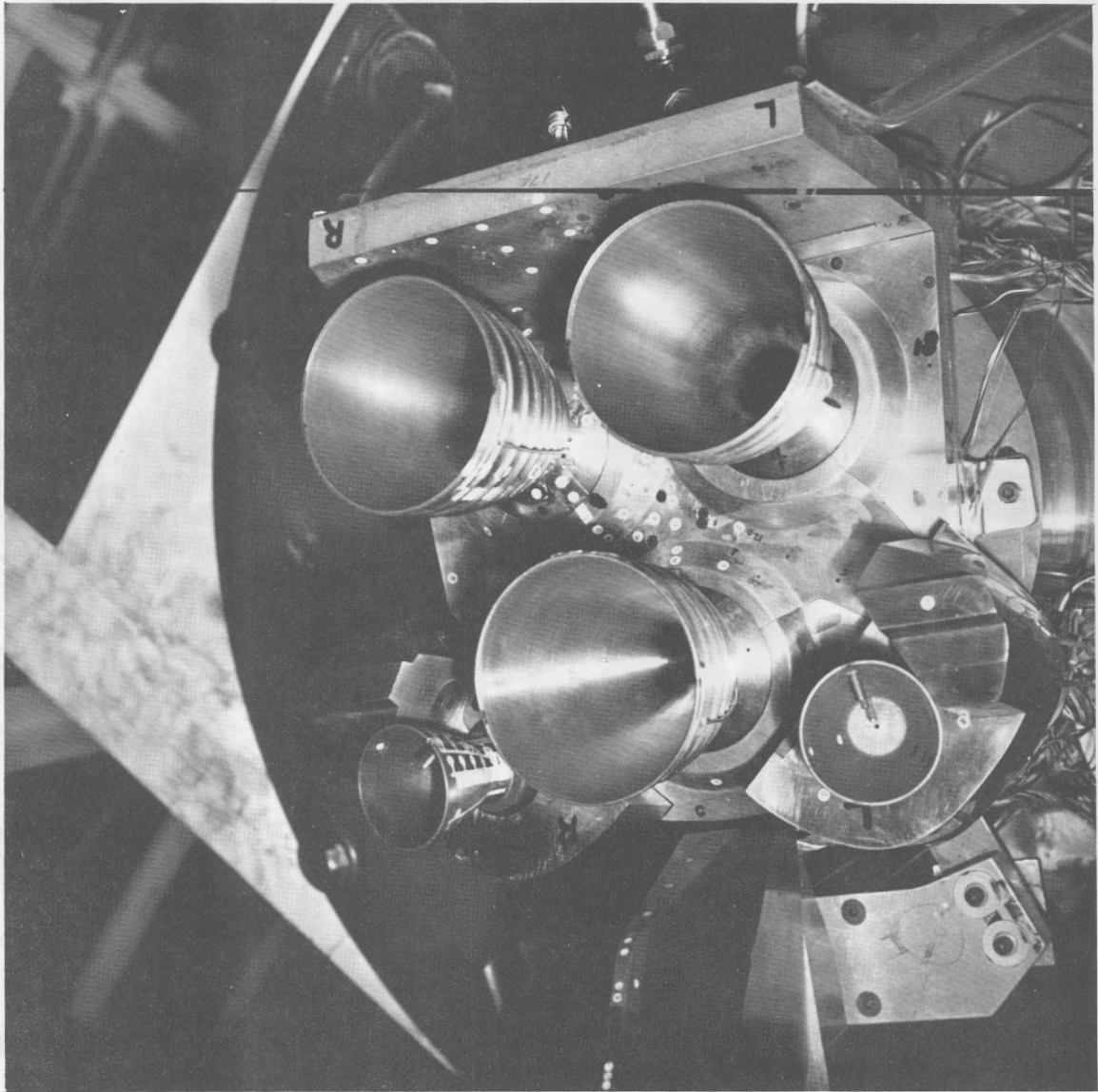
c. Center Base Heat Shield and Body Flap  
Figure 3. Concluded.



a. #1 SSME Position  
Figure 4. SSME hatband nozzle heat transfer gauges.



b. #2 SSME Position  
Figure 4. Continued.



c. #3 SSME Position  
Figure 4. Concluded.

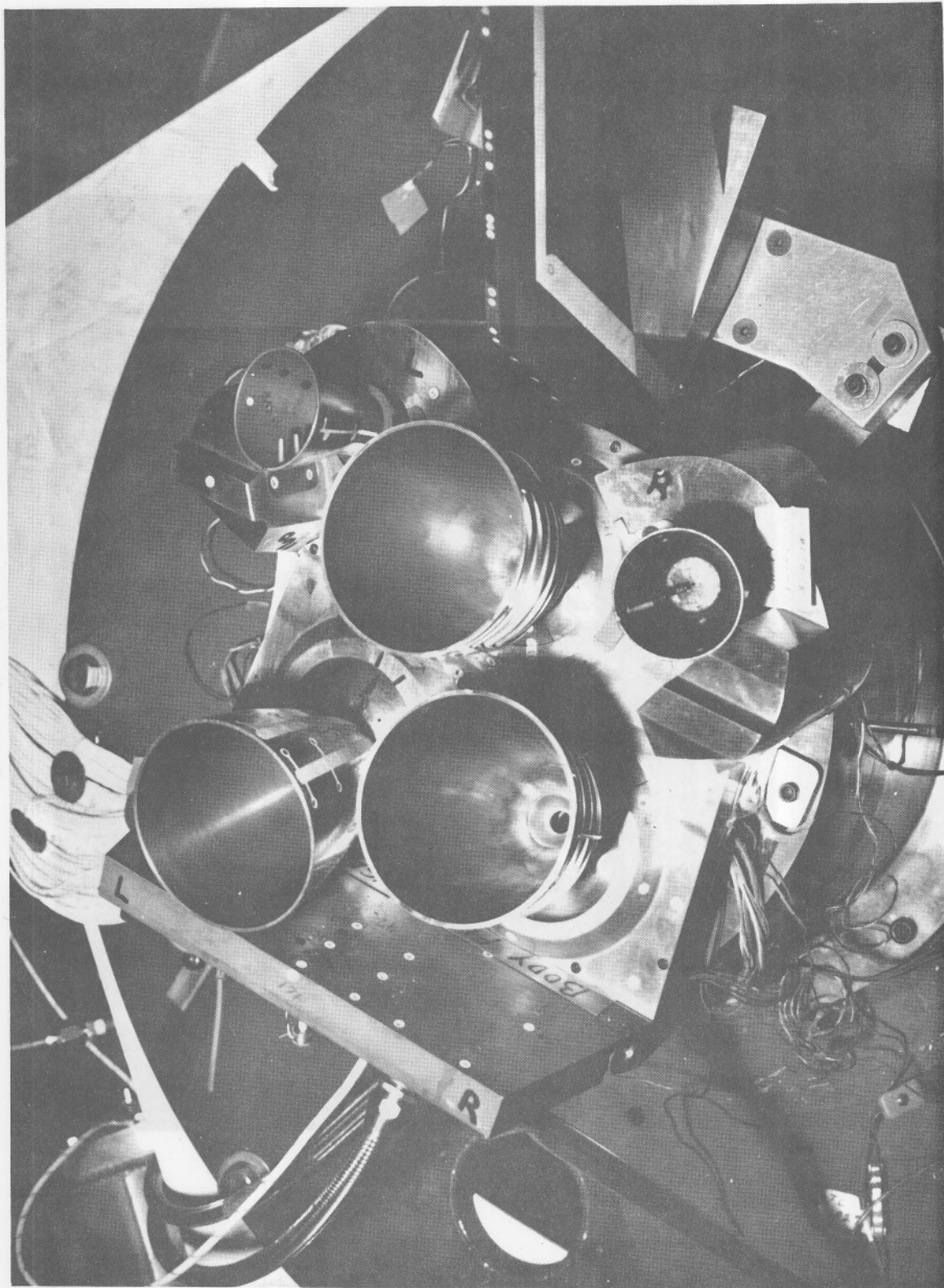
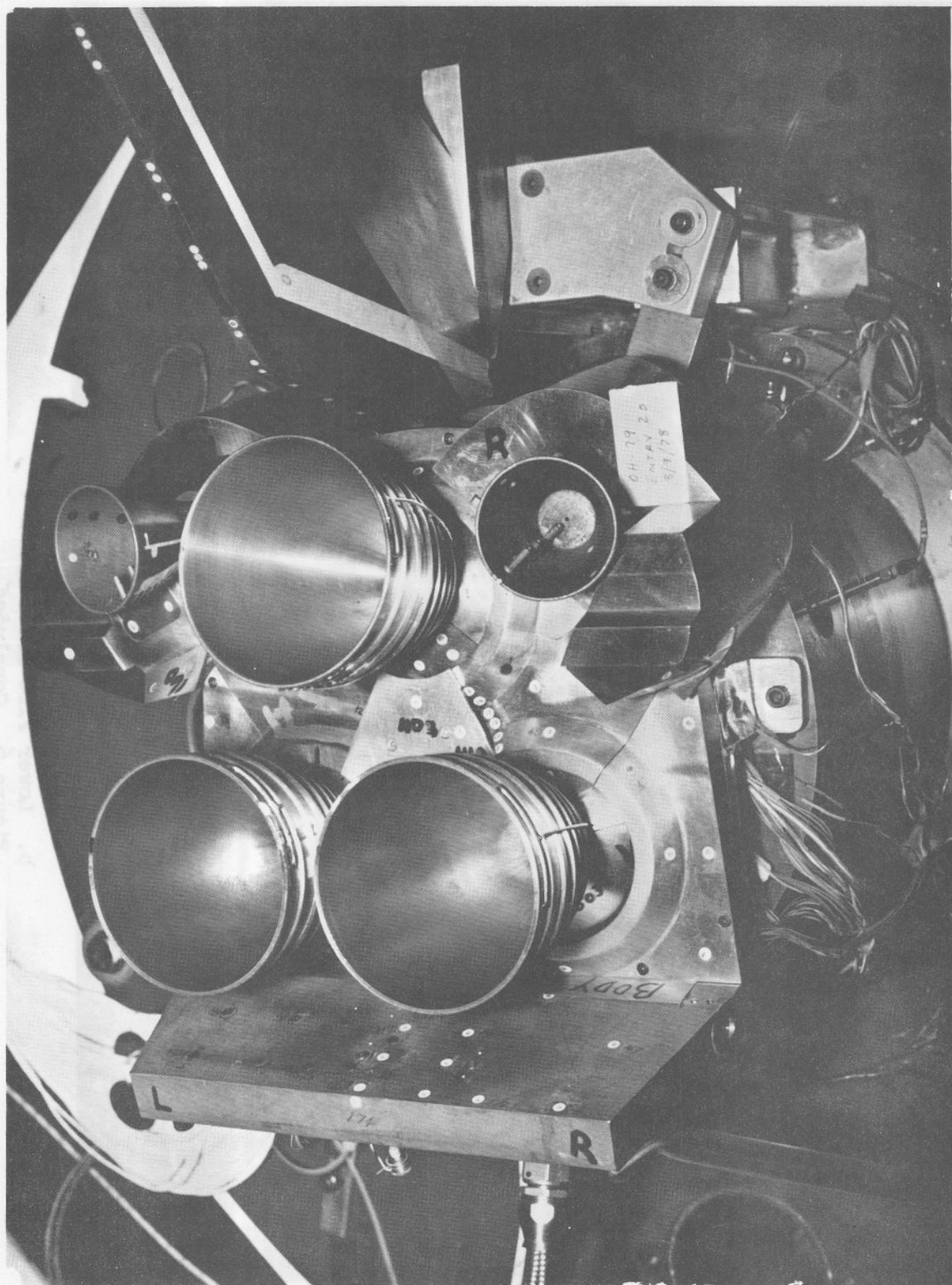
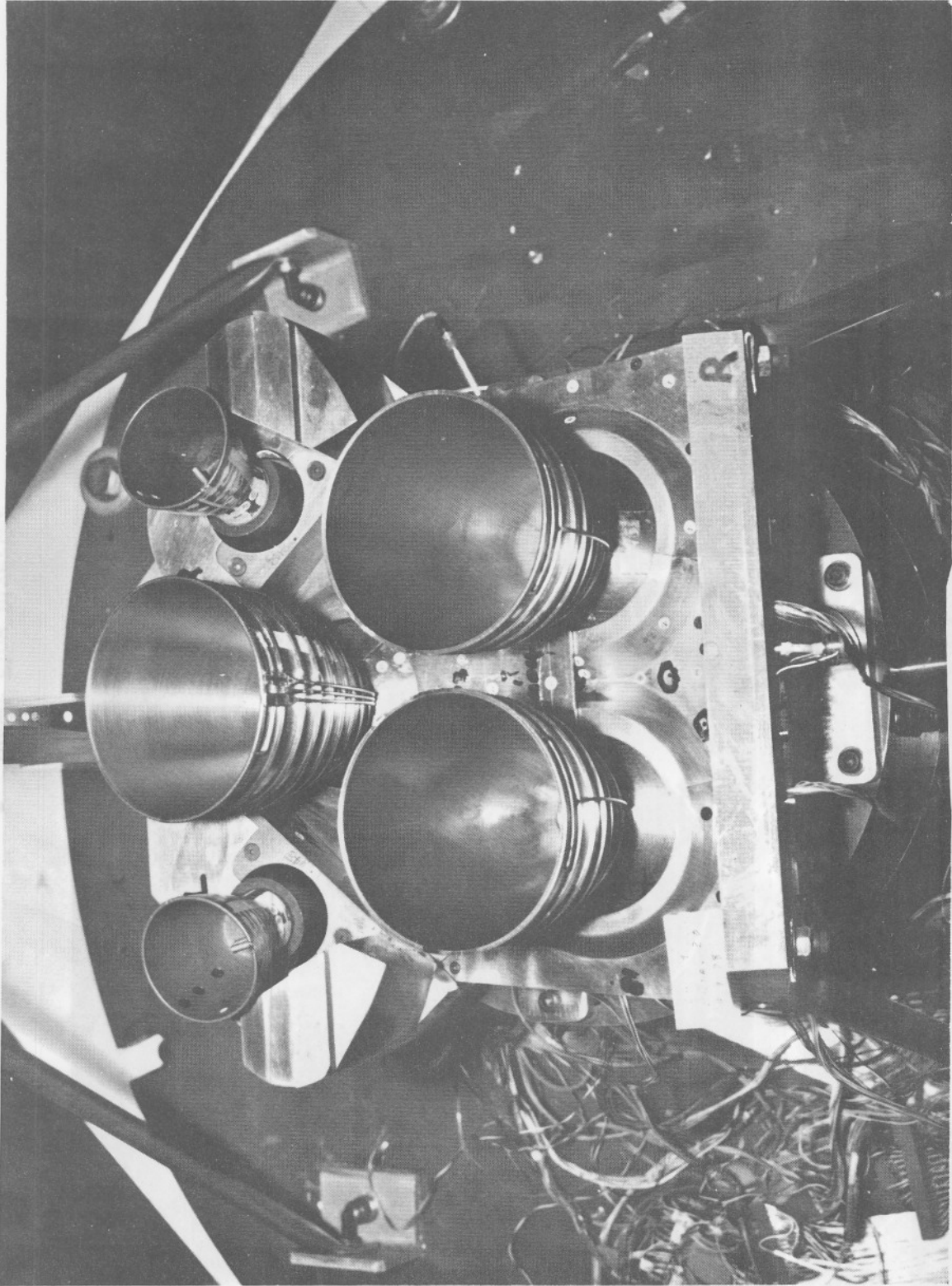


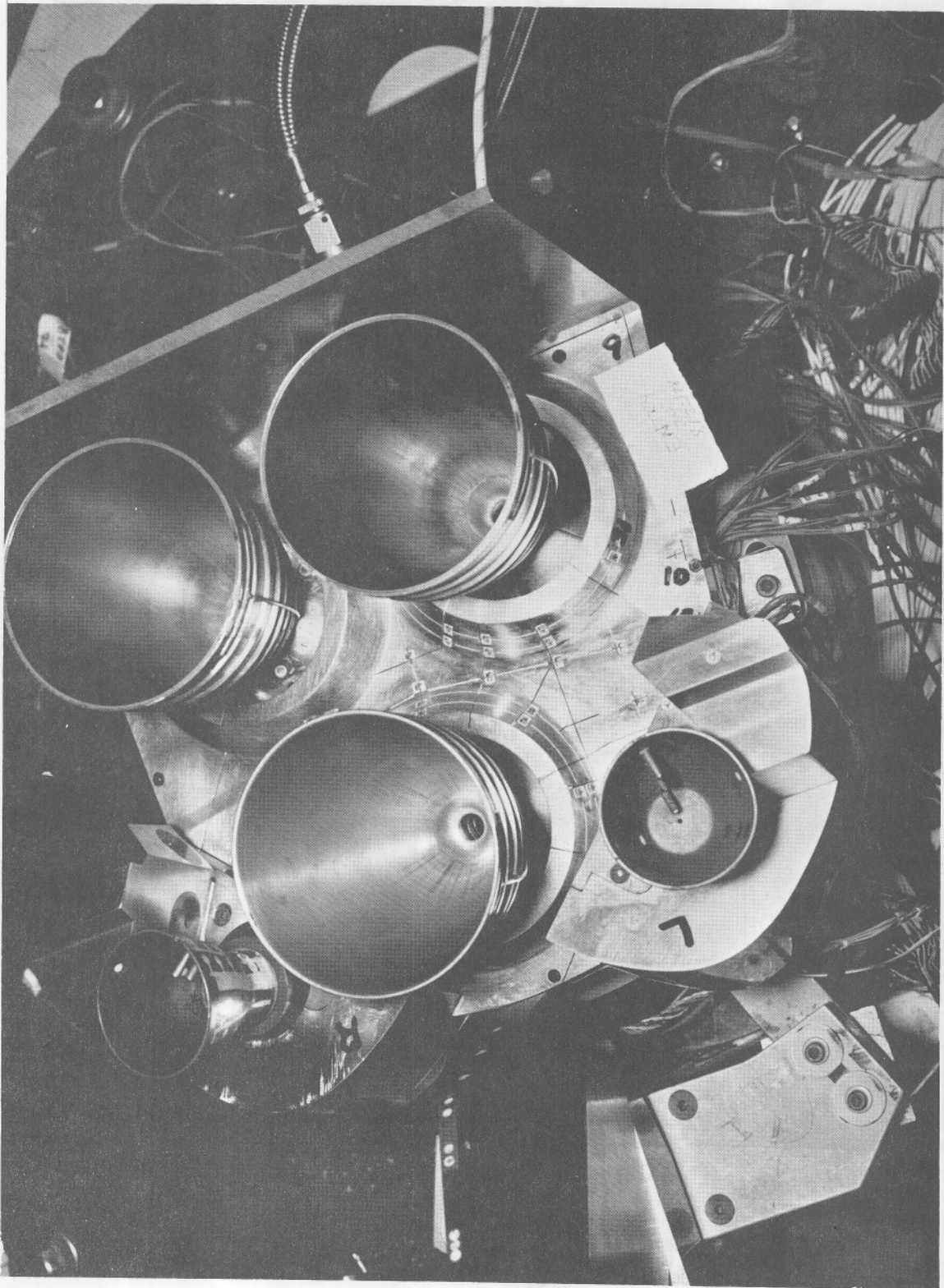
Figure 5. SSME smooth wall nozzle heat transfer gauges.



a. Upper Flow Diverter  
Flow diverter heat transfer gauges.

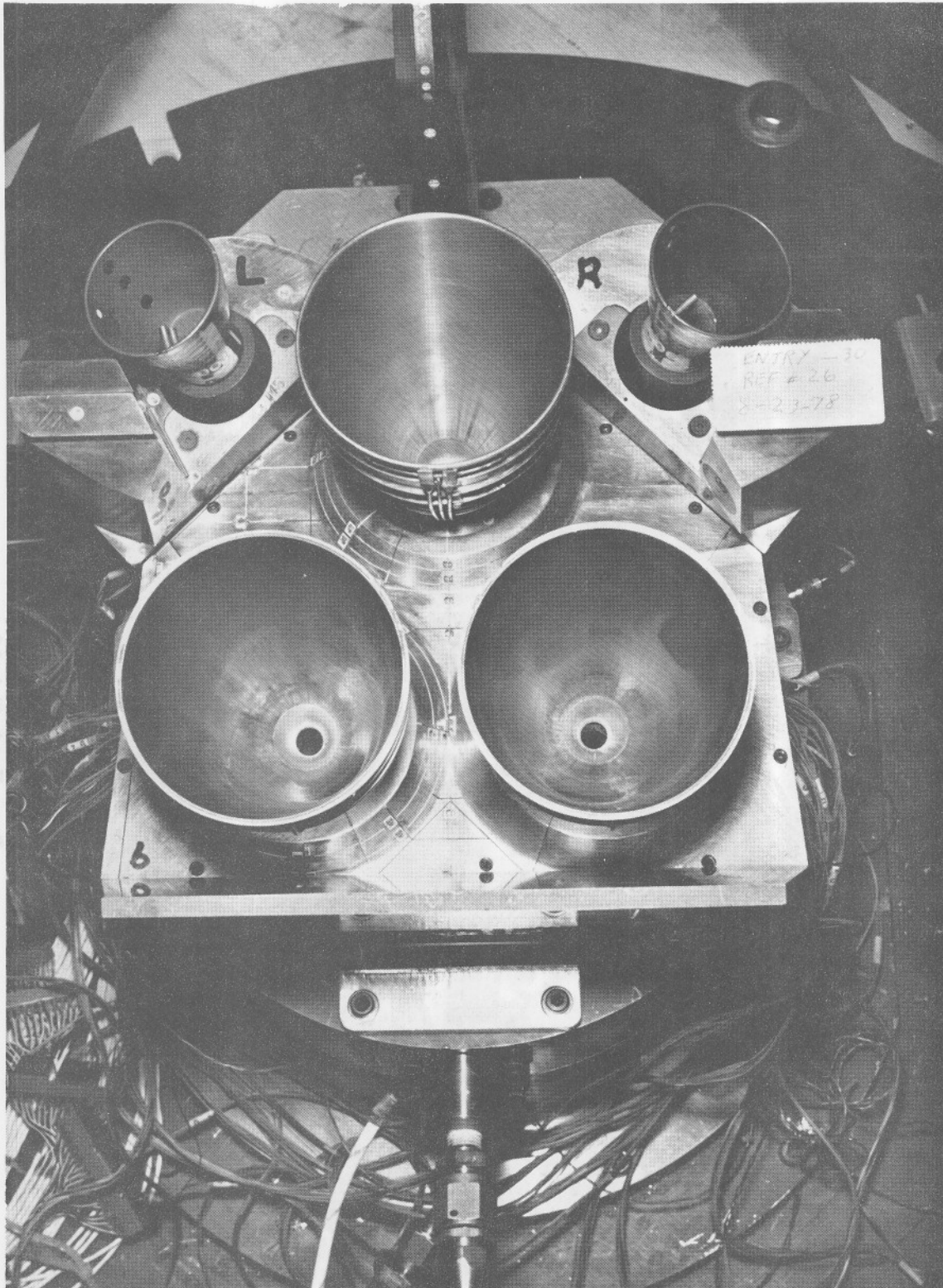


b. Lower Flow Diverter  
Figure 6. Concluded.

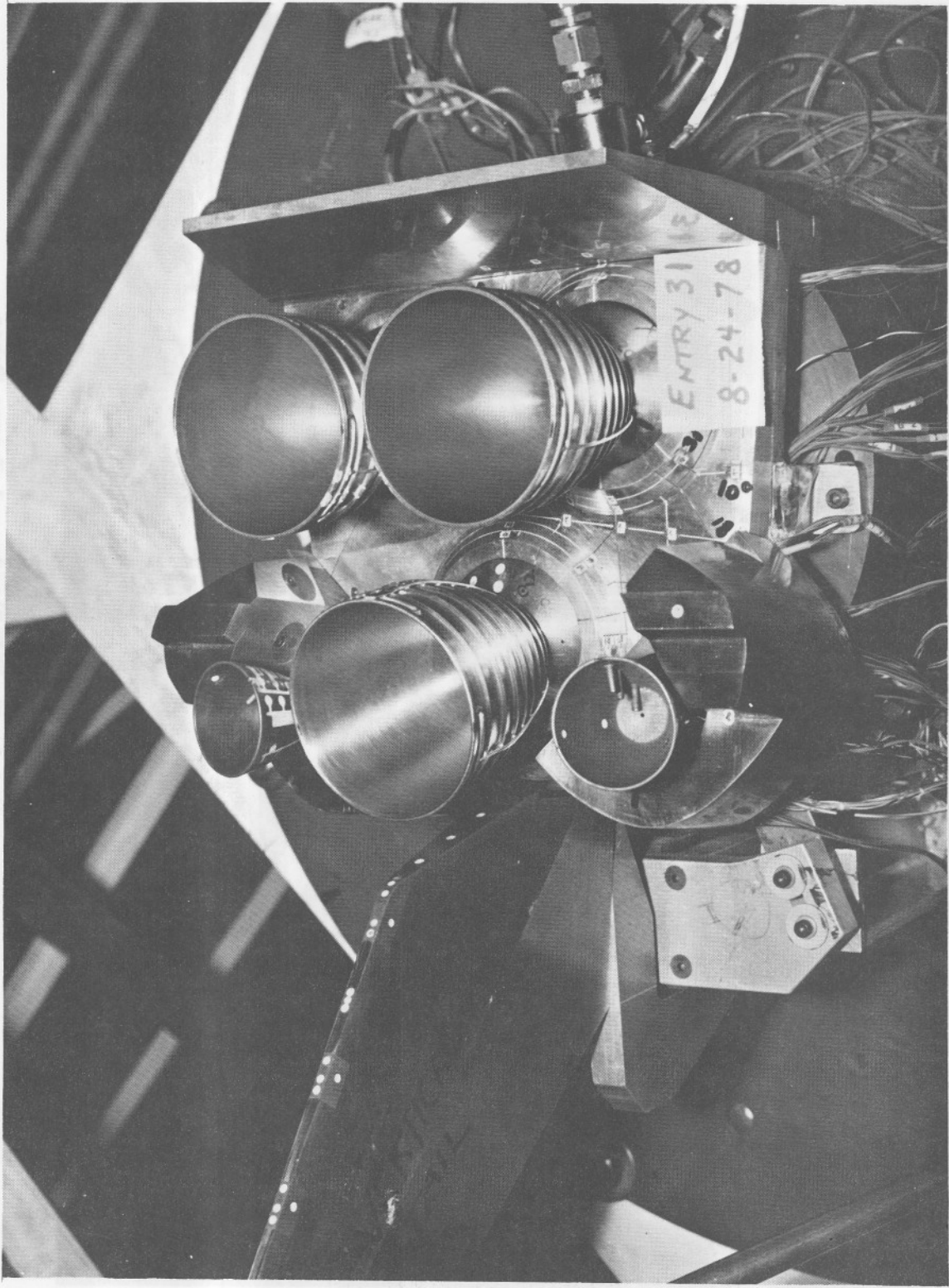


a. Base Heat Shield  
Figure 7. Tile gap base heat shield and body flap heat transfer gauges.

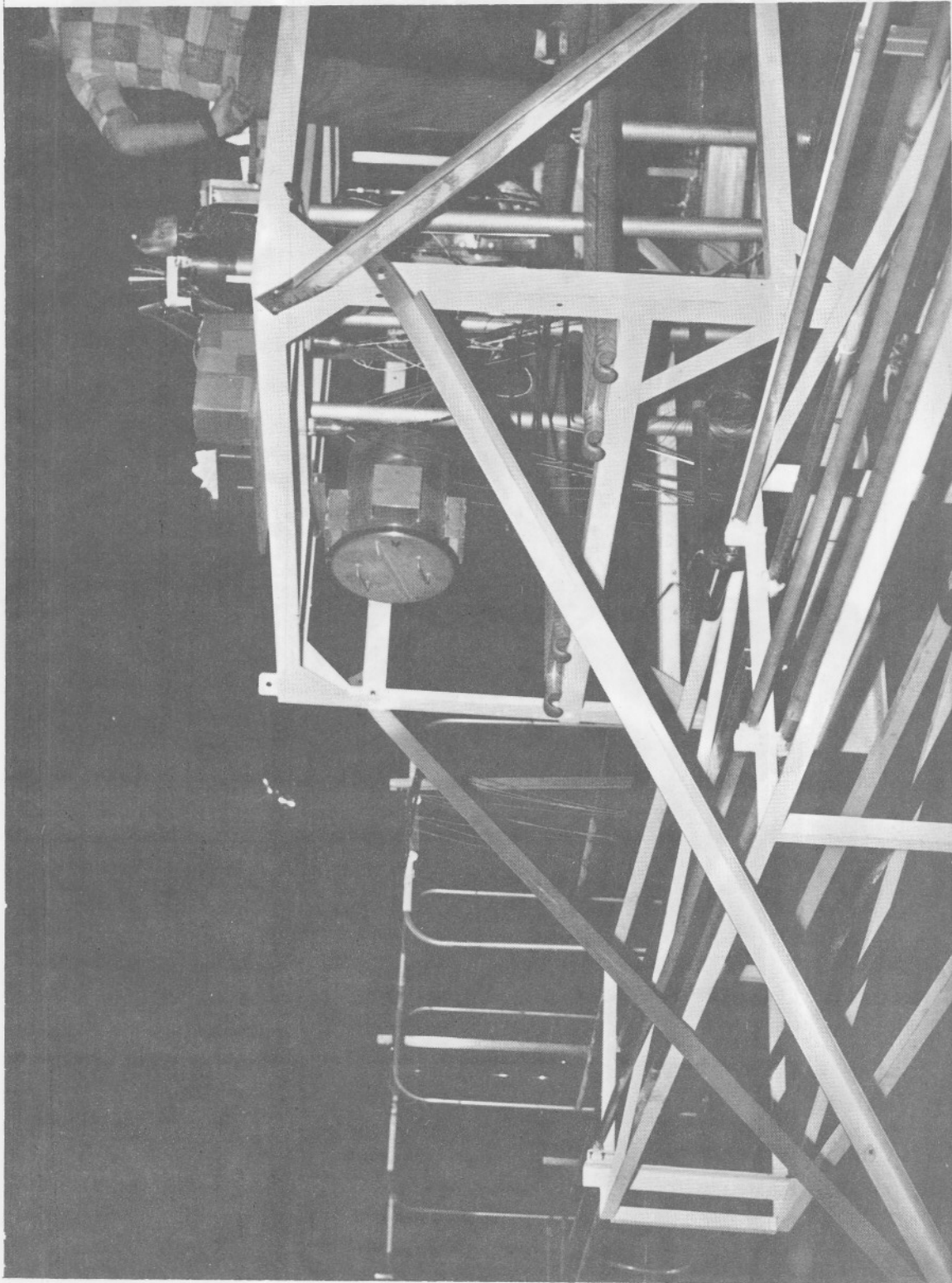




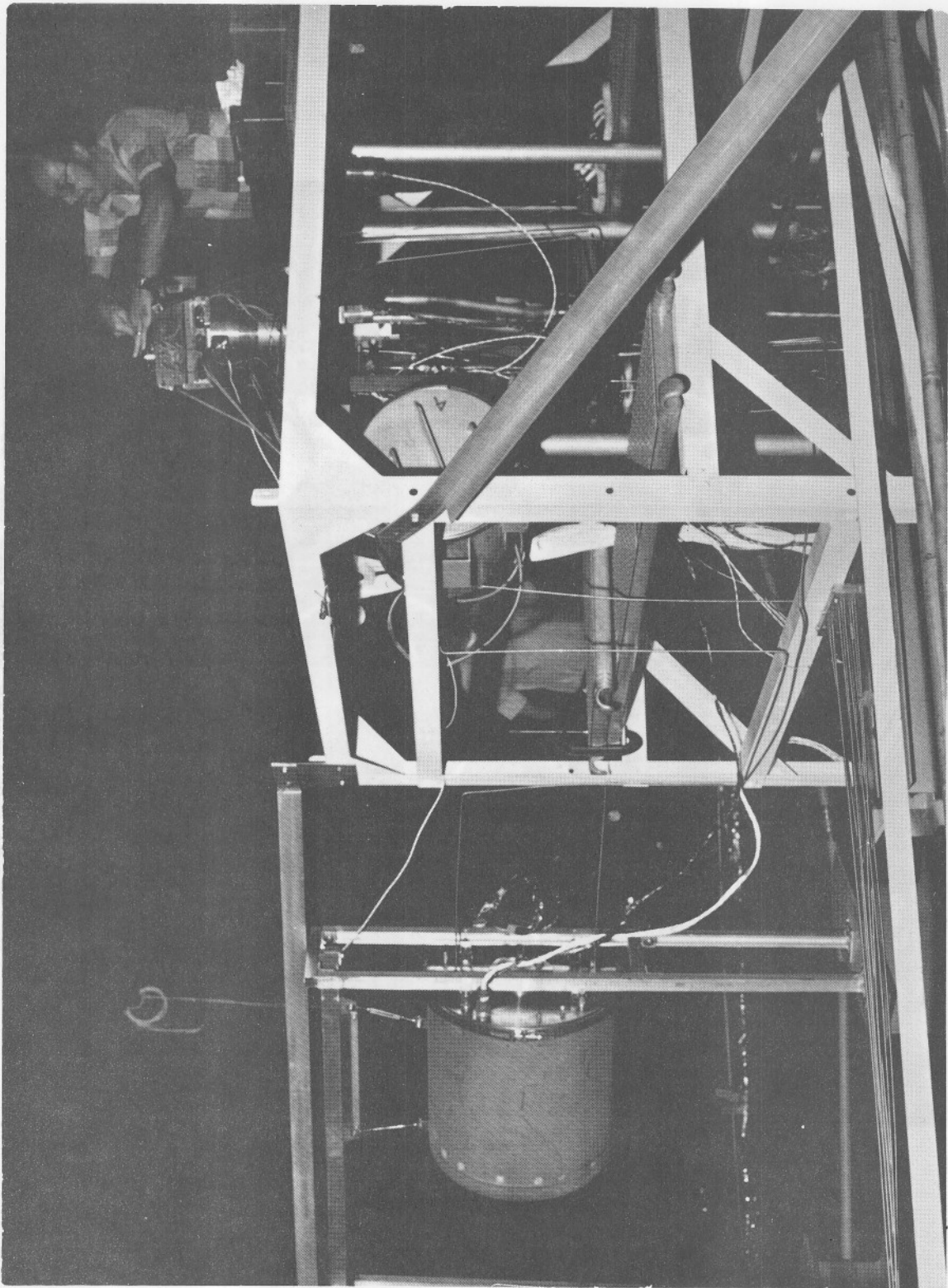
b. Base Heat Shield  
Figure 7. Continued.



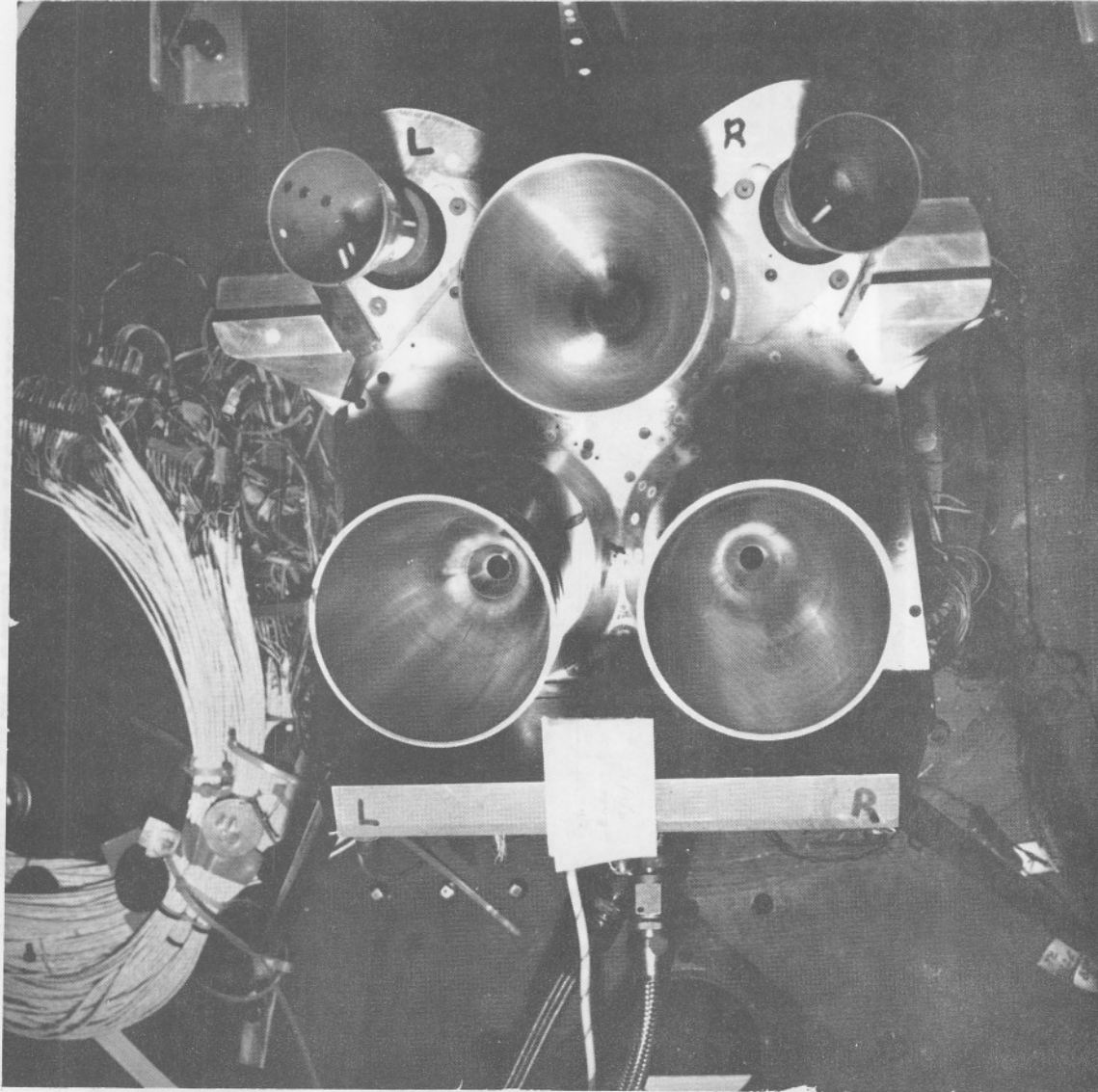
c. Body Flap  
Figure 7. Concluded.



a. Model, Thrust Stand, and Charge Tubes  
Figure 8. Model 65-0 installation and general arrangement.



b. Model, Thrust Stand, and Pressurized Containers  
Figure 8. Concluded.



9. Model 65-0 strip connectors and wire bundles.



Figure 10. Gas line arrangement inside Chamber A.

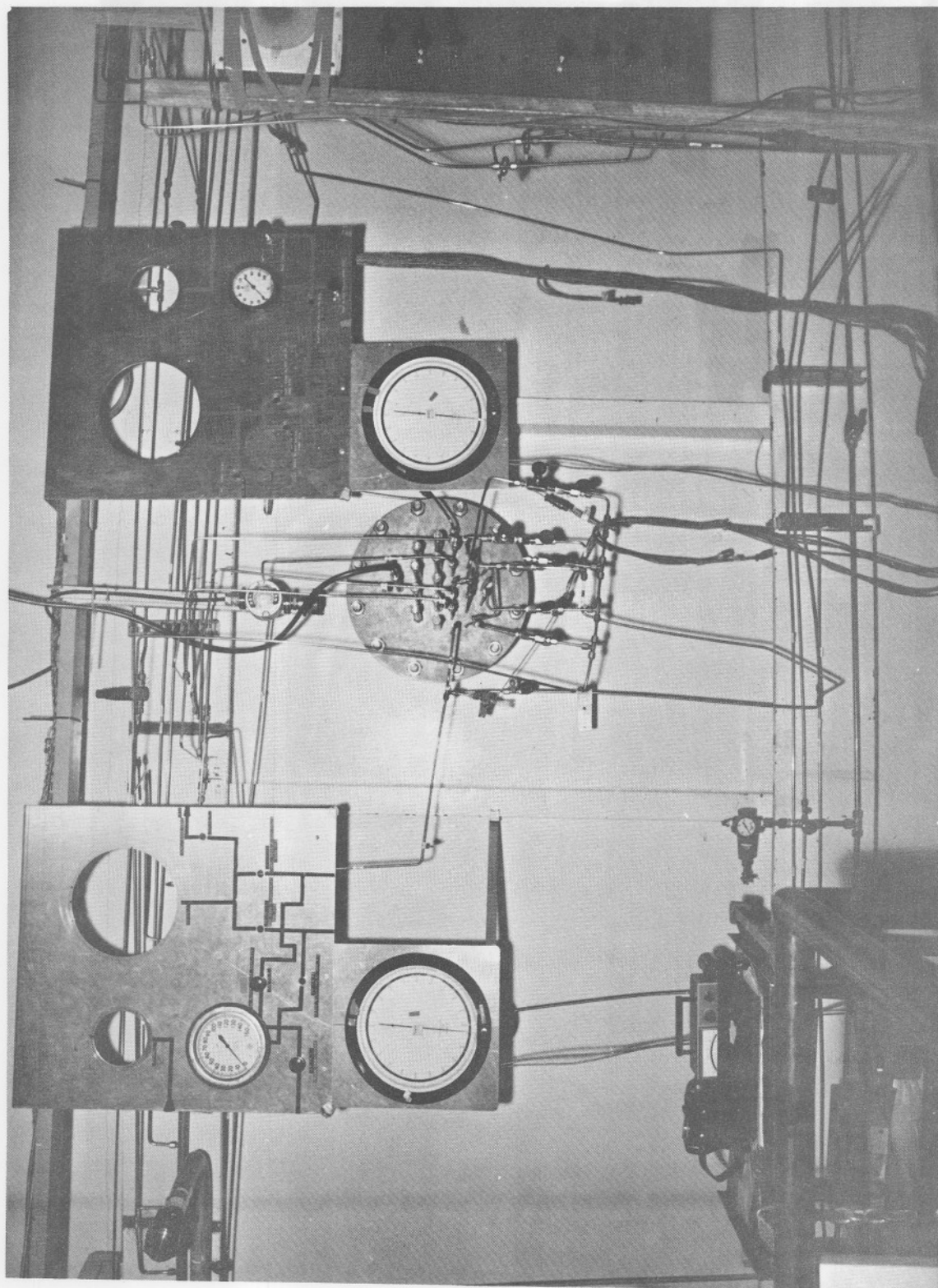


Figure 11. Gas control panels.

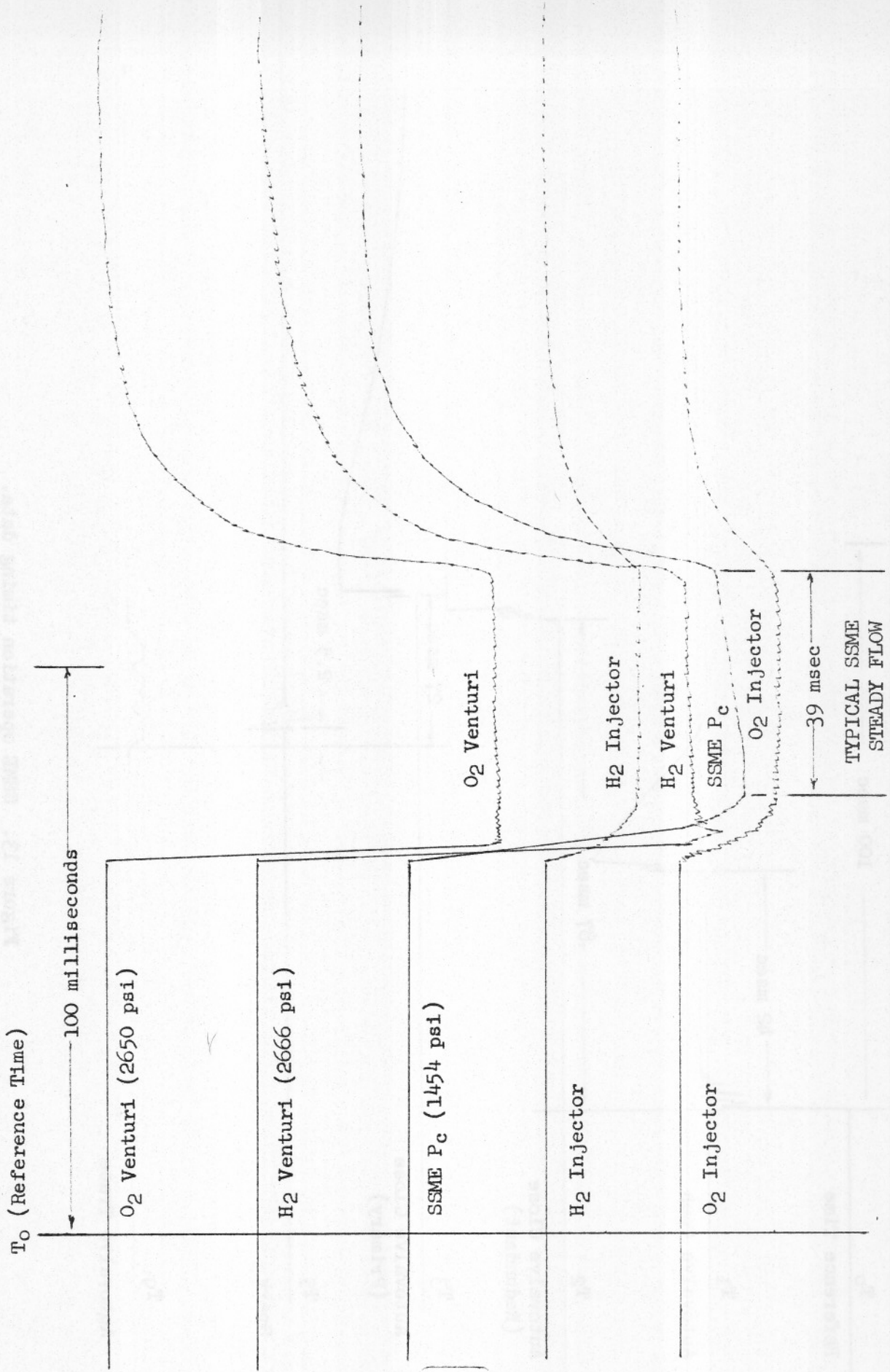


Figure 12. SSME operation pressure data.



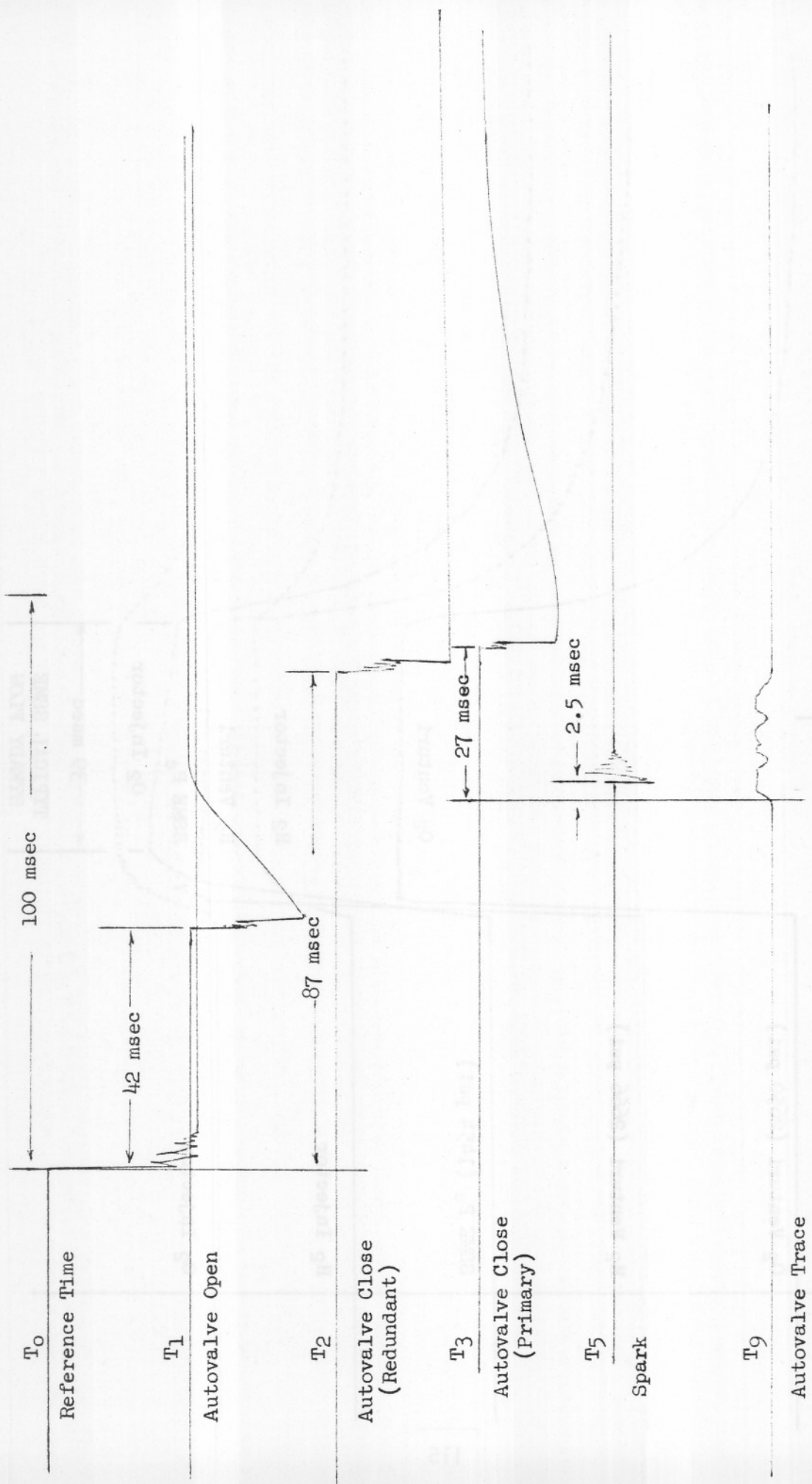
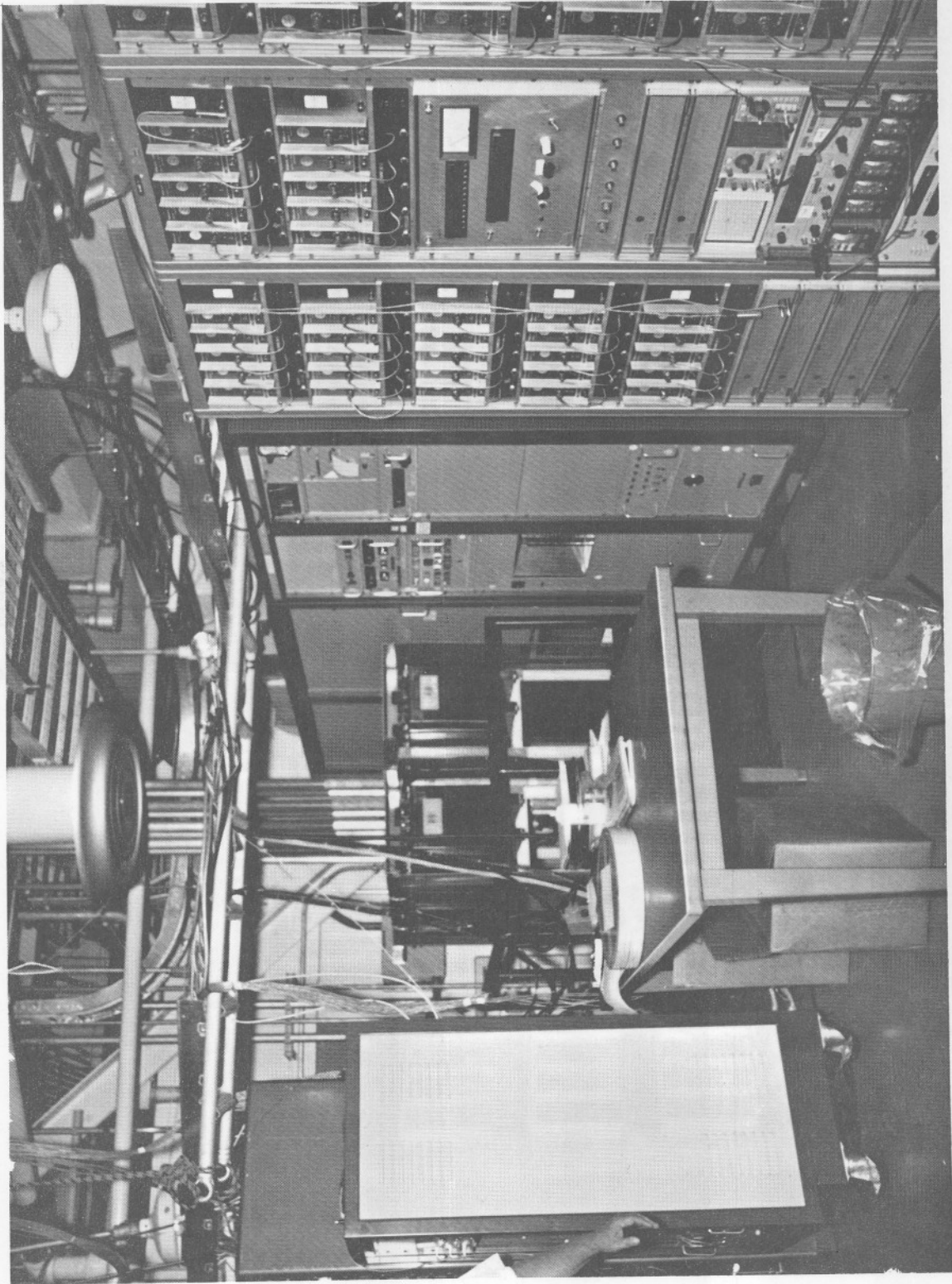
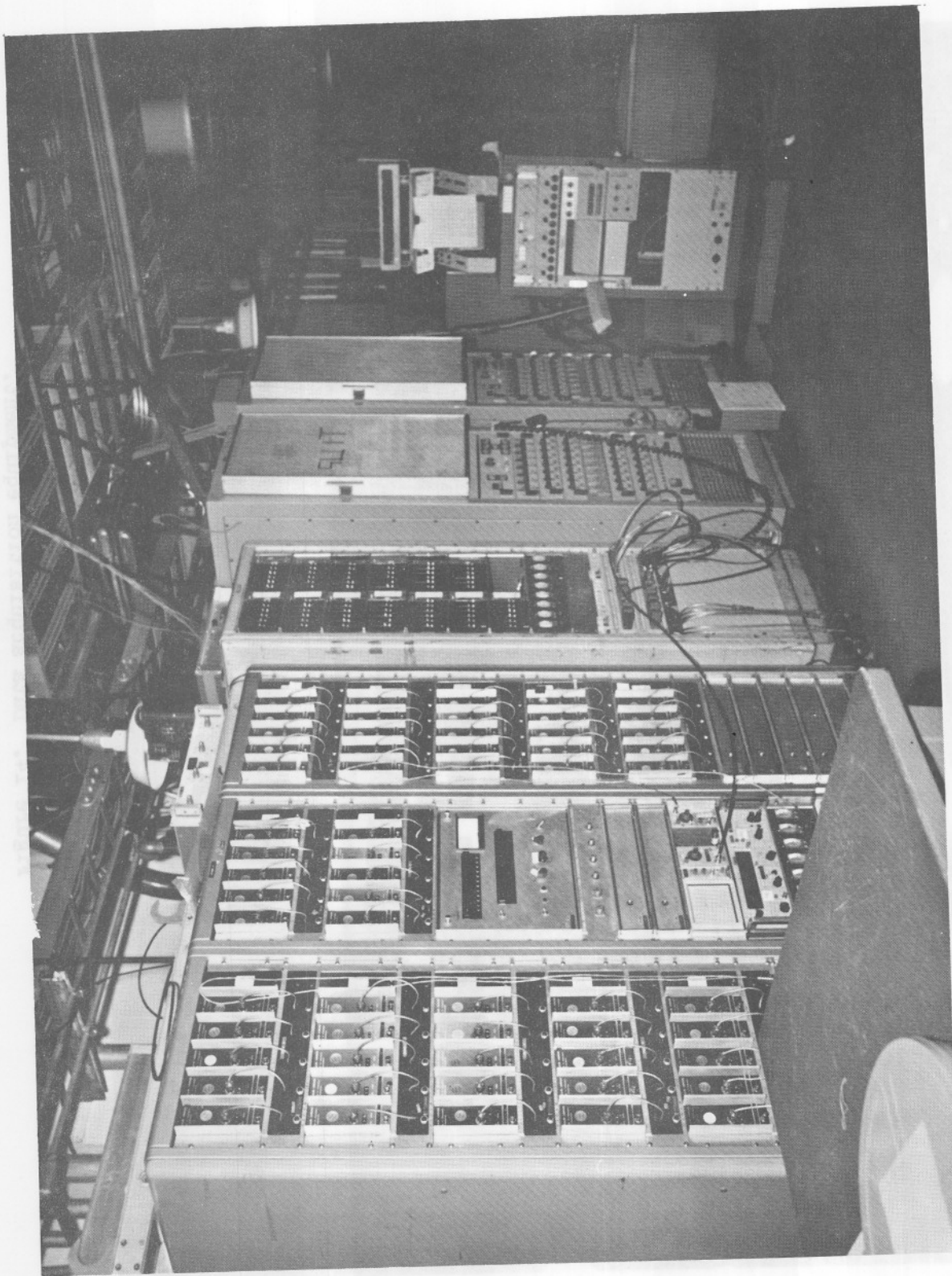


Figure 13. SSME operation timing data.

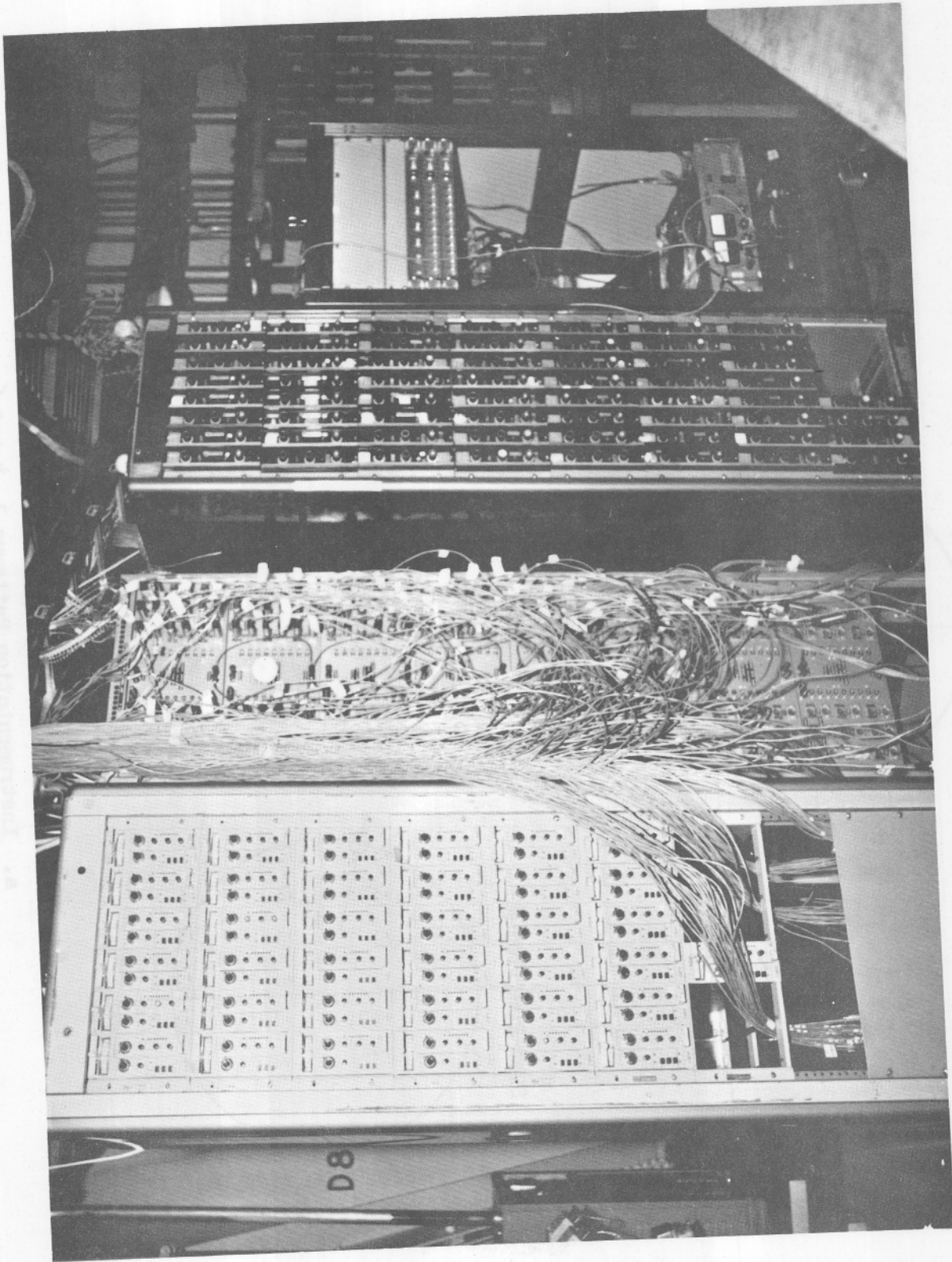
Exhibit 111 - Copying



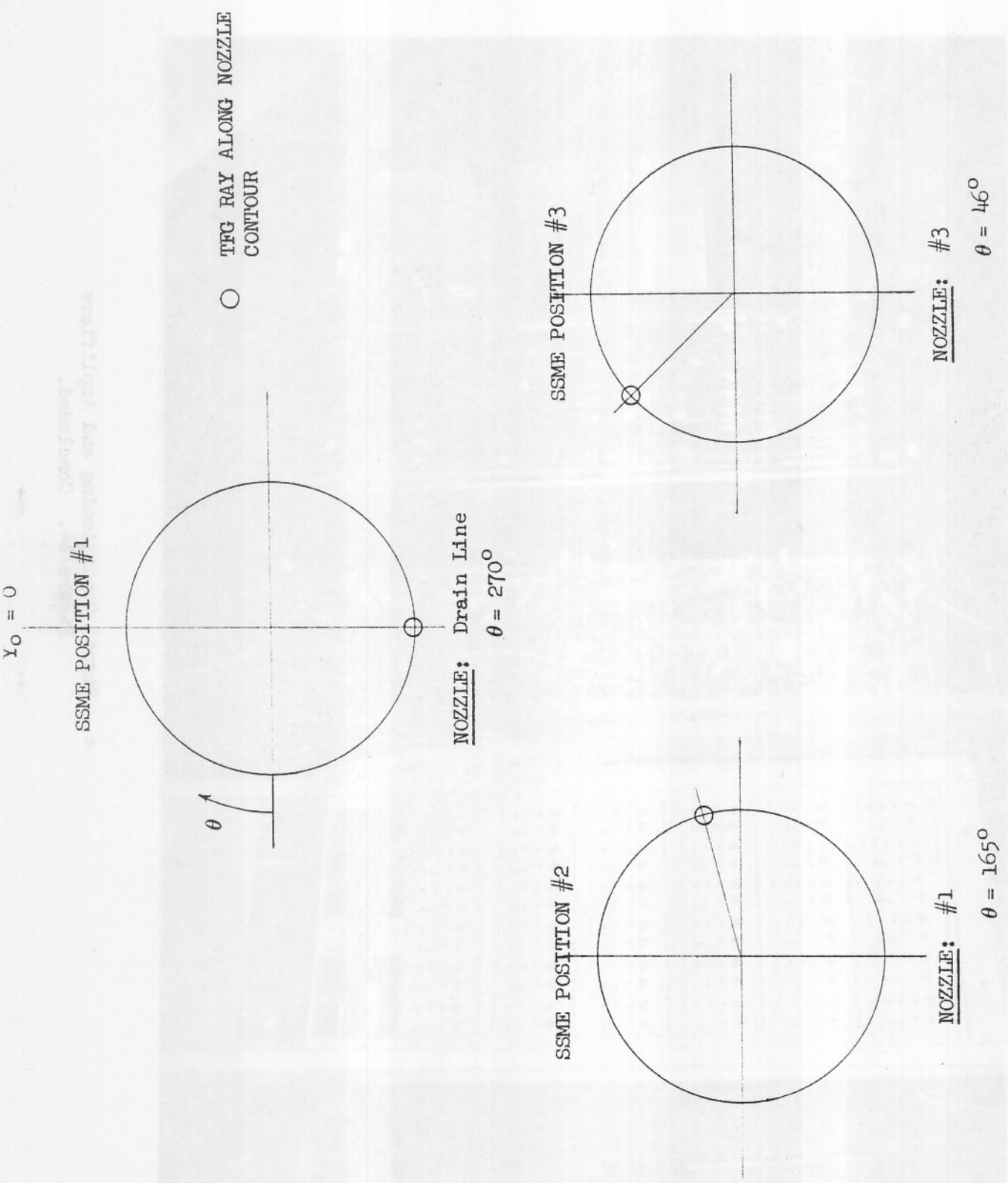
a. FACT  
Figure 14. Data acquisition equipment.



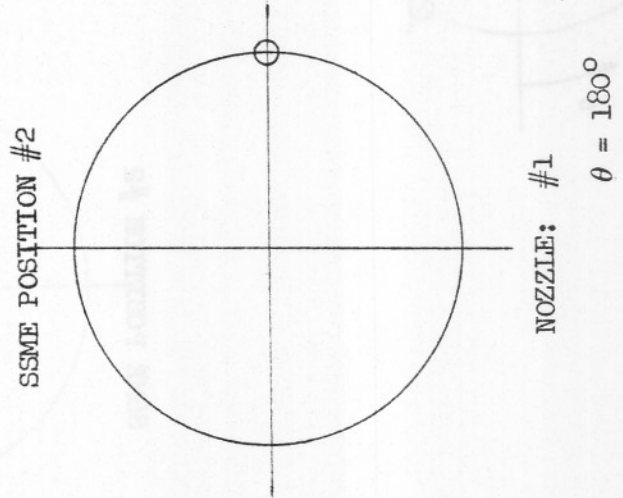
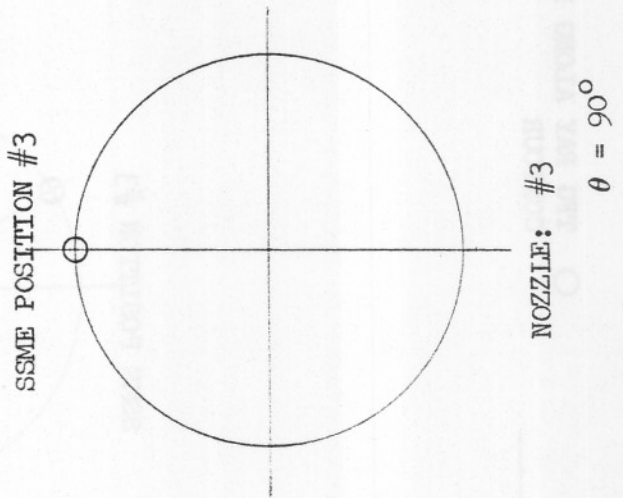
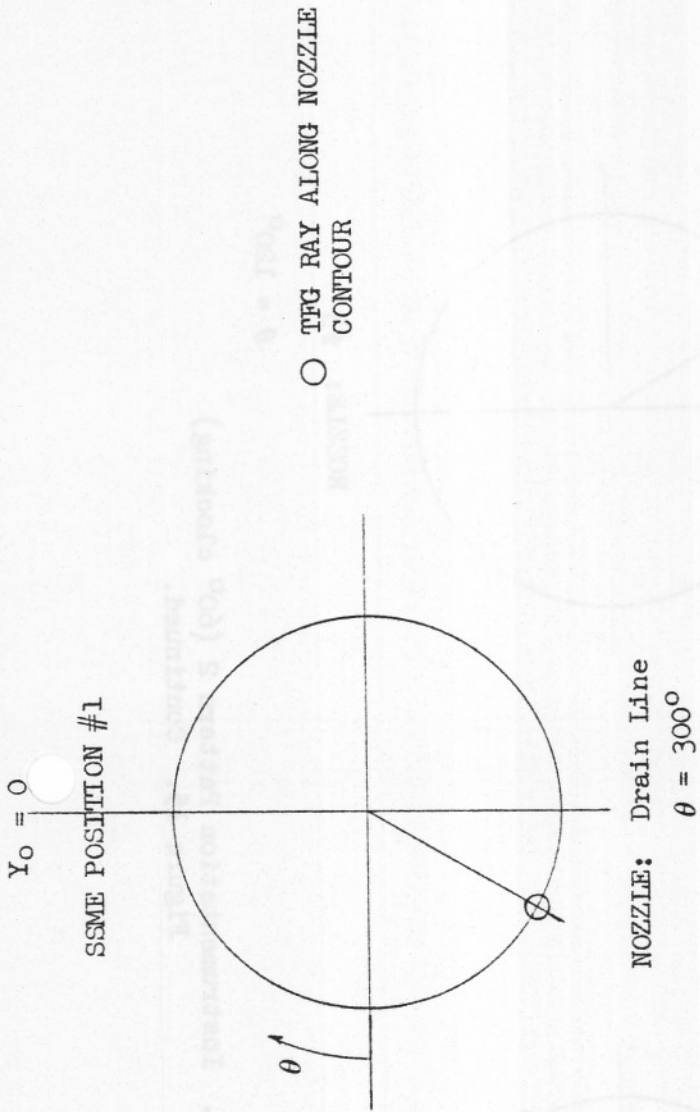
b. Vidar  
Figure 14. Continued.



c. Signal Conditioning and Amplifiers  
Figure 14. Concluded.

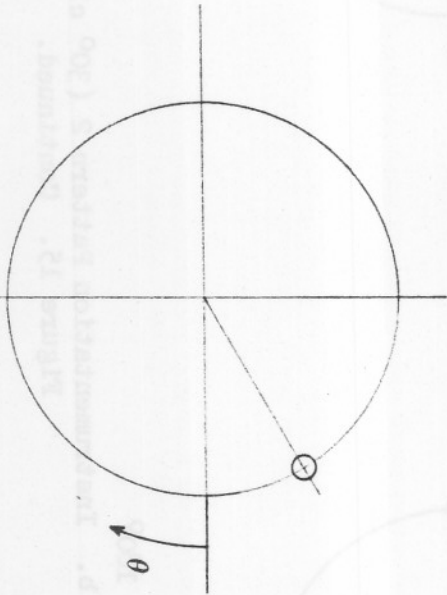


a. Instrumentation Patterns 1, 4 and 6  
 Figure 15. SSME nozzle orientation.



b. Instrumentation Pattern 2 (30° clocking)  
Figure 15. Continued.

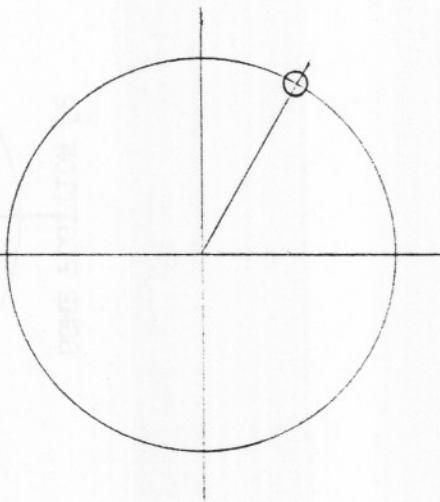
SSME POSITION #1



NOZZLE: Drain Line  
 $\theta = 330^\circ$

○ TFG RAY ALONG NOZZLE  
CONTOUR

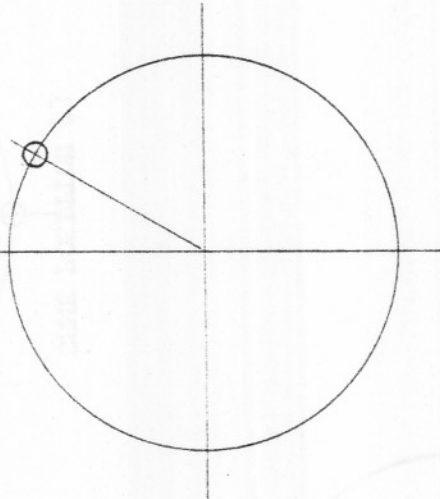
SSME POSITION #2



NOZZLE: #1

$\theta = 210^\circ$

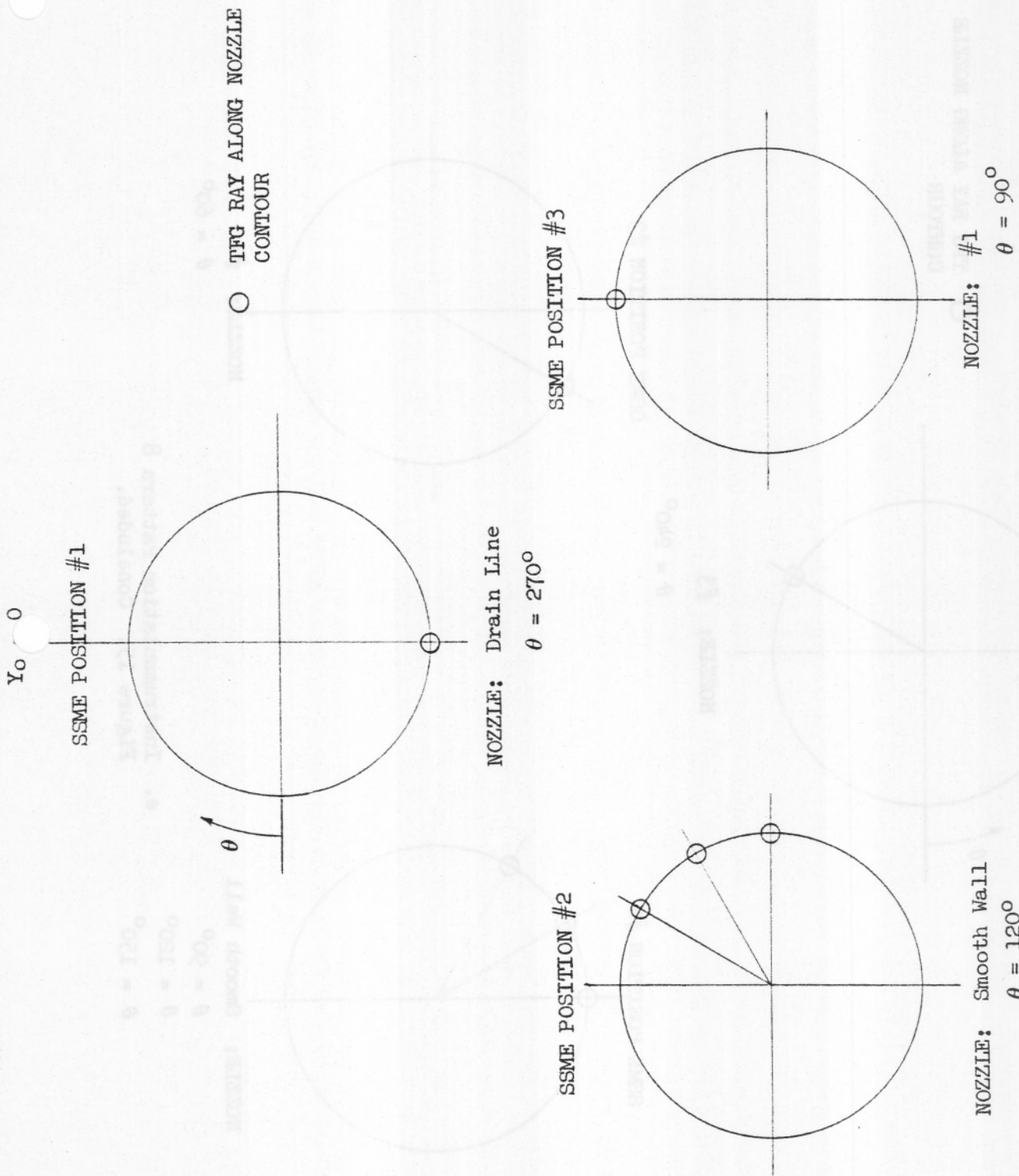
SSME POSITION #3



NOZZLE: #3

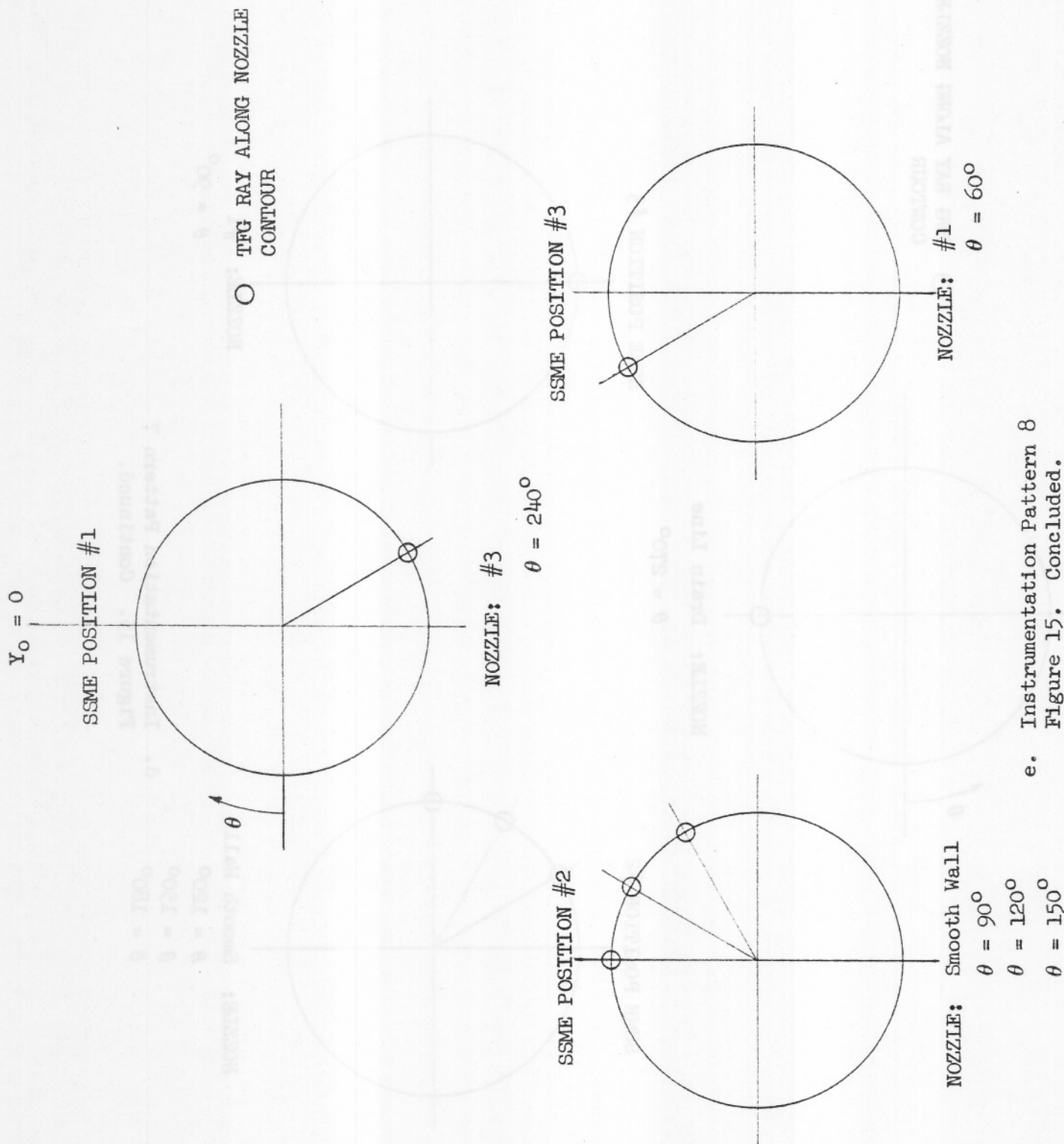
$\theta = 120^\circ$

c. Instrumentation Pattern 2 (60° clocking)  
Figure 15. Continued.

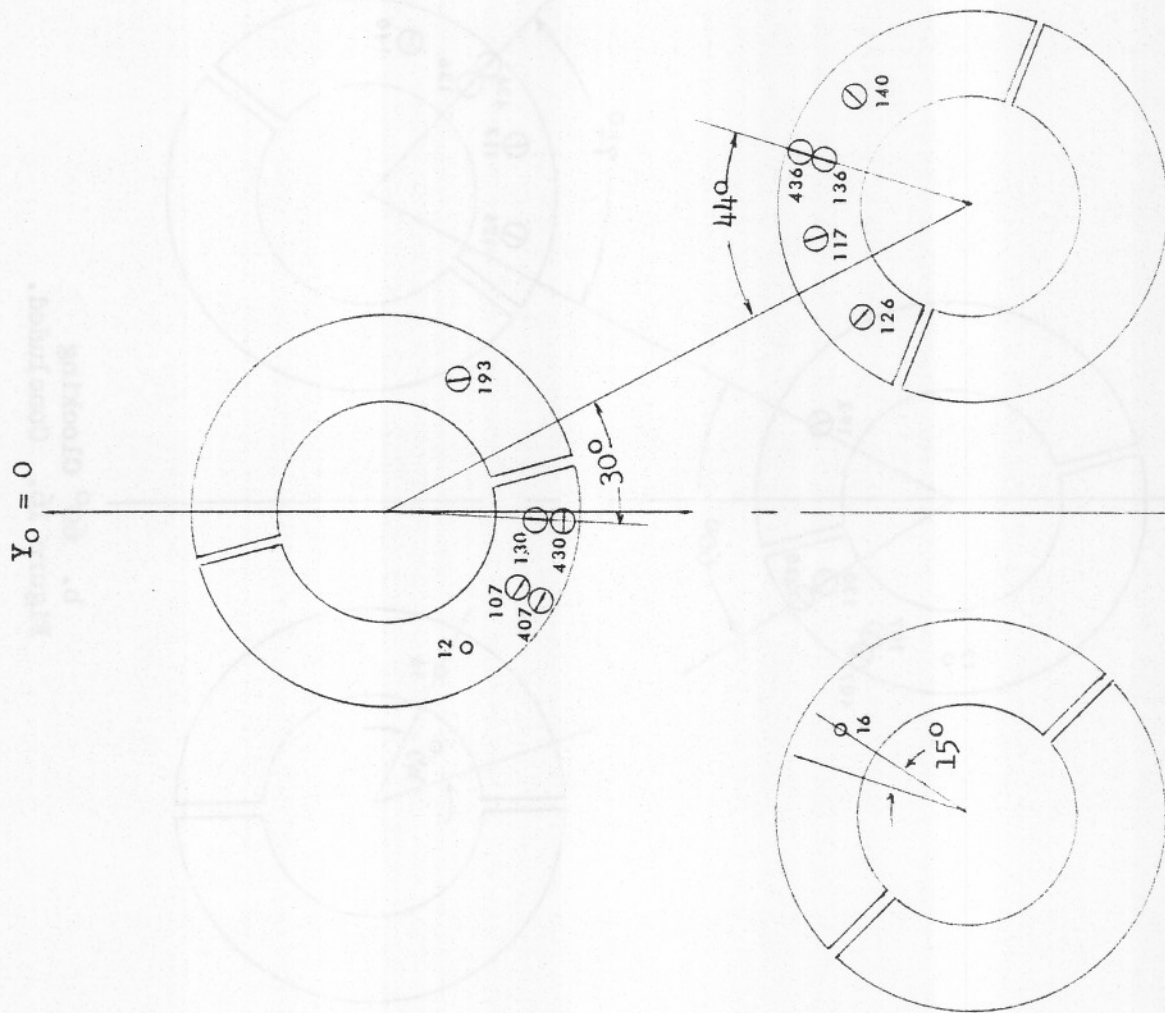


d. Instrumentation Pattern 7  
Figure 15. Continued.



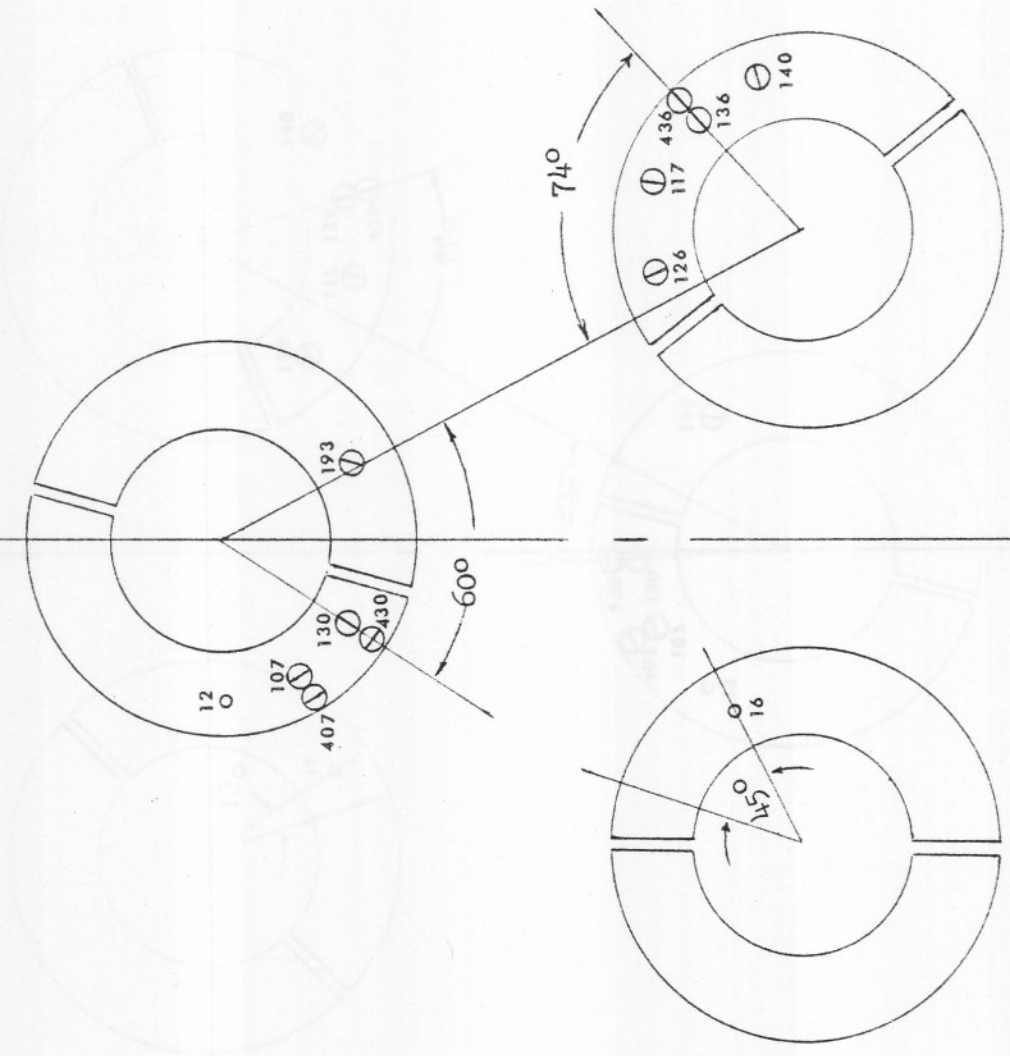


e. Instrumentation Pattern 8  
Figure 15. Concluded.



a.  $30^\circ$  Clocking  
 Figure 16. Instrumentation pattern 2 engine-mounted heat shield orientation.

$Y_0 = 0$



b. 60° Clocking  
Figure 16. Concluded.

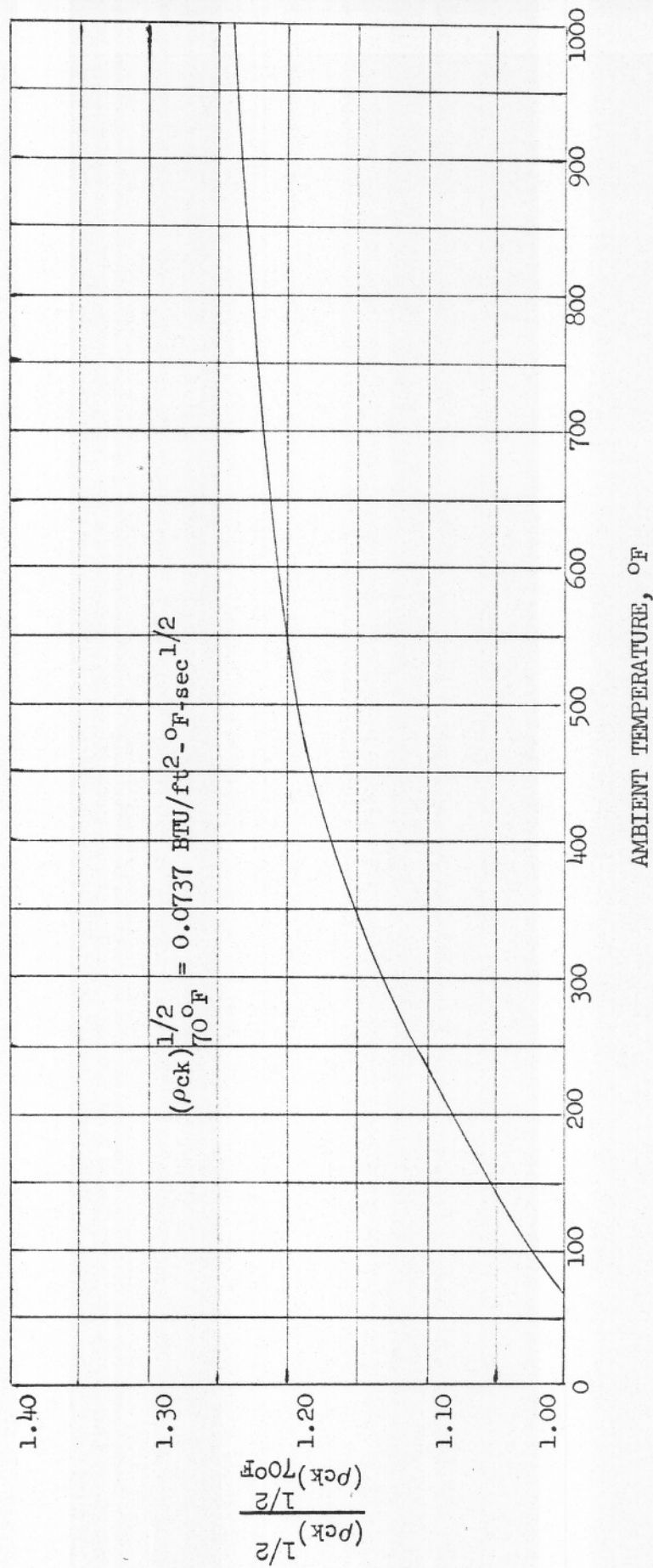


Figure 17. Variation of thin-film gauge substrate (#7740 Pyrex) properties with temperature.

APPENDIX A

SOURCE DATA REFERENCES

SOURCE DATA REFERENCES

DATA	ROCKWELL INTERNATIONAL STS AEROSCIENCES DEPARTMENT	
Tabulated	Wind Tunnel Operations Group  (R. S. Crowder, Supervisor)	Aero Heating Group  (M. H. Harthun, Supervisor)
Plot		Aero Heating Group  (M. H. Harthun, Supervisor)

APPENDIX B

TABULATED SUMMARY HEAT TRANSFER

DATA CORRECTION FACTORS

SUMMARY HEAT TRANSFER DATA CORRECTION FACTORS

$$\text{Corrected } \bar{q}_{ss} = \text{Correction Factor} \times \bar{q}_{ss}$$

CHAMBER ENTRY	R <sub>p</sub> USED FOR DATA REDUCTION (EQ. 16)	ACTUAL R <sub>p</sub> (1/R <sub>p</sub> ) (R <sub>p</sub> c)	CORRECTION FACTOR (1/R <sub>p</sub> <sup>2</sup> ) <sup>0.8</sup>
02-4	0.986	1.014	1.0228
02-5	0.950	1.053	1.0855
02-6	0.973	1.028	1.0448
02-7	0.973	1.028	1.0448
03-1	0.931	1.074	1.1212
03-2	0.942	1.062	1.1003
03-3	0.942	1.062	1.1003
03-4	0.944	1.059	1.0966
04-1	0.990	1.010	1.0162
04-2	0.994	1.006	1.0097
04-3	0.999	1.001	1.0016
05-1	0.954	1.048	1.0783
05-2	0.961	1.041	1.0657
06-1	0.989	1.011	1.0179
06-2	0.994	1.006	1.0097
07-1	0.981	1.019	1.0312
07-2	0.905	1.105	1.1732
07-3	0.923	1.083	1.1368
07-4	0.970	1.031	1.0499
07-5	0.923	1.083	1.1368



SUMMARY HEAT TRANSFER DATA CORRECTION FACTORS (Continued)

$$\text{Corrected } \bar{q}_{ss} = \text{Correction Factor} \times \bar{q}_{ss}$$

CHAMBER ENTRY	R <sub>p</sub> USED FOR DATA REDUCTION (EQ. 16)	ACTUAL R <sub>p</sub> (1/R <sub>p</sub> ) (R <sub>p,c</sub> )	CORRECTION FACTOR (1/R <sub>p</sub> <sup>2</sup> ) <sup>0.8</sup>
08-1	0.956	1.046	1.0747
08-2	0.969	1.032	1.0517
08-3	0.973	1.028	1.0448
08-4	0.977	1.024	1.0379
09-1	0.959	1.043	1.0693
09-2	0.969	1.032	1.0517
09-3	0.986	1.014	1.0228
09-4	0.931	1.074	1.1212
10-2	0.990	1.010	1.0162
10-3	0.952	1.050	1.0819
10-4	0.969	1.032	1.0517
10-5	0.977	1.024	1.0379
11-1	1.058	0.945	0.9137
11-2	1.049	0.953	0.9263
11-3	1.055	0.948	0.9179
11-4	1.036	0.965	0.9450
12-1	1.070	0.935	0.8974
12-2	1.040	0.962	0.9392
12-3	1.028	0.973	0.9568
12-4	1.020	0.980	0.9688

SUMMARY HEAT TRANSFER DATA CORRECTION FACTORS (Continued)

$$\text{Corrected } \bar{q}_{ss} = \text{Correction Factor} \times \bar{q}_{ss}$$

CHAMBER ENTRY	R <sub>p</sub> USED FOR DATA REDUCTION (EQ. 16)	ACTUAL R <sub>p</sub> (1/R <sub>p</sub> ) (R <sub>p</sub> c)	CORRECTION FACTOR (1/R <sub>p</sub> <sup>2</sup> ) <sup>0.8</sup>
12-5	1.020	0.980	0.9688
13-1	1.0575	0.946	0.9144
13-2	1.029	0.972	0.9553
13-3	1.036	0.965	0.9450
14-1	1.045	0.957	0.9320
14-2	1.032	0.969	0.9509
14-3	1.045	0.957	0.9320
15-1	1.041	0.961	0.9377
15-2	1.041	0.961	0.9377
15-3	1.015	0.985	0.9765
15-4	0.998	1.002	1.0032
15-5	1.015	0.985	0.9765
15-5	1.011	0.989	0.9826
15-7	0.973	1.028	1.0448
16-2	1.007	0.993	0.9889
16-3	0.9901	1.010	1.0160
16-4	0.9817	1.019	1.0300
16-5	0.986	1.014	1.0228
17-2	1.0323	0.969	0.9504
17-3	1.049	0.953	0.9263

SUMMARY HEAT TRANSFER DATA CORRECTION FACTORS (Continued)

$$\text{Corrected } \bar{q}_{ss} = \text{Correction Factor} \times \bar{q}_{ss}$$

CHAMBER ENTRY	R <sub>p</sub> USED FOR DATA REDUCTION (EQ. 16)	ACTUAL R <sub>p</sub> (1/R <sub>p</sub> ) (R <sub>p</sub> c)	CORRECTION FACTOR (1/R <sub>p</sub> <sup>2</sup> ) <sup>0.8</sup>
17-4	1.011	0.989	0.9826
19-1	0.9859	1.014	1.0230
19-2	1.01133	0.989	0.9821
20-1	1.0154	0.985	0.9758
20-2	0.9969	1.003	1.0050
20-3	0.9986	1.001	1.0022
20-4	0.9817	1.019	1.0300
21-1	0.982	1.018	1.0295
21-2	0.9775	1.023	1.0371
21-3	0.969	1.032	1.0517
22-1	0.96485	1.036	1.0589
22-2	0.9775	1.023	1.0371
22-3	0.9738	1.027	1.0434
22-4	0.96485	1.036	1.0589
23-2	1.02384	0.977	0.9630
23-3	1.02805	0.973	0.9567
23-4	0.9943	1.006	1.0092
23-5	1.0028	0.997	0.9955
24-1	0.9943	1.006	1.0092
24-2	0.965	1.036	1.0587

SUMMARY HEAT TRANSFER DATA CORRECTION FACTORS (Continued)

$$\text{Corrected } \bar{q}_{ss} = \text{Correction Factor} \times \bar{q}_{ss}$$

CHAMBER ENTRY	R <sub>p</sub> USED FOR DATA REDUCTION (EQ. 16)	ACTUAL R <sub>p</sub> (1/R <sub>p</sub> ) (R <sub>p</sub> c)	CORRECTION FACTOR (1/R <sub>p</sub> <sup>2</sup> ) <sup>0.8</sup>
24-3	0.948	1.055	1.0892
25-1	0.948	1.055	1.0892
25-2	0.9354	1.069	1.1128
25-3	0.9227	1.084	1.1374
25-4	0.9227	1.084	1.1374
26-2	1.0154	0.985	0.9758
26-3	0.961	1.041	1.0657
26-4	1.0007	0.999	0.9989
26-5	0.944	1.059	1.0966
27-1	0.851	1.175	1.2945
27-2	0.872	1.147	1.2450
27-3	0.792	1.263	1.4522
27-4	0.864	1.157	1.2635
28-1	0.943	1.060	1.0985
28-2	0.943	1.060	1.0985
29-1	0.906	1.104	1.1711
29-2	0.902	1.109	1.1794
29-3	0.890	1.124	1.2050
29-4	0.910	1.099	1.1629
30-1	0.973	1.028	1.0448

SUMMARY HEAT TRANSFER DATA CORRECTION FACTORS (Concluded)

$$\text{Corrected } \bar{q}_{ss} = \text{Correction Factor} \times \bar{q}_{ss}$$

CHAMBER ENTRY	R <sub>p</sub> USED FOR DATA REDUCTION (EQ. 16)	ACTUAL R <sub>p</sub> (1/R <sub>p</sub> ) (R <sub>p</sub> c)	CORRECTION FACTOR (1/R <sub>p</sub> <sup>2</sup> ) <sup>0.8</sup>
30-2	1.072	0.933	0.8947
30-3	1.079	0.927	0.8855
30-4	1.063	0.941	0.9069
31-1	1.070	0.935	0.8974
31-2	1.078	0.928	0.8868